

Spectroscopy of Extra-galactic Globular Clusters

Michael J. Pierce, BSc(Hons)

A dissertation presented in fulfilment of the requirements for the degree of **Doctor
of Philosophy**

Faculty of ICT

Swinburne University of Technology

December 2006

Abstract

The focus of this thesis is the study of stellar populations of extra-galactic globular clusters (GCs) by measuring spectral indices and comparing them to simple stellar population models. We present the study of GCs in the context of tracing elliptical galaxy star formation, chemical enrichment and mass assembly.

In this thesis we set out to test how can be determined about a galaxy's formation history by studying the spectra of a small sample of GCs. Are the stellar population parameters of the GCs strongly linked with the formation history of the host galaxy?

We present spectra and Lick index measurements for GCs associated with 3 elliptical galaxies, NGC 1052, NGC 3379 and NGC 4649. We derive ages, metallicities and α -element abundance ratios for these GCs using the χ^2 minimisation approach of Proctor & Sansom (2002).

The metallicities we derive are quite consistent, for old GCs, with those derived by empirical calibrations such as Brodie & Huchra (1990) and Strader & Brodie (2004). For each galaxy the GCs observed span a large range in metallicity from approximately $[Z/H]=-2$ to solar.

We find that the majority of GCs are more than 10 Gyrs old and that we cannot distinguish any finer, age details amongst the old GC populations. However, amongst our three samples we find two age distributions contrary to our expectations. From our sample of 16 GCs associated with the 1-2 Gyr old merger remnant NGC 1052, we find no young GCs. If a significant population of GCs formed during this merger we would expect those GCs to have low mass-to-light ratios and be included in our sample of bright GCs. We find 4 young GCs in our sample of 38 around NGC 4649, an old massive cluster elliptical. There are no signs of recent star formation and therefore we do not expect any GCs to have formed within the galaxy. These results seem to indicate that the GC systems of elliptical galaxies are not strongly associated with recent field star formation.

We find a correlation between the α -element abundance ratio and the metallicity for all three samples. Using Thomas, Maraston & Korn (2004) models, we measure much higher α abundance ratios for low metallicity GCs than high metallicity GCs. With current data and models we are limited in both the accuracy and the detail with which we can probe this relationship.

We suggest that there are some difficulties reconciling measured GC parameters with our expectations and propose some future work which could help to resolve these and other issues.

Acknowledgements

There are lots of people to thank for being a part of the process at various points. My supervisors have all filled different roles. Duncan helping to keep track of the big picture, interpreting results and setting deadlines for different tasks. Rob for all his hands-on help with data and software and helping figure out why things don't work. Mike and Terry for reading sections and slices of text and giving feedback on different ideas. From early on I'd like to thank Jean and Jay from UCSC for their enthusiasm about GCs and for sharing their expertise and data.

Thanks to Jarrod and Jeremy for their discussions on particular topics that came up writing this thesis and their expert advice and suggestions on which references to read and include. Thanks to Sarah for comments and feedback on several of the papers.

Thanks to the other students at Swinburne for being people sharing a similar experience with small pieces of advice and wisdom.

Major thanks to my family for keeping encouraging me on the way through. For dealing with the frustrating times of slow progress and reminding me to keep plugging away at it. Thanks to Alex for reading through text and identifying misplaced apostrophes. Thanks to Bron for patience and understanding that finishing a thesis takes time and brain energy and encouraging me to take breaks and get out of town.

Contents

1	Introduction	1
1.1	The Big Picture	1
1.1.1	Elliptical Galaxy Formation Simulations	1
1.1.1.1	N-body Simulations	2
1.1.1.2	Hydro-dynamic Simulations	2
1.1.2	Galaxy Observations	3
1.1.2.1	High Redshift Observations	3
1.1.2.2	Nearby Galaxy Observations	4
1.1.3	Globular Cluster Systems	5
1.2	Globular Clusters	5
1.2.1	Individual Globular Cluster Formation	6
1.2.2	Models of Globular Cluster System Formation	7
1.2.2.1	Major Gas-Rich Mergers	7
1.2.2.2	In-Situ Formation	8
1.2.2.3	Dissipationless and Accretion models	9
1.2.2.4	Miscellaneous	9
1.2.2.5	Testing Formation Models	10
1.2.3	Previous Observational Results	10
1.2.3.1	Galactic Globular Clusters	10
1.2.3.2	Extra-galactic Globular Cluster Luminosities	11
1.2.3.3	Extra-galactic Globular Cluster Colours	12
1.2.3.4	Extra-galactic Globular Cluster Spectroscopy	13
1.3	Spectroscopic Measurements of Stellar Population Parameters	14
1.3.1	Previous Approaches	15
1.3.2	Our Approach	16
1.4	Thesis Layout	17
2	Evolutionary History of the Elliptical Galaxy NGC 1052	19
2.1	Introduction	19
2.2	Observations and data reduction	21
2.3	GC Spectral Line Indices	24
2.3.1	Measurement of Indices	24
2.3.2	Blue Horizontal Branches	28
2.3.3	Fitting Indices to Simple Stellar Population Models	29
2.4	Derived GC Ages, Metallicities and Alpha Abundances	30
2.4.1	Age	30
2.4.2	Metallicity	33

2.4.3	Abundance Ratio	33
2.5	Galaxy Spectrum	33
2.5.1	Long-slit Observations	33
2.5.2	Derived Parameters	36
2.6	Discussion	39
2.7	Conclusions	42
3	Gemini/GMOS Spectra of Globular Clusters in the Leo Group El- liptical NGC 3379	44
3.1	Introduction	44
3.2	Observations and data reduction	46
3.3	Ages, Metallicities and α -Element Abundance Ratios	48
3.4	Discussion	55
3.5	Conclusions	58
4	Gemini/GMOS Spectra of Globular Clusters in the Virgo Giant Elliptical NGC 4649	59
4.1	Introduction	59
4.2	Observations and data reduction	61
4.3	Ages, Metallicities and α -Element Abundance Ratios	62
4.4	Discussion	72
4.5	Conclusions	75
5	Future Directions	76
5.1	Stellar Population Models and Measurements	76
5.1.1	Horizontal branch morphology as a parameter	77
5.1.2	The effect of dynamical processes on globular cluster evolution	77
5.1.3	Modelling of elemental abundances	79
5.1.4	Improving the index system	79
5.2	Globular Cluster Observations	80
5.2.1	Studying a young globular cluster population	80
5.2.2	Resolving the NGC 4365 near-IR photometry controversy . . .	81
5.2.3	Are Ultra-Compact Dwarfs galaxies or globulars?	82
5.2.4	Globular clusters across the luminosity function	82
6	Conclusions	84
6.1	Individual galaxies	84
6.2	Stellar Population Parameters	85
6.2.1	Metallicities	85
6.2.2	Age distributions	86
6.2.3	Alpha element abundance ratios	87
6.3	Summary	89

List of Figures

2.1	NGC 1052 Candidate globular cluster colour magnitude distribution.	22
2.2	Spatial distribution of the confirmed NGC 1052 GCs	24
2.3	Sample of NGC 1052 GC Spectra	25
2.4	CaII Index values against Brodie-Huchra Metallicities	29
2.5	Index-index plot of $H\gamma_F$ vs $Fe50Mg_1$ for NGC 1052 GCs.	31
2.6	Age-metallicity distribution of NGC 1052 GCs	32
2.7	A comparison of empirical metallicities and observed colours with total metallicity	34
2.8	B–V model colour from the spectroscopic metallicity and age vs the observed B–V colour for NGC 1052 GCs	35
2.9	NGC 1052 GC α -abundance ratio vs Metallicity	35
2.10	NGC 1052 galaxy light recession velocity and velocity dispersion as functions of radius	36
2.11	NGC 1052 galaxy light indices with radius	38
2.12	NGC 1052 galaxy light $\langle Fe \rangle$ vs Mgb	39
2.13	NGC 1052 galaxy light derived stellar population parameters with radius	40
2.14	NGC 1052 and NGC 1316 GC colour magnitude diagram comparison	42
3.1	Example NGC 3379 GC spectra	47
3.2	NGC 3379 GC $H\gamma_A$ vs $Fe4383$ plot	52
3.3	NGC 3379 GC age-metallicity relation	53
3.4	Brodie-Huchra metallicity comparison with χ^2 fit metallicity for NGC 3379 GCs	54
3.5	Predicted colours for NGC 3379 GCs vs observed $g-i$ colour	54
3.6	α -element ratio vs metallicity for NGC 3379 GCs	55
3.7	α -element sensitive indices vs Iron indices for NGC 3379 GCs	56
4.1	NGC 4649 GC colour magnitude diagram	61
4.2	NGC 4649 sample spectra	68
4.3	NGC 4649 SSP fit metallicities and ages	70
4.4	Comparison of Brodie-Huchra metallicity and χ^2 fit metallicity for NGC 4649 GCs	71
4.5	NGC 4649 GC α -element abundance ratios vs metallicity	72
4.6	GC age vs projected galactocentric radii for NGC 4649	74
6.1	Comparison of observed colour and metallicity	86
6.2	Comparison of alpha-element abundance trends with metallicity	88

List of Tables

2.1	Globular Cluster candidates around NGC 1052	23
2.2	NGC 1052 GC indices $\lambda < 4500 \text{ \AA}$	26
2.3	NGC 1052 GC indices $\lambda > 4500 \text{ \AA}$	27
2.4	NGC 1052 GC derived parameters	30
2.5	NGC 1052 Galaxy parameters with radius	37
3.1	Properties of GCs around NGC 3379	48
3.2	NGC 3379 GC indices $\lambda < 4600 \text{ \AA}$	49
3.3	NGC 3379 GC indices $\lambda > 4600 \text{ \AA}$	50
3.4	Derived NGC 3379 Globular Cluster Properties	51
4.1	Properties of GCs around NGC 4649	63
4.2	NGC 4649 GC indices $\lambda < 4600 \text{ \AA}$	64
4.3	NGC 4649 GC index errors $\lambda < 4600 \text{ \AA}$	65
4.4	NGC 4649 GC indices $\lambda > 4600 \text{ \AA}$	66
4.5	NGC 4649 GC index errors $\lambda > 4600 \text{ \AA}$	67
4.6	NGC 4649 GCs derived properties	69

Declaration

This thesis contains no material that has been accepted for the award of any other degree or diploma. To the best of my knowledge, this thesis contains no material previously published or written by another author, except where due reference is made in the text of the thesis. All work presented is primarily that of the author with paper co-authors making contributions to the relevant chapters.

Chapter 2 includes all the stellar population sections published in Pierce, M.J., Brodie, J.P., Forbes, D.A., Beasley, M.A., Proctor, R. & Strader, J., "Evolutionary history of the elliptical galaxy NGC 1052", 2005, MNRAS, 358, 419. The work relating to the globular cluster kinematics mass estimate in Section 6 of this paper was primarily that of Jay Strader and has not been included in this thesis.

Chapter 3 is an extract from the published paper Pierce, M.J., Beasley, M.A., Forbes, D.A., Bridges, T.J., Gebhardt, K., Faifer, F.R., Forte, J.C., Zepf, S.E., Sharples, R., Hanes, D.A., & Proctor, R., "Gemini/GMOS spectra of globular clusters in the Leo group elliptical NGC 3379", 2006, MNRAS, 366, 1253. The published paper section 4, focusing on the globular cluster kinematics, is primarily that of Karl Gebhardt and has not been included in this thesis. Chapter 3 includes all sections (1,2,3,5 and 6) related to the stellar population study which is primarily the work of the author. Several paragraphs on kinematics from sections 1, 5 and 6 of the paper are not included in this thesis.

Chapter 4 has been published as Pierce, M.J., Bridges, T.J., Forbes, D.A., Proctor, R., Beasley, M.A., Gebhardt, K., Faifer, F.R., Forte, J.C., Zepf, S.E., Sharples, R., & Hanes, D.A., "Gemini/GMOS spectra of globular clusters in the Virgo giant elliptical NGC 4649", 2006, MNRAS, 368, 325.

Minor alterations have been made to these works in order to maintain consistency of style.

Michael Pierce

Publications

The following publications have arisen from the work presented in this thesis.

1. *Evolutionary history of the elliptical galaxy NGC 1052* Pierce, M.J., Brodie, J.P., Forbes, D.A., Beasley, M.A., Proctor, R., Strader, J. Monthly Notices of the Royal Astronomical Society, 2005, 358, 419
2. *Gemini/GMOS spectra of globular clusters in the Leo group elliptical NGC 3379* Pierce, M.J., Beasley, M.A., Forbes, D.A., Bridges, T.J., Gebhardt, K., Faifer, F.R., Forte, J.C., Zepf, S.E., Sharples, R., Hanes, D.A., Proctor, R. Monthly Notices of the Royal Astronomical Society, 2006, 366, 1253
3. *Gemini/GMOS spectra of globular clusters in the Virgo giant elliptical NGC 4649* Pierce, M.J., Bridges, T.J., Forbes, D.A., Proctor, R., Beasley, M.A., Gebhardt, K., Faifer, F.R., Forte, J.C., Zepf, S.E., Sharples, R., Hanes, D.A. Monthly Notices of the Royal Astronomical Society, 2006, 368, 325
4. *The globular cluster kinematics and galaxy dark matter content of NGC 4649 (M60)* Bridges, T., Gebhardt, K., Sharples, R., Faifer, F.R., Forte, J.C., Beasley, M.A., Zepf, S.E., Forbes, D.A., Hanes, D.A., Pierce, M.J. Monthly Notices of the Royal Astronomical Society, 2006, in press

Chapter 1

Introduction

1.1 The Big Picture

The focus of this thesis is the study of Globular Cluster (GC) systems of elliptical galaxies with the aim of revealing some of the formation and evolution details of these galaxies.

The detailed formation and evolution history of elliptical galaxies, both mass assembly and star-formation, is an unsolved problem facing astronomy. A large fraction of the stellar mass in the universe at $z=0$ resides in spheroids, such as elliptical galaxies ($\sim 75\%$; Fukugita, Hogan & Peebles 1998). However, exactly when and how that stellar mass came to be in large ellipticals has not yet been constrained.

There are several methods being pursued to resolve this problem. These include cosmological N-body and hydrodynamic simulations, photometric and spectroscopic observations of high-redshift galaxies, detailed studies of local galaxies, and observations of globular cluster systems in local galaxies. Each approach has its advantages and limitations. The use of several complimentary, independent methods will be required to identify and resolve the bias that can result from the use of a single approach in isolation. The models associated with each method also require refinement for the approaches to be reconciled. This thesis is focused on the study of globular cluster systems. We will first briefly describe some of the alternate means of studying elliptical galaxy formation.

1.1.1 Elliptical Galaxy Formation Simulations

From the theoretical realm there are two common approaches to modelling elliptical galaxy formation. These are based on the two current dominant formation paradigms, hierarchical merging and monolithic collapse.

According to hierarchical galaxy formation, ellipticals form through the merging of smaller systems (e.g. Kauffmann, White & Guiderdoni 1993). In cold dark matter (CDM) simulations dark matter (DM) halos merge hierarchically. Assuming that galaxies live in DM halos and that there is a close relationship between the assembly history of galaxies and their host DM halos, then CDM simulations map the hierarchical galaxy formation paradigm. This scenario predominantly describes the mass assembly rather than the star formation history of the galaxies.

In the alternate scenario, ellipticals form by the rapid monolithic collapse of baryons at high redshift (Larson 1975). This scenario can naturally explain the tightness of many elliptical scaling relations, such as the fundamental plane and colour-magnitude relations (e.g. van Dokkum & Stanford 2003).

In the following two sub-sections we describe two modelling methods which are aligned to some extent with the formation paradigms described.

1.1.1.1 N-body Simulations

Cosmological N-body simulations can be used to trace the assembly of dark matter (DM) particles and halo mergers. Recent simulations, such as the Millennium run (Springel *et al.* 2005), include large volumes ($500 h^{-1}$ Mpc per side) and thousands of galaxy-size halos. Assuming that the DM dominates the dynamical processes on scales larger than that of individual galaxies (10-100 kpc), it is reasonable to use semi-analytic models to populate these DM halos with baryons (e.g. Bower *et al.* 2006) and produce a statistical sample of simulated galaxies. These semi-analytic models usually aim to reproduce the observed mass and luminosity functions at $z=0$ as well as observed scaling relationships, such as galaxy colour with velocity dispersion and the mass-to-light ratio with galaxy mass. This style of simulation is capable of making predictions regarding the assembly of mass with redshift, the number of mergers and accretions a standard galaxy has undergone and the distribution of bulk properties such as luminosity. The effect of mergers on the kinematics of stars and GCs can be inferred from N-body simulations (e.g. Bekki *et al.* 2005).

A drawback with this approach is that baryon physics is highly non-linear and complex. Therefore semi-analytic models require implicit assumptions (e.g. virialisation of the dark matter and gas) and phenomenological parameterisations of complex physics that are not well constrained. For example, star formation is poorly understood, which means the semi-analytic prescriptions are usually simple and empirical (Somerville & Primack 1999). Another problem is that the baryons can affect the dark matter halo shape and concentration (Kazantzidis *et al.* 2004), especially in the inner regions where baryons dominate (Lintott, Ferreras & Lahav 2006).

It is important to note that different parameterisations of the baryons can lead to highly different predictions from the simulations. De Lucia *et al.* (2006) show that when they do not include AGN feedback to suppress gas cooling flows they find similar results to earlier simulations (e.g. Baugh *et al.* 1996; Kauffmann 1996b; Kauffmann & Charlot 1998) and obtain extended star formation histories for massive galaxies, contrary to observations. When they do suppress gas cooling the most massive galaxies are found to have old and metal-rich stellar populations, similar to observations (e.g. Nelan *et al.* 2005). One advantage with semi-analytic approaches is that particular physical processes can be turned off and on for a simulation making it possible to determine which physics is the most important for reproducing particular observational properties (Baugh 2006).

1.1.1.2 Hydro-dynamic Simulations

Commonly starting from the collapse of a single primordial gas cloud, hydro-dynamic simulations aim to reproduce detailed features of individual galaxies (e.g. Pipino,

Matteucci & Chiappini 2006). These simulations tend to focus on properties such as metallicity gradients, stellar kinematics and star-formation histories.

Similar to semi-analytic models, an ever increasing number of physical processes are modelled including multi-phase gas physics, supernova feedback, active galactic nuclei feedback, chemical enrichment, radiative cooling and stellar winds (e.g. Kobayashi 2004 and references therein). The implementation of each of these processes in the simulation requires a solid observational basis. The results of such complex models are limited by the input physics, which is gradually evolving and improving as constraints are improved. For example, Matteucci *et al.* (2006) includes an updated formulation of SN type Ia and the effect this has on galactic chemical evolution, and find that more Iron is created earlier in their models.

There are also now a few fully cosmological hydro-dynamic simulations that produce elliptical galaxies (e.g. Kawata & Gibson 2003; Saiz, Dominguez-Tenreiro & Serna 2003). These are consistent with the hierarchical formation paradigm, but also form a large fraction of their stars rapidly at high redshift in the largest galaxies similar to the predictions of monolithic collapse.

1.1.2 Galaxy Observations

To provide constraints and tests of galaxy formation models we observe galaxies. Nearby and distant galaxies can be used to probe different elements of galaxy formation and evolution. We will briefly introduce both approaches.

1.1.2.1 High Redshift Observations

Observing galaxies at high redshift can allow the study of galaxy properties over a long baseline in time. Therefore it is a direct method of determining their mass assembly and star-formation history (Renzini 2006).

Often, high redshift observations of early-type galaxies have focused on clusters of galaxies, because it is observationally more efficient. For a given galaxy cluster various observational relationships can be measured, such as the colour-magnitude relation and the star-formation rate with environmental density. The luminosity functions and co-moving number densities of galaxies at different redshifts offer an insight into mass assembly (Wake *et al.* 2006).

Observations of high redshift galaxies have shown that the star-formation rate was much higher in large galaxies at earlier epochs (e.g. Bell *et al.* 2005). We also now know that there used to be a higher fraction of blue star-forming galaxies in clusters than is observed at the present day (Butcher & Oemler 1978) and that very large stellar systems, such as Ultra-luminous Infra-red Galaxies (ULIRGs) are already assembled at redshifts of $z \sim 3$ (e.g. Genzel & Cesarsky 2000, Genzel *et al.* 2003).

There are several difficulties with studying high-redshift galaxies. Firstly, objects are fainter, require longer integration times to achieve useful signal-to-noise and fewer resolved properties are measurable than for local galaxies. Secondly, it is much more difficult to assess environmental effects at high redshift, where all but the brightest galaxies are difficult to detect. Finally, and perhaps most importantly, high redshift observations suffer from progenitor selection bias (van Dokkum *et al.*

2000), i.e. when trying to select high- z galaxies that will evolve into current day large ellipticals, it is difficult to avoid making target selection assumptions that bias the sample (e.g. Cannon *et al.* 2006, Wake *et al.* 2006).

1.1.2.2 Nearby Galaxy Observations

Detailed studies of galaxies in the local universe, often called “Galactic Archaeology”, provide constraints on the current content of these galaxies as well as some clues to their formation history (see Section 3 of Renzini 2006).

Obviously the nearest galaxy to study is our own. Freeman & Bland-Hawthorn (2002) present an excellent review of the formation of the Milky Way, the detailed observations of various sub-components and how they contribute to our overall understanding of how the Milky Way formed. Venturing further abroad, local group galaxies can be resolved into their stellar populations in order to study their star formation histories in great detail. Brown *et al.* (2003) show that the halo of M31 contains a significant fraction of intermediate age (6–8 Gyr) stars as well as an old (11–13 Gyr) population. The star-formation histories of local group dwarf galaxies are shown to vary between galaxies as well as spatially within galaxies (Grebel 2001).

To study massive elliptical galaxies we must go beyond the local group to distances beyond 10 Mpc where individual stars cannot easily be resolved or studied. In this case star-formation histories can be measured from the spectra of integrated stellar populations. A standard approach is to compare the observed spectra to simple stellar population models (see Section 1.3). However, if there are multiple epochs of star-formation, it is almost impossible to disentangle the contributions of each epoch. The low M/L ratio of young stellar populations means that a relatively small burst of recent (< 2 Gyr) star-formation can dominate the observed spectrum, even when the underlying old population comprises more than 90% of the mass. This domination by a low-mass, bright component is sometimes called “frosting” (see Trager *et al.* 2000a) and often leads to a misleading galaxy-age estimation: approximately the luminosity weighted mean of the two populations.

A two-burst stellar population fit can be made. However, this involves fitting at least 7 parameters (2 ages, 2 metallicities, 2 α -element enhancements and a luminosity ratio), with the underlying assumption that the old and young populations are each composed of a uniform metallicity and α -element abundance. Several groups are beginning to develop methods to attempt to find such solutions. These are generally based on fitting admixtures of spectral indices (e.g. Serra & Trager 2006) or principal component analysis of the spectra (e.g. Ferreras *et al.* 2006). One interesting result found by Serra & Trager (2006) is that in many situations the SSP estimated age is not the luminosity weighted age of the two input components, but is the Balmer Index weighted age of the two. This causes stellar populations younger than ~ 2.5 Gyrs to influence index-index measurements based on spectra more strongly than their luminosity weighting would suggest.

An additional complication to account for in the interpretation of observations is the effect of mergers and accretions, both gas-rich and gas-poor. Gas-rich major mergers can result in a large burst of star-formation contributing a sizeable percentage of the galaxy’s stars. Such a merger is usually detectable observationally

due to the recently formed bright young stars, disturbed morphology, HI and stellar tidal tails. However, other processes that may be responsible for building elliptical galaxy mass are the merger of two gas-poor progenitors or the accretion of satellite dwarf galaxies. In these cases there may be minor star formation in the centre of the galaxy, but after several Gyrs such an event is often difficult to detect (with the exception of “shell” galaxies, which are believed to be an example of minor mergers where long lived, faint stellar shells are created by gravitational resonances).

1.1.3 Globular Cluster Systems

One of the major motivations behind studies of globular clusters is that they are good tracers of several of their host galaxies’ properties (see Brodie & Strader 2006). During both initial proto-galactic collapse and gas-rich major mergers we expect globular clusters to form. GCs trace both the field stars they form alongside and the host galaxy they are found orbiting. They can be used to quantify the “frosting” effect, to trace the chemical enrichment history of gas and stars and to pinpoint the epoch of major star-formation activity.

As mentioned in the previous section the disentangling of an unknown number of stellar populations that are inter-mixed is an unenviable task. However, globular clusters are surviving tracers of the individual stellar populations that are not contaminated by mixing, to first order. A large percentage of Galactic GCs (e.g. M22) show star to star variation in C and N abundance, probably due in part to the effects of dredge-up and the CNO cycle. However, some of the variations could be due to contamination of the GC sample by field stars (Ivans *et al.* 1999; Cohen *et al.* 2002; Cohen *et al.* 2005).

The accretion of an almost gas-free dwarf galaxy will not create many, if any, new globular clusters. However, it will add to the host galaxy GC system a small number of GCs that previously belonged to the consumed dwarf. Detailed analysis of the kinematics and stellar populations of GC can show the difference between the GCs originally belonging to the host galaxy and those imported alongside the accreted dwarf. Forbes, Strader & Brodie (2004) present this case for the Sagittarius dwarf.

1.2 Globular Clusters

Globular star clusters contain tens of thousands to millions of stars, with typical total masses between 10^4 and 10^6 solar masses. They span a luminosity range in the V band from $M_V = -5$ to -10 . To be considered a GC the star cluster must be older than a few hundred Myrs. They typically have half-light radii of a few pcs. The stellar velocity dispersions are <10 km/s and GCs possess little or no gas. There is currently no evidence that GCs possess dark matter haloes (Heggie & Hut 1996).

GCs are found around galaxies, of all morphological types, brighter than approximately $M_V = -15$. A GC system typically contains around 0.25% of the total stellar mass of their host galaxy (McLaughlin 1999).

We know from high resolution spectroscopy of individual stars in Local Group GCs that, with a few notable exceptions, the age, metallicity and α -element abun-

dance ratios are very similar for all the stars contained within the cluster and therefore that the cluster formed in a single star formation episode (e.g. Leep, Wallerstein & Oke 1986; Brown & Wallerstein 1992; Carney 1996; Ferraro *et al.* 2006). In the Milky Way there is at least one counter example, Omega Cen, which has historically been identified as a GC, but contains two distinct giant branches and main sequences with an age spread of at least 2 Gyrs (Lee *et al.* 1999; Hughes *et al.* 2004). Morgan & Lake (1989) and Tsujimoto & Shigeyama (2003) show that Omega Cen can be modelled as a self-enriched object with several bursts of star formation. Objects such as this and G1 in M31 are thought to be stripped dwarf galaxies rather than GCs (Lee *et al.* 1999; Meylan *et al.* 2001).

GCs span a wide range of metallicities from less than one hundredth to several times solar ($[\text{Fe}/\text{H}]^1 = -2.3$ to $+0.5$). Based on the well studied Milky Way GC system and photometric studies of other galaxies (see Section 1.2.3.3), there are believed to be at least two sub-populations of GCs around most galaxies, the photometrically blue ($V-I < 1.05$) metal-poor $[\text{Fe}/\text{H}] < -0.8$ and the red ($V-I > 1.05$) metal-rich $[\text{Fe}/\text{H}] > -0.8$ (West *et al.* 2004). This separation into two populations photometrically and presumably in metallicity is referred to as GC system bi-modality.

1.2.1 Individual Globular Cluster Formation

GCs are typically thought to form during major star formation episodes: proto-galactic collapse, gas-rich major mergers or other large star-formation bursts (Larsen & Richtler 2000). There is little to no GC formation observed in low-level continuous quiescent star-forming regions (e.g. in spiral disks). Larsen & Richtler (2000) find the fraction of star formation occurring in star clusters scales with the total star-formation rate of the galaxy. So efficient star cluster formation will only occur during the most major star formation events, such as initial star-formation at high- z or during gas-rich galaxy mergers.

The global conditions under which GCs form are somewhat understood. There are several postulated sites and formation mechanisms for individual GCs. The cores of giant molecular clouds possess high gas densities and mass and a similar mass function to GCs above $10^5 M_\odot$ indicating that GCs could form from giant molecular clouds (Harris & Pudritz 1994; McLaughlin & Pudritz 1996).

Another possible means of forming individual GCs is modelled by Scannapieco, Weisheit & Harlow (2004), who propose that GCs can be formed from gas in “minihalos” that surround large galaxies, with the formation triggered by galactic outflows from star-burst galaxies. According to their models the gas originally in the “minihalo” can be stripped from the dark matter halo. The outflow gas mixes with the primordial gas from the halo to produce star clusters with homogeneous metallicities and a range of metallicities between star clusters. They claim that formation by this means can explain the upper mass limit of GCs ($10^6 M_\odot$), as below this mass limit a gas cloud is unable to independently start forming stars and that therefore some triggering mechanism is required to start star-formation below $10^6 M_\odot$.

In another scenario, Elmegreen & Efremov (1997) suggest a universal formation mechanism for all type of star clusters. They claim that globular clusters form in

¹Chemical abundances are commonly defined as the logarithm of the ratio to solar abundance. e.g. $[\text{X}/\text{Y}] = \log_{10}(\frac{\text{X}}{\text{Y}})_{\text{Obs}} - \log_{10}(\frac{\text{X}}{\text{Y}})_{\odot}$

high pressure regions such as shocks during galaxy mergers or in regions of turbulence compression. Formation in a region of high density makes the cluster more tightly bound which implies a longer disruption timescale for GCs compared with other star clusters.

These scenarios are difficult to test. While star clusters may be formed by each process it is very difficult to determine whether these will survive and evolve into the GC populations observed.

1.2.2 Models of Globular Cluster System Formation

The formation details of individual GCs, like star-formation, are not well understood. However despite these uncertainties, there are several hypotheses to describe the assembly of the GC systems of large elliptical galaxies, that do not rely on individual GC formation details. These are predominantly driven by observations of the GC specific frequency and colour bi-modality described in Sections 1.2.3.2 and 1.2.3.3. These models fall into three broad classes: major gas-rich mergers, in-situ formation and dissipationless (gas-free) accretion.

1.2.2.1 Major Gas-Rich Mergers

Ashman & Zepf (1992) suggested that major disk-disk galaxy mergers, which they considered a common formation mechanism for elliptical galaxies, should contribute significantly to the GC populations of large ellipticals. The final GC system would then be composed of GCs from both progenitor galaxies and a younger population of metal-rich GCs formed during the merger.

The best example of young massive star clusters (YMCs, which presumably are the progenitors of GCs) forming in a major star-formation event is the Antennae galaxy merger (Whitmore & Schweizer 1995), where hundreds of YMCs are seen forming in conjunction with the galaxy-galaxy merger. There are numerous other cases of YMCs forming during major star-formation events, however the fraction of clusters that survive to become GCs is not well constrained (e.g. McCardy, Gilbert & Graham 2003; Smith & Gallagher 2001).

The luminosity distribution of YMCs formed during major mergers is observed to follow a power-law (Whitmore & Schweizer 1995; Schweizer *et al.* 1996; Miller *et al.* 1997; Carlson *et al.* 1998; Zepf *et al.* 1999). There is some disagreement as to whether the dynamical interactions of a star cluster with its host galaxy can convert the power-law luminosity function of young clusters to the observed log-normal GC luminosity function (GCLF).

For example Vesperini (2000, 2001), based on simulations incorporating semi-analytic prescriptions, claimed that it is quite difficult to change a GCLF from the power-law form observed for YMCs to the log-normal form observed for GCs. Dynamical evolution can remove star clusters from the low mass end of the GCLF, however the resulting turnover mass is lower than observed for GCs and varies with galactocentric radius, contrary to observations. This suggests that the initial GCLF of GCs at early times is different from that observed for YMCs forming now. However, Vesperini & Zepf (2003) show that if the density of the individual GCs is related to mass then a log-normal GCLF, with little variation in turn-over mass

with galactic radius, can be reproduced. This is because low-concentration GCs are more easily destroyed at all radii.

Fall & Zhang (2001) present a semi-analytic study of GCLF evolution for a Milky Way-like galaxy. A cluster's orbit, rather than mass or concentration, determines its mass loss rate in this model. They find that for a wide variety of initial GCLFs, eventually a log-normal GCLF evolves, with turn-over masses similar to those observed. The turn-over mass in this model varies strongly with radius, contrary to observations, unless the outer regions GCs display strong radial anisotropy. Vesperini *et al.* (2003) came to a similar conclusion, requiring strong radial anisotropy in GC kinematics to evolve a power-law GCLF to a log-normal GCLF, when they modelled M87 in detail.

1.2.2.2 In-Situ Formation

Forbes, Brodie & Grillmair (1997) highlight several problems with the major merger scenario, most importantly that the fraction of metal-poor GCs increases with GC specific frequency ($S_N = N_{GC} \times 10^{0.4(M_V + 15)}$, the number of GCs per unit luminosity of the host galaxy), contrary to the expectation of the merger model (see also Rhode, Zepf & Santos 2005). Instead they suggest a multi-phase collapse during initial galaxy formation, which involves two distinct in-situ formation events for metal-poor and metal-rich GCs.

Beasley *et al.* (2002) presented a semi-analytic galaxy formation model within a cosmological formation simulation. This method intrinsically includes mergers, both gas-rich and gas-poor and biased galaxy formation, which is the tendency for large galaxies to be found near to other large galaxies. In this scenario metal-poor GCs form early in low-mass proto-galaxies and then metal-rich GCs are formed during the gas-rich merger of these proto-galaxies. Artificial truncation of the formation of metal-poor GCs at $z \sim 5$ was necessary to prevent the over-production of metal-poor GCs. One key prediction is that the metal-rich GCs should be 2-4 Gyrs younger than the metal-poor sub-population.

Strader, Brodie & Forbes (2004b) and Rhode *et al.* (2005), propose similar hierarchical scenarios to Beasley *et al.* (2002). Metal-poor GCs are proposed to form at redshifts of $z = 10-15$ in low-mass dark matter halos, with truncation of formation likely due to reionisation. Subsequent mergers of these halos form both the final galaxy and the metal-rich GCs by $z > 2$ for L^* galaxies. These proposals are consistent with the Forbes *et al.* (1997) multi-phase collapse model and provide plausible mechanisms for the truncation of metal-poor GC formation and the subsequent formation of metal-rich GCs.

The truncation of metal-poor GC formation by reionisation has been applied in several simulations of GC formation that seek to reproduce particular observational relationships. Assuming that reionisation truncates metal-poor GC formation then the surface density profile of metal-poor GCs around a galaxy can be used to set limits on the epoch of reionisation (Bekki 2005; Moore *et al.* 2006). Bekki & Forbes (2006) show that the properties of the GC systems of elliptical galaxies will be affected by the galaxy's merger history and therefore disentangling the merger history and epoch of reionisation will not be a trivial task.

1.2.2.3 Dissipationless and Accretion models

With a view to producing a model consistent with hierarchical formation, as predicted by CDM cosmological simulations, Cote, Marzke & West (1998) propose that a substantial component of an elliptical galaxy’s GC system is accreted from dwarf galaxies. The mean metallicity of GC systems is known to correlate with galaxy mass (Brodie & Huchra 1990). The Cote *et al.* model proposes that the metal-rich GCs are formed in the massive galaxy and that the metal-poor sub-population is accreted from dwarf galaxies.

Dissipationless accretions involve little or no gas and therefore almost no star-formation. In this case the ages of GCs do not reflect when the merger occurred, but do reflect the epoch when the stars formed. One problem with this scenario is that a large number of low metallicity stars from the dwarf galaxy will be accreted alongside the metal-poor GCs. These low metallicity stars are not observed within the fields of elliptical galaxies (Harris & Harris 2002). Another potential problem is that the metal-poor GCs of dwarf galaxies have metallicities that are lower than those in massive ellipticals by up to 0.5 dex (Strader *et al.* 2004b). The assumption that present day dwarfs are identical to those accreted at earlier times by massive ellipticals does not include the effects of biased structure formation (Brodie & Strader 2006), meaning that some of the issues raised may not be as serious as expected.

A similar suggestion to the Cote *et al.* (1998) accretion model is the tidal stripping of GCs from a neighbouring galaxy. Bekki *et al.* (2003) model the massive Fornax cluster ellipticals NGC 1404 and NGC 1399 and seek to understand the difference in S_N of 2 for NGC 1404 vs 10 for NGC 1399. By assuming an eccentric orbit for NGC 1404 and that the scale-length of the GC system is twice that of the galaxy, then the difference in S_N for the two galaxies can be explained by the tidal stripping of NGC 1404 GCs by the cluster potential. These stripped GCs will create a tidal stream orbiting the centre of the cluster potential and therefore would be assigned to NGC 1399 in an imaging study.

1.2.2.4 Miscellaneous

Kravtsov & Gnedin (2005) present a cosmological simulation of a Milky Way-like galaxy to $z \sim 3$, focusing on the formation of the GC system. In their simulation, GCs are assumed to form in the baryon dominated cores of supergiant molecular clouds. However, too many $[\text{Fe}/\text{H}] = -1$ GCs were formed towards the end of their simulation, even though it incorporates standard feedback mechanisms, suggesting that normal “stellar” feedback mechanisms (i.e. star-formation, supernovae, active galactic nuclei) may not suppress metal-poor GC formation and thus some other mechanism, such as reionisation (see Section 2.2.2), is required.

While not a formation model as such, it is worth noting the suggestion of Yoon, Yi & Lee (2006). When they apply a new stellar population colour-metallicity relationship (which is discussed further in Section 1.2.4.3), they propose that the GC systems of large elliptical galaxies could have uni-modal metallicity distributions. This contradicts the commonly accepted bi-modal metallicity distribution that the previously mentioned formation models have attempted to reproduce and the validity of these results and models is currently disputed.

1.2.2.5 Testing Formation Models

Across the various models there is general consensus that metal-poor GCs form very early, however precisely determining their ages offers a strong test and constraint on formation models. To determine the relative contributions of different galaxy formation and assembly processes, accurately measured ages for metal-rich GCs are crucial. Also important are the relative ages of metal-poor and metal-rich GCs. Metallicity distributions for entire GC systems across a range of galaxy masses and environments will also be necessary to distinguish between the proposed models.

1.2.3 Previous Observational Results

Globular clusters are useful probes of galaxy formation for a number of reasons. Firstly, several globular cluster system properties are correlated with those of their host galaxies, implying that the formation of these star clusters is linked to the formation of the galaxy itself. Secondly, the stars within an individual globular cluster are a coeval and generally chemically homogeneous population, which makes them relatively simple stellar systems to understand, unlike the complex stellar population in galaxies, which often span a wide range of ages and chemical abundances. Thirdly, the luminosity and compact size of GCs make them among the brightest and most readily identifiable individual objects within galaxies. This allows them to be traced to large galactocentric distances, whereas the surface brightness of the host galaxy rapidly drops with increasing galactocentric radius.

To measure the stellar population parameters of GCs there are several different observations that can be made. There is commonly a trade off between required observation time, the number of GCs sampled and the amount of information measurable for individual GCs.

1.2.3.1 Galactic Globular Clusters

For Milky Way GCs, because we can measure individual stars, it is possible to obtain both colour-magnitude diagrams (CMD), including stars as faint as the main sequence, as well as high-resolution spectra of individual bright stars. In conjunction these two methods make it possible to tightly constrain the metallicity, age and α -element abundances of GCs.

The ages of clusters can be measured both from the main sequence turn-off mass (magnitude) and from the white dwarf cooling sequence (Piotto *et al.* 2002). The metallicity of a cluster can be measured by comparing the slope of the red giant branch with isochrones of known metallicity or by the location of the main sequence in colour space. These measures are based on relatively well-understood stellar evolution physics.

Abundances of individual elements can be measured from tens of lines with high-resolution optical spectroscopy of individual stars in Galactic GCs. Carney (1996) finds an $[\alpha/\text{Fe}]$ ratio of +0.3 dex for GCs more metal-poor than $[\text{Fe}/\text{H}]=-1$ with the α -element abundance ratio decreasing to solar at solar metallicity. Pritzl, Venn & Irwin (2005) show the same trend in α -element ratios as Carney (1996) and also show that the trend matches those in Galactic halo stars.

The Galactic system has been well sampled (although some GCs are more difficult to observe due to dust extinction) and it is commonly used to calibrate empirical metallicity estimates (e.g. Zinn & West 1984; Brodie & Huchra 1990; Strader & Brodie 2004). There is a drawback to this approach: the Galactic GC system is almost completely confined to old ages and metallicities below solar. Therefore calibration is difficult for young ages or super-solar metallicities.

1.2.3.2 Extra-galactic Globular Cluster Luminosities

Photometric studies of more distant globular cluster systems have been made over many years (e.g. Racine 1968; Hanes 1976; Harris 1999). There are an assortment of quantities that can be measured by imaging GC systems. We will introduce several of them in this and the following section.

Harris & van den Bergh (1981) introduced a way to quantify the richness of a GC system. The specific frequency (S_N , see Section 1.2.2 for definition) is a measure of the number of GCs per unit luminosity of the host galaxy, such that a $M_V=-15$ galaxy with one GC has a S_N equal to one. For a galaxy with no interaction history it is a function of formation efficiency of GCs relative to field stars and the survival probability. Typical values vary between galaxy types, suggesting different GC formation and destruction efficiencies. Somewhat surprisingly, S_N does not correlate monotonically with galaxy mass, but forms a “U shape” (Harris 1991; Durrell *et al.* 1996; Forbes 2005), with both dwarf (low mass) and large elliptical (high mass) galaxies possessing significantly richer GC systems (higher S_N) than spirals (intermediate mass) and intermediate mass ellipticals.

Zepf & Ashman (1993) introduce a different way to quantify the richness of a GC system. They define the T parameter as $T_N=N_{GC}/[M_G/10^9 M_\odot]$. This is the specific frequency with mass, which is more fundamental than luminosity, although more difficult to measure. In many studies (e.g. Rhode, Zepf & Santos 2005), mass is determined from the observed luminosity and an assumed mass-to-light ratio, rather than from dynamical measures. In this situation T_N and S_N are equivalent.

After quantifying the richness of a GC system, it is natural to construct a luminosity function. For GC systems the luminosity distribution can generally be fit by a Gaussian or t_5 (Secker 1992). Another very useful finding, first shown by Hanes (1976; 1977a; 1977b; 1979), is that the turn-over luminosity appears to be universal: M_{TO} is -7.4 in the V band, within errors, for all observed GC systems, even amongst galaxies of different Hubble types (Harris 2001). The dispersion of the distribution is related to the host galaxy’s absolute magnitude (Jordan *et al.* 2006), varying from 1.3 mags for the brightest galaxies ($M_B=-22$) to 0.8 mags for galaxies with $M_B=-16$. The GCLF is now a commonly used distance indicator for nearby galaxies, where it is possible to sample the GC system below the turn-over magnitude. However, Jordan *et al.* (2006) recently warned that for host galaxies fainter than $M_B=-18.5$, the GCLF may not be an entirely accurate distant indicator. This is because in their HST ACS sample of Virgo galaxies the turn-over magnitude appears to become fainter amongst the least massive galaxies.

1.2.3.3 Extra-galactic Globular Cluster Colours

An almost ubiquitous feature of GC systems is a bi-modal colour distribution. This was first noted for large elliptical galaxies by Zepf & Ashman (1993) and Ostrov, Geisler & Forte (1993). Histograms of common filter combinations such as V–I are generally found to have two peaks, which reside at similar colours for most galaxies. These are referred to as the red and blue peaks or sub-populations.

In the late 1990s with the Wide Field and Planetary Camera 2 (WFPC2) on the Hubble Space Telescope (HST), many galaxies were studied, with much improved spatial resolution and photometric accuracy (e.g. Kissler-Patig & Gebhardt 1999, Kundu & Whitmore 2001). This improved the identification of GCs, foreground stars, and background galaxies, for galaxies to distances of the Virgo and Fornax clusters. At those distances (~ 17 -20 Mpc) a typical GC with a half-light radius of a few pc is partially resolved and, with a well modelled point spread function (PSF), the size of individual GCs is measurable.

The mean colours of the red and blue sub-populations scale with host galaxy luminosity. Forbes *et al.* (1997) found that the colour of the red sub-population is correlated with host galaxy luminosity and also with galaxy halo star colour. Strong evidence that a similar correlation exists for the blue sub-populations was provided by Strader, Brodie & Forbes (2004). The correlation of GC sub-population colours with host galaxy luminosity and mass is taken as evidence that there is a strong link between GC and galaxy star formation and that a dominant fraction of GCs form in association with their final host galaxy.

Further interest in the details of GC colours has been sparked by the recent Advanced Camera for Surveys (ACS) GC studies of Strader *et al.* (2006), Harris *et al.* (2005) and Peng *et al.* (2006). All three find that for at least some galaxies the mean colour at a given magnitude within the blue GC sub-population reddens with increasing GC luminosity. This trend is referred to as the “blue tilt” and has been interpreted as a mass/metallicity relationship for metal-poor GCs.

The relationship between metallicity and observed colour is of great interest, both because of the colour bi-modality seen for large ellipticals and in trying to understand the “blue-tilt”. We know that both varying age and horizontal branch morphology affect a stellar population’s integrated colour in very similar ways to metallicity (Lee *et al.* 2000). A simplifying set of assumptions for understanding GC colours is that a dominant fraction (80-90%) of GCs have ages close to the age of the universe (see Section 1.2.3.4), and that horizontal branch morphology depends primarily on metallicity (see Fig 3. Reico-Blanco *et al.* 2006). Therefore, under these assumptions, the colour bi-modality and trends with galaxy mass are primarily metallicity effects.

The most common colour used to study GC systems with WFPC2 was V–I (e.g. Larsen *et al.* 2001a; Strader *et al.* 2004b), mostly due to exposure time considerations. The relationship of V–I to metallicity has been empirically calibrated as a linear function using a combination of Milky Way and M31 GCs (e.g. Barmby *et al.* 2000). It is important to note that there are very few metal-rich Galactic GCs without high dust reddening, because the majority are in the galactic bulge. Therefore it is very difficult to calibrate GC relationships at high metallicity with just Galactic data. Model V–I colours, in general, are not linear with metallicity;

however the deviation from linear is often within the normal observational errors.

More recent observations in $g-z$ (a colour which has much higher metallicity sensitivity than V-I), show clearly that the transformation of colour to metallicity, for old GCs is not linear for this combination of filters and presumably most (if not all) colour combinations (see Peng *et al.* 2006). Instead there are significantly different slopes for metal-poor ($[\text{Fe}/\text{H}] < -0.8$, $g-z < 1.05$) and metal-rich ($[\text{Fe}/\text{H}] > -0.8$, $g-z > 1.05$) GCs.

Yoon, Yi & Lee (2006) present results of models of GC colour with much closer metallicity spacing ($\Delta[\text{Fe}/\text{H}] = 0.1$ dex) that focus on horizontal branch morphology. They find a non-linear ‘‘S-shaped’’ metallicity-to-colour relationship for old GCs (13 Gyrs), which is driven by horizontal branch morphology at intermediate metallicity ($[\text{Fe}/\text{H}] = -1$ to -0.6). The colour-metallicity relationship plotted in Yoon, Yi & Lee (2006) figure 1 can predict the commonly observed bi-modal colour distribution (for elliptical galaxy GC systems) from a uni-modal metallicity distribution. The detailed models have not been published yet nor have they been tested by other groups. However, they highlight the importance of considerations beyond age and metallicity and also the need to accurately model horizontal branch morphology.

One method suggested by Kissler-Patig (2000) to break the age-metallicity degeneracy for integrated colours is the inclusion of near-IR photometry. Colours such as R-K and I-K are strongly dependent on metallicity, but quite insensitive to age. Therefore a comparison of B-I and I-K colours should be quite effective in breaking the age-metallicity degeneracy. There is some controversy over the effectiveness of this method, mostly relating to the GC system of NGC 4365 and the accuracy of SSP model colours and photometric errors (Puzia *et al.* 2002; Larsen *et al.* 2003; Brodie *et al.* 2005; Larsen, Strader & Brodie 2005; Kundu *et al.* 2005).

1.2.3.4 Extra-galactic Globular Cluster Spectroscopy

For all galaxies’ GC systems studied spectroscopically, a range of metallicities are found. However, due to the relatively small numbers of well constrained GC metallicities for elliptical galaxies, it is not clear if the metallicity distribution is actually bi-modal, as the colour distribution is.

Across many studies based on high S/N spectra and using Lick indices the majority of GCs associated with large elliptical galaxies are generally found to be old with a small fraction of young GCs (see Brodie & Strader 2006). For example, Strader *et al.* (2003, 2004a) selected 10 likely intermediate age candidates around the merger remnant NGC 3610 and found that only two of those GCs had ages consistent with the merger. Large cluster ellipticals such as NGC 1399 (Forbes *et al.* 2001), M87 (Cohen *et al.* 1998) and M49 (Beasley *et al.* 2000, Cohen *et al.* 2003) have predominantly old measured GC ages, with a minor fraction of GCs which may have young or intermediate ages. However, the S/N of the data for many of the GC spectra from these three large cluster ellipticals is low enough to make age determination unreliable.

One atypical elliptical galaxy is NGC 5128. This galaxy shows signs of recent merger activity, including a large dust lane, disturbed morphology and young stars and OB associations in the halo (Israel 1998). Therefore we may expect a large fraction of the GCs to be young. Spectroscopically there is evidence that about 10%

of GCs in this galaxy are younger than 8 Gyrs (Beasley *et al.* 2006 in prep).

We discuss in more detail our spectroscopic results for several individual galaxies GC systems in Chapters 2-4.

1.3 Spectroscopic Measurements of Stellar Population Parameters

One of the intrinsic uncertainties any observation aiming to determine ages and metallicities must overcome is the “age-metallicity degeneracy” (Worthy, 1994). The effects of increasing age or increasing metallicity are very similar; both make photometric colours redder, increase the depth of metal absorption lines and decrease the strength of Balmer absorption lines. Breaking the age-metallicity degeneracy is crucial for the interpretation of spectroscopic results.

For the spectroscopic studies of elliptical galaxy GC systems, measuring the ages of individual GCs is often the primary aim. Accurately measured ages help distinguish between the different formation scenarios described in Section 1.2.2.

Linked to GC age is the metallicity, through both the age-metallicity degeneracy and through the expected monotonic relationship. The metallicity of GCs forming within an isolated system should monotonically increase, due to metal enhancement of the host galaxy’s gas by stellar evolution and supernova ejecta, unless less enhanced gas is accreted. GC metallicity offers a direct link to the host galaxy’s field stars. One complication to be aware of is that metallicity is expressed in several different ways: as either the total metallicity $[Z/H]$ or the iron abundance $[Fe/H]$. If the α -element abundance is a constant value then these total metallicity and iron abundance are offset from each other, however if the α -element abundance varies significantly it is important to be aware which version of metallicity is being measured.

The α -element abundance, usually expressed relative to iron abundance as $[E/Fe]$ (note the modelled $[E/Fe]$ is not strictly $[\alpha/Fe]$; see Thomas, Maraston & Bender 2003), is used to infer the relative contributions of different SN types and masses. This measure of SN contributions is commonly interpreted as a “timescale” indicator for how long a star-burst continued (e.g. Puzia, Kissler-Patig & Goudfrooij 2006). High $[E/Fe]$ values imply rapid star formation from a SN-II enriched interstellar medium. Lower $[E/Fe]$ values indicate that there has been significant contribution from SN Ia, which only occurs more than a Gyr after the initial starburst.

As some of the brightest stars within the GC, horizontal branch stars have a large influence on the observed integrated properties. The relative contribution of those stars towards either end of the horizontal branch is significant for measurement of the integrated colour, age and metallicity. Therefore the morphology of the horizontal branch (HB) affects the measurement of several GC properties (Lee *et al.* 2000; Thomas *et al.* 2003). Blue HB stars are both luminous and hot; therefore, they increase the blue continuum of the spectrum, increase the strength of Balmer indices and decrease the strength of metal lines. These effects mimic those of a younger stellar population.

The strength of the contribution of blue horizontal branch stars scales inversely with metallicity. That means that at low metallicity and old ages the blue hori-

zonal branch stars become major contributors to the GCs luminosity, whereas at metallicities close to solar most GC have almost no blue horizontal branch stars. This metallicity-HB morphology relationship is inferred from Galactic GCs (e.g. Recio-Blanco *et al.* 2006, Thomas *et al.* 2003). It is not clear if the trend is similar for GC systems around elliptical galaxies or if there is an offset in metallicity. It is also not clear how strongly the blue HB contribution varies with age. SSP models include horizontal branch morphologies based on the isochrones from which they are constructed. These isochrones are often based on Galactic GCs and therefore the observed trend of HB morphology with metallicity is built into the SSP models (Thomas *et al.* 2003).

Fainter GCs will begin to suffer from stochastic variations due to the exact mass distribution of the brightest stars. For GCs fainter than $M_V \sim -5$ the contribution of the individual brightest stars becomes important. Fagiolini, Riamondo & Degl’Innocenti (2006) present the results of Monte Carlo simulations of cluster observed properties based on standard IMF inputs and show that for fainter GCs there is significant stochastic variation in the observed colours for an input age, metallicity and luminosity. This means that for faint GCs there is increased uncertainty measuring integrated properties.

1.3.1 Previous Approaches

Several methods have been commonly used to measure GC properties such as age and metallicity from integrated spectra.

Empirical metallicity calibrations such as the method of Brodie & Huchra (1990, hereafter BH90), based on absorption-line features and the principal components analysis (PCA) of 11 absorption-line features of Strader & Brodie (2004, hereafter SB04) are both tied to the Zinn & West (1984) metallicities of Galactic GCs and assume that the GCs have old ages (>10 Gyrs).

Methods involving Lick spectral indices usually rely on the comparison of an age-sensitive index (e.g. $H\gamma$) and a metallicity-sensitive index (e.g. Fe5270) to break the age-metallicity degeneracy (Worthey 1994). Puzia *et al.* (2005) determine the “relative best Age indicator” amongst the Balmer indices and find in order of decreasing age indicating strength $H\gamma_A$, $H\delta_A$, $H\beta$, $H\gamma_F$, $H\delta_F$. However, these methods suffer greatly when either index is contaminated, by cosmic rays, sky-line subtraction or galactic emission. If the contamination effect is not substantial enough to be obvious then a spurious age and metallicity can be measured.

One complicating factor is that GCs predominantly possess non-solar α -element abundance ratios. These non-solar α -element abundances cannot be determined from simple index-index plots and require a more complex approach. It is only recently that α -element abundances have become a topic of major interest in extra-galactic GC studies. Thomas *et al.* (2003) produced the first models to include the effects of non-solar α -element abundances. Previously Trager *et al.* (2000b) described a method for estimating $[Mg/Fe]$ based on the models of Worthey (1994) and the Trippico & Bell (1995) enhancement corrections.

Puzia *et al.* (2005, 2006) use an iterative approach involving diagnostic grids of

Balmer lines and $\langle \text{Fe} \rangle$, Mg_2 and $[\text{MgFe}]'$ ². The weighted mean is taken of age and metallicity, derived from diagnostic plots of $\text{H}\gamma_A$, $\text{H}\beta$ and $\text{H}\delta_A$ vs $[\text{MgFe}]'$. Assuming the measured age, α -enhancement can be derived by constructing an Mg_2 vs $\langle \text{Fe} \rangle$ grid for that age. This value is then used to construct age-metallicity grids of that α -enhancement for each Balmer line vs $[\text{MgFe}]'$. The whole process is iterated until the parameter values converge.

Lilly & Fritze-v. Alvensleben (2006) present a χ^2 minimisation method similar to that of Proctor & Sansom (2002). They compare the measured indices with SSP models and select the point with the lowest χ^2 . They do not explicitly discuss the identification and exclusion of contaminated indices. Their models do not include α -element ratios.

None of these methods offer a comprehensive robust approach to measuring stellar population parameters. Empirical metallicity calibrations only provide a metallicity estimate and require the assumption of an old age. Index-index plots are susceptible to index contamination and can only measure two parameters (e.g. age and metallicity) at once, while the third parameter (e.g. α -element abundance) subtly affects the indices. The Puzia *et al.* approach is an improvement on index-index methods, but does not include all the indices and as an iterative approach does not simultaneously sample the full three dimensional parameter space. This could possibly lead to finding a local, but not global, best fit. The most sophisticated method discussed so far is the Lilly & Fritze-v. Alvensleben (2006) approach. While utilising all the information in all indices, they do not include α -element abundance ratios nor do they explicitly describe a method for detecting and excluding contaminated includes from their fitting process.

1.3.2 Our Approach

We use the multi-index χ^2 minimisation method presented by Proctor & Sansom (2002) to measure age, metallicity and α -element abundance of GCs. We use the same SSP models, from Thomas, Maraston & Korn (2004), for all GCs. These models include the effect of variable α -element abundances on all indices, including the $\text{H}\gamma$ and $\text{H}\delta$ Balmer indices.

The multi-index χ^2 minimisation method was originally applied to study the Lick indices of nearby late- and early- type galaxies (Proctor & Sansom 2002). The basis is that all indices have some sensitivity to age, metallicity and α -element abundance and that this information can be extracted. It is ideally suited to studying GC spectra for several reasons. GCs often have non-solar α -element abundances. A 2D index-index fit cannot measure the ages, metallicities *and* α -element abundances, whereas this multi-index method simultaneously measures all 3 parameters.

We compare the measured Lick indices to all combinations of age, metallicity and α -element abundance ratio in the TMK04 SSPs and obtain a minimum χ^2 fit. This fit is obtained using all the indices measured. Simultaneously a set of χ^2 minimisation fits are found with each of the indices omitted. From this set, we select the fit with the lowest total χ^2 , remove the necessary index and repeat until a stable fit is achieved with no highly aberrant ($> 3\sigma$) indices remaining. Contaminated

² $[\text{MgFe}]' = \sqrt{\text{Mgb} \times (0.72 \times \text{Fe5270} + 0.28 \times \text{Fe5335})}$

indices, such as those affected by cosmic rays, are easily identified during this fitting process, because their value is incompatible with that of the other 15+ indices.

One common difficulty faced by extra-galactic GC spectra is calibration. These calibrations involve both flux calibration and calibration to the Lick system if comparing to SSP models based on the Lick stellar library. Multi-index fitting can identify index calibration offsets, systematics and individually deviant indices which can then be excluded from the fitting process. It is important that we fit all 3 parameters simultaneously, otherwise we risk assuming that indices are poorly calibrated, when in fact they are sensitive to α -elements and they have high or low enhancement. Proctor *et al.* (2004) discuss this for Galactic GC data.

Another issue, which is more specific to extra-galactic GCs than galaxy spectra, is host galaxy and background light subtraction. Often the host galaxy counts are of equal number to that of the GC and any imperfection in background subtraction, often due to the background varying, is a significant error on individual index measurements. Emission fill-in of Balmer lines and Fe5015 is one example. As long as less than 50% of the indices for a given GC are contaminated, we can identify the deviant indices in the χ^2 minimisation fit and exclude them.

The accuracy of the models is a limiting factor for analysing high S/N data. We can identify potential HB morphology irregularities, but these are unquantifiable until HB morphology is modelled as an independent parameter. We can suggest that there are abundance anomalies, such as C and N, but again we cannot quantify these, yet.

1.4 Thesis Layout

In this thesis we set out to test how information can be determined about a galaxy's formation history by studying the spectra of a small sample of GCs. Are the stellar population parameters of the GCs strongly linked with the formation history of the host galaxy, as implied by photometric observations? (see Sections 1.2.3.2 and 1.2.3.3)

We study in detail GCs associated with three galaxies. These galaxies are chosen to represent three common galaxy stereo-types. NGC 1052 is a merger remnant galaxy in a small group with multiple signs of recent star formation. NGC 3379 also resides in a small group, but has no indications of star formation or merger activity in the last 8+ Gyrs. NGC 4649 is a larger cluster elliptical, representing large galaxies in high density environments. We expect the GC systems studied to reflect the characteristics of their host galaxies and to be distinguishable on that basis.

In this thesis we apply the χ^2 fitting method of Proctor & Sansom (2002), as described in Section 1.3.2, to present robust measurements of extra-galactic GC ages, metallicities and α -element abundances. For three separate large elliptical galaxies GC systems we compare these measured ages and metallicities against both empirical metallicity methods and the observed colours (from the SSP predicted colours for that age and metallicity).

This adds another 76 extra-galactic GC spectra to the existing literature samples. While these do not allow us to discriminate between the different formation

scenarios, we highlight some stellar population measurement concerns and suggest some additional constraints.

The multi-index method we use allows us to test for the stability of our “best fit” to the inclusion or exclusion of indices. This allows us to estimate the minimum acceptable S/N and calibration accuracy for indices, because below a certain S/N stable fits are no longer found.

We identify some of the important considerations when measuring stellar population parameters for GCs, such as horizontal branch morphology and trends in α -element abundance ratio.

In Chapter 2 we present Keck/LRIS spectra and Lick Indices of 16 GCs associated with the merger remnant elliptical NGC 1052. We measure ages, metallicities and α -element abundance ratios for the GCs as well as from a long-slit spectrum of the galaxy.

In Chapter 3 we focus on Gemini/GMOS spectra of 22 GCs associated with the Leo group elliptical NGC 3379. Ages, metallicities and α -element abundance ratios for our 22 GCs are measured and compared to other indicators to test their accuracy.

In Chapter 4 we study Gemini/GMOS spectra of 38 GCs around the large Virgo cluster elliptical NGC 4649. Again, the stellar populations of the GCs is the main focus.

Chapter 5 contains suggestions for the directions future work in this area could take both theoretically and observationally.

Chapter 6 is a summary of our results followed by a discussion and conclusion regarding GC stellar population measurements.

Chapter 2

Evolutionary History of the Elliptical Galaxy NGC 1052

This chapter is based upon Pierce et al. 2005, MNRAS, 358, 419. One Section involving Globular Cluster kinematics from the published paper has not been included.

2.1 Introduction

Globular clusters (GCs) are generally considered to be good tracers of a galaxy's star formation history. Bimodal colour distributions are observed in many GC systems, suggesting that galaxies undergo multiple epochs of star and GC formation (Harris 2001). The exact nature of how these multiple star formation events occur is crucial to understanding galaxy formation.

Ashman & Zepf (1992) describe the production of metal-rich GCs during the merger of two gas-rich disc galaxies. This scenario results in similar ages for the metal-rich GCs and the merger event. In this model the blue, metal-poor GCs which belonged to the progenitor galaxies are universally old (~ 13 Gyr). Forbes, Brodie & Grillmair (1997) propose a multi-phase collapse, during which metal-poor GCs form early during the pre-galaxy collapse phase and, at a later time, metal-rich GCs form out of more enriched gas at a similar time to the galaxy field stars. This model implies a metal-rich population that is a few Gyr younger than the metal-poor population. The exact age difference may depend on mass and environment (Beasley *et al.* 2002). On the other hand, Cote, Marzke & West (1998) suggest the bimodality of GC colours in large ellipticals is due to the gradual accretion of metal-poor GCs from dwarfs, with metal-rich GCs being indigenous to the elliptical. In this picture, the metallicity of the metal-rich population is a function of the galaxy's luminosity and both sub-populations should be old.

These physical processes may all occur to some extent. To distinguish between the relative contributions of each process, we need examples of elliptical galaxies covering a range of masses and in different environments. Given that the above GC formation scenarios have different expectations concerning the ages of the metal-poor and metal-rich sub-populations, determining the age of individual GCs is a crucial step in testing these models.

There are several methods to measure GC properties such as age and metallicity from integrated spectra. Examples include the method of Brodie & Huchra (1990; hereafter BH90), who present an empirical metallicity measure based on absorption line features. Another method is that of Strader & Brodie (2004; hereafter SB04), based on a principal components analysis (PCA) of 11 absorption line features. Methods involving spectral indices, predominantly the Lick system, and their comparison to simple stellar population (SSP) models can break the age-metallicity degeneracy (Worthey 1994). These methods usually rely on an age sensitive index (e.g., $H\beta$) and a metallicity sensitive index (e.g., Mgb) to break the degeneracy. However, these methods suffer difficulties when individual indices are contaminated, due to cosmic rays, skyline subtraction or galactic emission. Another complication is non-solar α -abundance ratios, which are difficult to determine from index-index plots and can affect the higher order Balmer indices (Thomas, Maraston & Korn 2004). Recently, Proctor & Sansom (2002; hereafter PS02) have used a multi-index χ^2 -minimisation method to obtain ages, metallicities and abundance ratios for the stellar populations of late and early-type galaxies. Another advantage of using many indices is that it maximises the information used to break the age-metallicity degeneracy. Here we extend this method to extragalactic GCs for the first time (see Proctor, Forbes & Beasley 2004 for an application to Galactic GCs).

Hot luminous blue horizontal branch (BHB) stars have a significant effect on the measurement of several indices (most notably the Balmer indices, see Lee, Yoon & Lee 2000). Studies of Galactic GCs show that those with similar ages and metallicities can have very different spectral contributions from their HB stars depending on whether the HB stars are hot (blue) or cool (red). The way the HB is modelled has a significant impact on a SSP model (Maraston, Greggio & Thomas 2001a). A colour-magnitude diagram is probably the best way to deduce HB morphology in a given GC, but such diagrams are limited to GCs in the very nearest galaxies. Thus information on HBs in extragalactic GCs must generally come from integrated spectra. Old metal-rich GCs with BHBs (e.g., NGC 6388 and NGC 6441; Rich *et al.* 1997) can falsely appear to be intermediate-age clusters due to this strengthening of the Balmer lines (Schiavon *et al.* 2004); therefore the ability to deduce HB morphology from integrated spectra is important. Schiavon *et al.* (2004) have recently introduced a method to detect anomalous HBs in GC spectra by differential comparisons of $H\delta$, $H\gamma$, and $H\beta$ line strengths.

There is evidence for a significant number of proto-GCs in galaxies which are currently merging (e.g., The Antennae; Whitmore & Schweizer 1995) and very recent (<500 Myr) mergers such as NGC 7252 (Maraston *et al.* 2001b; Schweizer & Seitzer 1998; Miller *et al.* 1997) and NGC 3921 (Schweizer, Seitzer & Brodie 2004; Schweizer *et al.* 1996). The outstanding questions are whether a substantial fraction of the proto-GC sub-population formed in these mergers survives, and hence whether it can account for the GC systems of ellipticals (see Forbes, Brodie & Grillmair 1997).

An important link between ongoing mergers and “old” elliptical galaxies is the intermediate aged (2-5 Gyr) merger remnants. Previous GC spectroscopic studies of merger remnant galaxies such as NGC 1316 (Goudfrooij *et al.* 2001) and NGC 3610 (Strader *et al.* 2003; Strader, Brodie & Forbes 2004a) have confirmed a small number of GCs with ages matching the time since the merger event (~ 3 Gyr and ~ 2 Gyr respectively). However, the total number of intermediate-age GCs in these

galaxies is currently poorly constrained spectroscopically.

In this work we examine the GC system of NGC 1052, which is an excellent candidate for an elliptical that has undergone a minor merger event in the last few Gyrs. NGC 1052 is an E4 galaxy, located in a small group at a distance of 18 Mpc (Forbes, Georgakakis & Brodie 2001b). Aside from containing an active nucleus, NGC 1052 displays several indications of a past merger or significant accretion event. The gas angular momentum is higher than that of the stellar component, with the gas and stars having different rotation axes (van Gorkom *et al.* 1986, Plana & Boulesteix 1996). NGC 1052 also reveals HI ‘tidal tails’ (van Gorkom *et al.* 1986), infalling HI gas onto the active nucleus (van Gorkom *et al.* 1989) and dust lanes (Forbes, Sparks & Macchetto 1990): all signs of an accretion or merger. van Gorkom *et al.* (1986) suggest that the HI observations could be explained by the accretion of a gas-rich dwarf, or other minor interaction, about 1 Gyr ago.

Despite the evidence for a recent accretion event, NGC 1052 shows almost no optical disturbance (it has a low fine structure value of $\Sigma = 1.78$, Schweizer & Seitzer 1992) and has a fundamental plane residual of +0.07 (Prugniel & Simien 1996) which is consistent with a normal galaxy on the fundamental plane (Forbes, Ponman & Brown 1998).

We can further probe the evolutionary history of NGC 1052 by measuring the ages and metallicities of individual GCs in the galaxy. The imaging of Forbes *et al.* (2001b) revealed a bimodal GC system as is typical for elliptical galaxies. The two sub-populations had a colour difference of $\Delta B-I=0.4\pm 0.1$. Using Worthey (1994) models, under the assumption that the blue GC sub-population is 15 Gyr old and metal-poor with $[Fe/H]=-1.5$, Forbes *et al.* (2001b) showed that any newly-formed red GCs (assuming ages of ≤ 2.5 Gyr) must have super-solar metallicities to fully account for the red sub-population.

In Section 2.2 we will present our observations and data reduction methods. Measured indices and our analysis of these Lick indices are given in Section 2.3. Using the method of PS02, metallicities, ages and abundance ratios are given in Section 2.4. Spectra of NGC 1052 itself are given in Section 2.5. Finally we discuss the implications of our results in Section 2.6 and present conclusions in Section 2.7.

2.2 Observations and data reduction

Spectra of GC candidates around NGC 1052 were obtained with the Low Resolution Imaging Spectrometer (LRIS; Oke *et al.* 1995) on the Keck I telescope. Candidate selection, based on the Keck imaging data of Forbes *et al.* (2001b), was designed to cover a wide range of potential GC colours (i.e. $1.2 < B-I < 2.5$, $0.6 < V-I < 1.7$). The properties of our candidates can be found in Table 2.1. Observations were obtained in 2003 January 25-27 with an integration time of $16 \times 1800s = 8$ hours for the slit-mask. However, the signal-to-noise ratios of the combined spectra were improved by excluding the exposures made at the highest airmass. These suffered from signal-to-noise degradation, especially at bluer wavelengths. Seeing ranged between $0.65''$ and $0.75''$ over the three nights. A 600 lines per mm grating blazed at 4000 \AA was used for the blue side, resulting in an approximate wavelength range of $3300 - 5900 \text{ \AA}$ and a FWHM spectral resolution of $\sim 3.3 \text{ \AA}$.

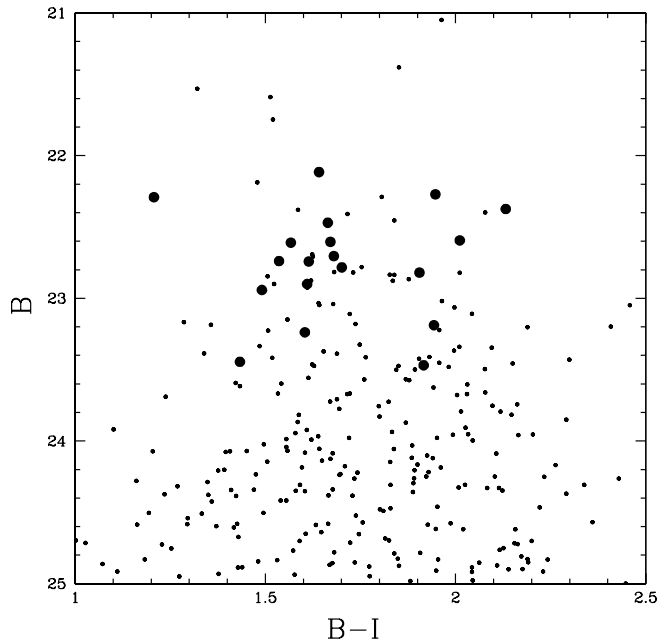


Figure 2.1: Candidate globular cluster colour magnitude distribution. GCs for which spectra were obtained are represented by large symbols. The small symbols are the full sample from the imaging study of Forbes *et al.* (2001b). Spectra were obtained for luminous GC candidates from both the blue and red sub-populations.

Table 2.1 presents observational data for the objects for which we obtained Keck spectra. Figure 2.1, a B-I colour magnitude diagram, shows that we have obtained spectra from both the blue and red sub-populations of GC candidates. We have also generally sampled the most luminous GCs in NGC 1052. If any young (\sim few Gyrs old) GCs exist then they will tend to be brighter than the old population. Plotted in Figure 2.2 are the spatial positions of the confirmed GCs.

Data reduction was carried out using standard IRAF¹ methods. Tracing of spectra was done using the two exposures from each night with the lowest airmass (both < 1.2). These were combined to increase the signal for aperture tracing. They were then used as the reference apertures for their respective nights and spectra were extracted from individual exposures.

Comparison lamp spectra of Hg, Ar, Ne, Cd and Zn were used for wavelength calibration (mostly based on 8 Hg lines). Zero-point corrections of up to 3 \AA were performed on the science spectra using the bright OI skyline at 5577.34 \AA . Different methods of spectral combining were tested. Average combining was used with median scaled pixel rejection, due to the significant difference in flux levels between high and low airmass observations. Sigma clipping was used to reject cosmic rays and reduce the effect of strong skylines. The resulting spectra have $S/N = 18\text{--}45 \text{ \AA}^{-1}$ measured at 5000 \AA .

Flux calibrations were provided by the flux standards Feige 34 and G191B2B.

¹IRAF is distributed by the National Optical Astronomy Observatories, which are operated by the Association of Universities for Research in Astronomy, Inc., under cooperative agreement with the National Science Foundation

Table 2.1: Globular Cluster candidates around NGC 1052. GC ID, R.A., Dec., V magnitude, B-I and V-I colours are from Forbes *et al.* (2001b). Galactocentric radii are calculated from GC positions assuming the distance to NGC 1052 of 18 Mpc. Heliocentric velocities are from this work.

ID GC	R.A. (J2000)	Dec. (J2000)	V (mag)	B-I (mag)	V-I (mag)	Radius (kpc)	V_{helio} (km/s)
GC7	02:41:00.0	-8:18:44.0	21.32	1.64	0.84	19.2	1659±74
GC9	02:41:05.7	-8:14:53.5	21.41	1.95	1.08	2.4	1649±105
GC11	02:41:00.2	-8:17:32.7	21.68	1.21	0.60	star
GC12	02:41:06.4	-8:12:33.9	21.40	2.13	1.16	14.2	1610±123
GC17	02:41:02.8	-8:15:18.6	21.72	1.66	0.92	1.9	1498±101
GC18	02:41:03.8	-8:16:04.9	21.71	2.01	1.13	4.3	1583±96
GC19	02:41:02.0	-8:15:50.1	21.85	1.67	0.92	4.7	1640±92
GC22	02:41:07.5	-8:13:13.1	21.87	1.68	0.85	star
GC28	02:41:02.6	-8:15:42.6	22.03	1.54	0.83	3.8	1414±86
GC29	02:41:01.0	-8:16:00.0	22.02	1.70	0.94	6.3	1273±78
GC30	02:41:04.7	-8:14:24.0	21.95	1.91	1.04	4.7	1537±122
GC37	02:41:01.3	-8:16:21.7	22.05	1.61	0.92	6.4	1443±76
GC38	02:41:03.9	-8:13:16.2	22.15	1.61	0.86	10.6	1295±122
GC45	02:41:03.0	-8:15:05.5	22.24	1.49	0.79	2.8	1765±74
GC47	02:41:02.8	-8:14:53.5	21.90	1.57	0.86	3.5	1781±83
GC55	02:41:00.8	-8:16:32.8	22.36	1.94	1.12	galaxy
GC60	02:41:07.2	-8:13:45.5	22.45	1.60	0.82	8.5	1415±122
GC74	02:41:05.7	-8:12:52.3	22.74	1.43	0.73	12.6	1675±93
GC78	02:41:01.6	-8:16:49.0	22.59	1.92	1.03	8.9	1619±92

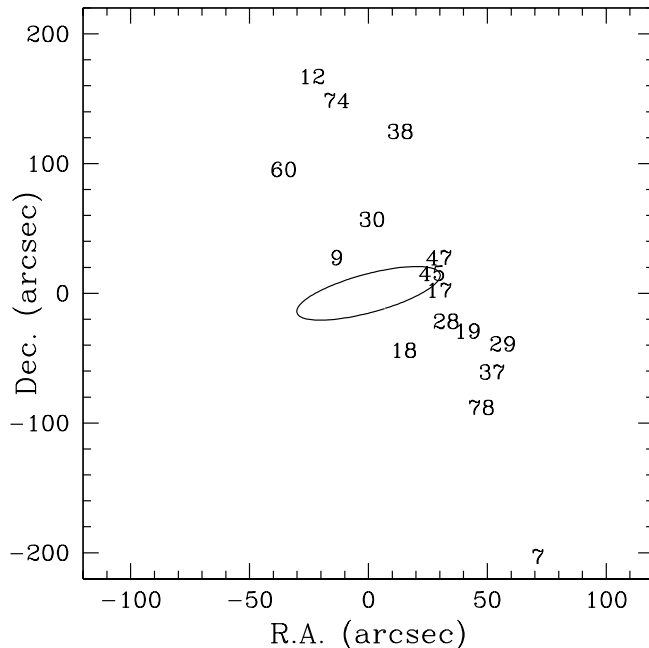


Figure 2.2: Spatial distribution of the confirmed GCs. The numbers correspond to the GCs listed in Table 2.1. The E4 ellipse represents the effective radius of NGC 1052 at $r_e \sim 34''$. The orientation is North up and East left. Note the x and y scales are different.

These were taken on the same run by long-slit and therefore have slightly different wavelength coverage to the multi-slit spectra. The velocities of GC candidates were determined by cross-correlation against high signal-to-noise M31 GC templates, i.e. 225–280 and 158–213 (see Beasley *et al.* 2004b). The typical variation of V_{helio} with respect to the different templates is ± 20 km/s.

Of the 19 spectra obtained, one is a background galaxy with $z=0.204$, two are Galactic stars and the remaining 16 have velocities consistent with being GCs associated with NGC 1052. Thus, we have a success rate of 16 out of 19. Figure 2.3 shows the confirmed GC spectra smoothed to the Lick resolution. Each spectrum has been normalized, then offset by a flux interval of one, to make visual comparison easier. These spectra show a wide variation in the ratio of the CaII H and K features around 3950 \AA . Other prominent lines are the G band at 4300 \AA , $H\beta$ (4863 \AA), Mg features (5200 \AA) and Fe lines around 5300 \AA .

2.3 GC Spectral Line Indices

2.3.1 Measurement of Indices

We measured Lick indices (Trager *et al.* 1998; Worthey & Ottaviani 1997), the Rose (1984) CaII index, and BH90 indices from our flux-calibrated spectra after convolving the spectra with a wavelength-dependent Gaussian kernel to broaden to the Lick resolution. We then applied small offsets to the Lick indices based on measurements of several Lick standard stars (see Beasley *et al.* 2004). Uncertainties

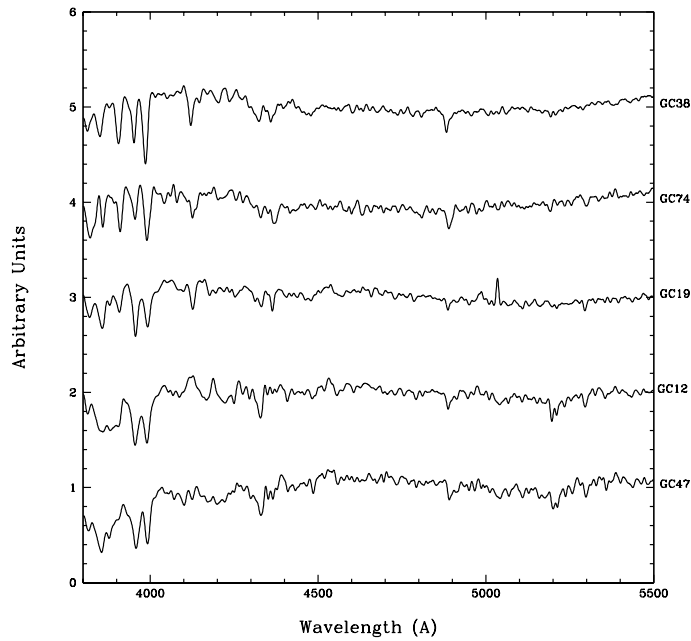


Figure 2.3: Selected Keck spectra of NGC 1052 GCs normalized and offset by 1 unit. These spectra have not been de-redshifted (which introduces a shift of ~ 25 Å). The spectra show the strong CaII H and K features around 3950 Å, the Gband at 4300 Å, H β (4863 Å), Mg feature (5200 Å), Fe lines around 5300 Å and other absorption lines. The emission line at ~ 5035 Å in GC19 is [OIII]5007 Å from the galaxy which did not fully subtract. The spectra indicate a range of metallicities and CaII ratios.

Table 2.2: Globular Cluster indices $\lambda < 4500 \text{ \AA}$. Central index values (first line) and errors (second line). Indices in brackets are removed during the fitting process.

ID GC	CaII ratio	H δ_A (\AA)	H δ_F (\AA)	CN ₁ (mag)	CN ₂ (mag)	Ca4227 (\AA)	G band (\AA)	H γ_A (\AA)	H γ_F (\AA)	Fe4383 (\AA)	Ca4455 (\AA)
GC7	1.01	2.07	2.60	(-0.039)	-0.038	(0.08)	(2.70)	-0.06	0.83	1.08	0.73
	0.07	0.33	0.21	0.010	0.012	0.19	0.34	0.35	0.22	0.52	0.27
GC9	1.41	0.06	0.70	(0.061)	(0.100)	1.19	(3.28)	-2.81	-0.15	3.72	1.00
	0.17	0.33	0.23	0.009	0.011	0.16	0.29	0.34	0.21	0.44	0.23
GC12	1.05	(0.86)	(4.07)	(-3.90)	(-1.04)	3.20	1.44
	0.10	0.17	0.30	0.35	0.22	0.47	0.24
GC17	0.94	2.81	2.20	(-0.057)	-0.050	(-0.33)	2.55	0.44	1.16	-1.16	1.24
	0.08	0.30	0.21	0.009	0.011	0.19	0.32	0.34	0.21	0.54	0.27
GC18	1.05	-2.05	-0.07	(0.010)	0.017	1.09	4.08	(-2.16)	(-0.03)	3.37	1.34
	0.13	0.41	0.27	0.011	0.013	0.21	0.36	0.42	0.26	0.57	0.28
GC19	1.17	2.79	(3.30)	(-0.024)	(0.020)	0.46	2.35	-0.36	1.30	1.40	0.21
	0.10	0.35	0.22	0.010	0.012	0.21	0.36	0.39	0.24	0.58	0.31
GC28	1.20	0.99	1.81	(0.029)	(0.049)	0.63	3.98	-3.01	-0.11	2.31	1.00
	0.15	0.39	0.25	0.011	0.013	0.21	0.38	0.42	0.26	0.62	0.31
GC29	0.96	1.83	(3.17)	-0.061	-0.022	(-0.22)	(1.26)	(-0.26)	1.21	2.66	1.12
	0.10	0.37	0.23	0.011	0.013	0.23	0.38	0.40	0.24	0.58	0.31
GC30	0.71	6.02	-4.99	-0.35	4.43	1.09
	0.21	0.34	0.44	0.26	0.55	0.30
GC37	0.94	2.23	1.89	(-0.071)	-0.056	0.63	1.99	-0.01	0.97	1.13	1.07
	0.11	0.39	0.27	0.011	0.014	0.21	0.41	0.41	0.25	0.63	0.32
GC38	0.78	3.68	3.01	(-0.089)	(-0.048)	-0.26	(1.45)	1.42	(1.40)	-1.13	0.50
	0.07	0.34	0.23	0.010	0.012	0.22	0.38	0.38	0.24	0.62	0.32
GC45	1.14	(-0.03)	(2.58)	3.02	2.72	-0.33	0.64
	0.12	0.29	0.48	0.47	0.29	0.68	0.35
GC47	1.13	-2.53	-0.11	(0.102)	0.104	(-0.39)	(3.59)	(-2.23)	(0.69)	4.48	1.48
	0.13	0.40	0.26	0.010	0.013	0.20	0.36	0.39	0.23	0.52	0.28
GC60	0.84	(-1.02)	(3.79)	0.49	1.81	0.27	(-1.58)
	0.10	0.27	0.41	0.44	0.27	0.71	0.38
GC74	0.81	3.98	(2.40)	-0.107	-0.083	0.36	0.27	2.55	1.96	1.94	0.61
	0.09	0.41	0.29	0.013	0.015	0.25	0.48	0.46	0.28	0.73	0.39
GC78	1.09	-0.03	1.21	-0.009	0.011	0.67	(-0.72)	(0.84)	(1.46)	2.31	0.13
	0.15	0.50	0.33	0.014	0.017	0.27	0.53	0.51	0.31	0.77	0.42

in the Lick indices were derived from the photon noise in the unfluxed spectra. Errors on the H β index range from ± 0.21 – 0.36 \AA . The Lick indices and Rose CaII index are presented for the confirmed GCs in Tables 2.2 and 2.3. We note that the 5202 \AA skyline falls in the central band for Mg₂ and Mgb for our redshifted spectra, but in the Mgb side band for the Lick standard stars, raising some doubt over the accuracy of the offsets applied to the Mgb index and possible systematic errors in Mg₂.

Missing values in Tables 2.2 and 2.3 indicate problematic indices due to various factors. Ionised gas emission from NGC 1052 has contaminated the H β index in GCs 9 and 19. This can be seen clearly by examining the [OIII] emission feature at 5007 \AA for GC19 in Figure 2.3. Difficulty subtracting the 5202 \AA skyline from the Mg indices (especially Mgb) affects GCs 45, 60 and 74. The presence of some weak light from internal reflections within the LRIS instrument from the guide stars affects wavelengths below 4200 \AA of GCs 12, 30, 45 and 60. Indices in parentheses are clipped from our fitting process due to their large deviance from the best fit age, metallicity and abundance ratio (see Section 2.3.3).

We have measured the BH90 indices, and using the method outlined in their paper, derived empirical metallicities. These values are obtained from an unweighted average of 6 metal-sensitive indices: CNB, G band, Fe52, MgH, Mg₂ and Δ (a

Table 2.3: Globular Cluster indices $\lambda > 4500 \text{ \AA}$. Central index values (first line) and errors (second line). Indices in brackets are removed during the fitting process.

ID	Fe4531	C4668	H β	Fe5015	Mg ₁	Mg ₂	Mgb	Fe5270	Fe5335	Fe5406
GC	(\AA)	(\AA)	(\AA)	(\AA)	(mag)	(mag)	(\AA)	(\AA)	(\AA)	(\AA)
GC7	(2.84)	1.34	2.50	3.10	(0.012)	(0.074)	(0.98)	1.46	1.46	0.94
	0.42	0.65	0.24	0.53	0.005	0.006	0.25	0.27	0.31	0.23
GC9	2.74	1.19	3.33	0.062	(0.182)	2.80	2.14	(0.76)	1.26
	0.35	0.54	0.45	0.004	0.005	0.21	0.23	0.26	0.19
GC12	3.30	3.15	1.76	4.93	0.085	(0.235)	3.56	2.02	1.97	1.05
	0.36	0.57	0.22	0.47	0.005	0.006	0.22	0.24	0.27	0.20
GC17	2.61	(-2.46)	2.34	(0.31)	(0.043)	0.089	0.91	0.42	(-0.55)	0.62
	0.41	0.67	0.25	0.56	0.006	0.006	0.27	0.30	0.34	0.24
GC18	2.61	2.62	(2.34)	3.78	0.087	(0.257)	3.32	(2.87)	1.27	0.64
	0.44	0.66	0.25	0.55	0.006	0.006	0.25	0.28	0.31	0.23
GC19	2.23	0.72	1.53	(0.058)	0.072	1.10	1.31	0.18	0.47
	0.46	0.72	0.62	0.006	0.007	0.29	0.32	0.37	0.26
GC28	2.25	(2.68)	2.17	(2.42)	0.062	(0.125)	1.93	2.55	(0.48)	1.22
	0.48	0.74	0.28	0.64	0.006	0.007	0.30	0.33	0.38	0.27
GC29	1.97	(2.35)	(2.81)	2.67	0.073	0.134	2.03	1.11	2.16	0.78
	0.48	0.74	0.28	0.64	0.007	0.008	0.30	0.34	0.39	0.28
GC30	2.56	2.75	2.40	3.94	0.090	0.197	2.60	1.78	(0.62)	0.68
	0.45	0.70	0.27	0.59	0.006	0.007	0.28	0.31	0.36	0.26
GC37	1.49	0.32	2.03	2.61	(0.066)	0.121	1.24	(1.97)	1.16	0.95
	0.50	0.77	0.29	0.64	0.006	0.007	0.30	0.33	0.37	0.27
GC38	1.07	(1.58)	2.95	(2.61)	0.006	(0.091)	1.03	1.19	-0.63	0.49
	0.50	0.77	0.29	0.66	0.007	0.008	0.32	0.36	0.43	0.30
GC45	1.38	(-2.02)	1.97	(5.98)	(0.104)	(0.144)	1.08	(2.91)	0.01
	0.58	0.88	0.35	0.75	0.008	0.009	0.40	0.45	0.32
GC47	(1.62)	(0.07)	1.26	5.92	0.114	0.239	3.46	2.92	1.91	1.38
	0.43	0.65	0.26	0.55	0.006	0.007	0.25	0.28	0.32	0.23
GC60	0.30	(2.68)	(2.36)	1.92	(0.040)	0.059	(2.07)	1.10	(1.09)
	0.57	0.83	0.31	0.71	0.007	0.008	0.36	0.41	0.29
GC74	-0.62	0.24	3.64	-0.67	0.034	0.050	1.09	0.01	0.10
	0.64	0.96	0.34	0.85	0.008	0.010	0.44	0.51	0.37
GC78	2.02	1.19	2.30	3.19	0.045	0.144	1.78	2.75	1.91	1.27
	0.63	0.96	0.36	0.79	0.008	0.009	0.38	0.40	0.45	0.33

measure of the 4000 Å break). The GCs affected by internal reflections do not have CNB or Δ included in their BH metallicity estimate. Similarly, GCs with poor 5202 Å skyline subtraction do not have MgH or Mg₂ included. The GCs 45 and 60 are affected by both internal reflections and poor sky subtraction so their BH90 metallicities are based only on the Gband and Fe52. The final BH90 metallicity estimate is presented in Table 2.4. We also include in Table 2.4 the PCA metallicities derived using the method of SB04. PCA metallicity errors include only propagated errors in index measurement, not possible systematic errors in the metallicity relation itself (see SB04 for details).

2.3.2 Blue Horizontal Branches

Before estimating the ages and metallicities of the GCs from integrated spectra it is necessary to consider the effect of the horizontal branch morphology on the indices. Hot, luminous stars on the blue section of the horizontal branch of a GC can make a significant contribution to its spectrum (e.g., Lee, Yoon & Lee 2000). The effects of BHB stars are to both increase the intrinsic strength of the Balmer absorption lines and raise the blue continuum level, which in turn slightly increases the strength of all indices in the blue. This means that if the BHB of a GC is stronger than modelled, younger ages and higher metallicities (due to the age-metallicity degeneracy) are inferred. Current SSP models do not cover the full range of observed BHB morphology. For example, Bruzual & Charlot (2003) SSPs incorporate the effect of a blue HB population for metal-poor GCs. Thomas, Maraston & Bender (2003; hereafter TMB03) allow a choice of a blue horizontal branch (BHB) or red horizontal branch (RHB) for old metal-poor populations, although this only applies to the Balmer indices. Thomas, Maraston & Korn (2004; hereafter TMK04) include BHB morphology for the old, metal-poor regime changing to RHB morphology in the metal-rich regime. We will show that anomalously blue HBs are likely present in several of our GCs.

One indicator for the presence of BHB stars in old populations is the Rose (1984) CaII index (Trippico 1989). The CaII index is defined as the ratio of the central intensity of CaII H + H ϵ at 3968 Å divided by the central intensity of CaII K at 3933 Å. The BHB stars greatly increase the absorption of H ϵ and therefore lower the value of this ratio (young GCs might be expected to show a similar behaviour). This effect, known as the “Ca Inversion”, can be clearly seen in GCs such as GC74 and GC38 of our sample (see Figure 2.3), which have CaII index values of 0.81 and 0.78 respectively. Our CaII indices are presented in Table 2.2 (we were unable to measure the CaII index for GC30). Although reflections may effect the measurement of the CaII index in some GCs, the lines are sufficiently strong so that the effect is minor. The CaII indices are plotted in Figure 2.4 against BH90 metallicities. This figure shows that, as expected, GCs with BHBs tend to be metal-poor.

Problems occur with fitting the indices to SSP models when the observed GC has a BHB contribution significantly greater than is modelled or when BHBs are present in metal-rich GCs (i.e. [Fe/H] > -1.0). Another difficulty arises for the case of metal-poor GCs with RHBs. Only the TMB03 SSP models cover this situation.

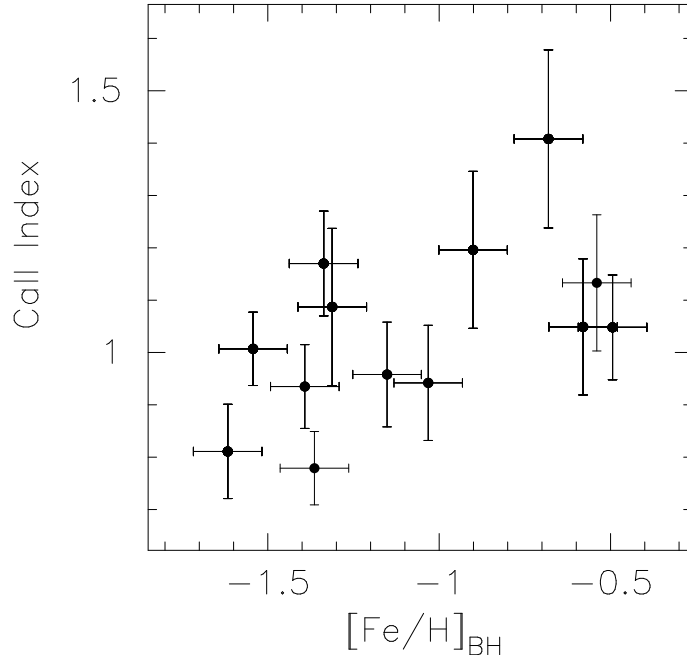


Figure 2.4: The CaII index against BH90 metallicity. There is a trend for low CaII values (indicating the presence of a blue horizontal branch) to be found in metal-poor globular clusters. The $[\text{Fe}/\text{H}]_{\text{BH}}$ errors are indicative only. GCs 45 and 60 are not plotted because their BH90 metallicities are based on only two indices.

2.3.3 Fitting Indices to Simple Stellar Population Models

Ages and metallicities are derived by comparing the measured indices with SSP models. The choice of which SSP model to use is not obvious since all the models have different advantages and limitations. We decided to use the recent models of TMK04, who modelled the affect of abundance ratios on the $\text{H}\gamma$ and $\text{H}\delta$ Balmer lines for the first time. These models only differ significantly from TMB03 at high metallicity (i.e. $[\text{Fe}/\text{H}] > -0.35$). We have also examined Vazdekis (1999), Bruzual & Charlot (2003) and TMB03 SSP models, and find qualitatively similar results for the derived ages, metallicities and abundance ratios ($[\text{E}/\text{Fe}]$). For a comparison of SSP models see Proctor *et al.* (2004).

To derive accurate measures of GC parameters, particularly in view of the problematic indices discussed in Section 2.3.1, we need to include as many reliable indices as possible in the fitting process. Here, we use all uncontaminated indices in a multi-dimensional fitting procedure (see PS02), using the SSP models of TMK04, which include α -enhancement. A χ^2 -minimisation fit is made to the SSP grid points, including an interpolation along all three parameter axes.

We reject outliers by iteratively excluding the index that has the greatest contribution to the overall χ^2 . This decision is based not only on the individual index's χ^2 value, but also on the change of the new fit obtained by excluding it. We also require the final fit to be stable to the further exclusion of indices (those that do not end up stable are GCs 45, 47 and 78). To achieve this it was often necessary to search for specific indices that destabilise the fit.

Indices that are excluded on this basis are in parentheses in Tables 2.2 and

Table 2.4: Globular Cluster derived parameters. Age, $[\text{Fe}/\text{H}]_{SSP}$, $[\text{E}/\text{Fe}]$, $[\text{Z}/\text{H}]$, $[\text{Fe}/\text{H}]_{BH}$ and $[\text{Fe}/\text{H}]_{PCA}$ for the 16 GCs. Errors given are 1σ statistical errors, the PCA errors only include index errors and thus may be underestimates. Values in brackets indicate unreliable BH90 metallicity estimates.

ID GC	Age (Gyr)	$[\text{Fe}/\text{H}]_{SSP}$ (dex)	$[\text{E}/\text{Fe}]$ (dex)	$[\text{Z}/\text{H}]$ (dex)	$[\text{Fe}/\text{H}]_{BH}$ (dex)	$[\text{Fe}/\text{H}]_{PCA}$ (dex)
GC7	15.0±5.4	-1.27±0.18	0.34±0.16	-0.95±0.15	-1.54	-1.32±0.08
GC9	13.3±3.5	-0.74±0.13	0.15±0.10	-0.60±0.11	-0.68	-0.38±0.07
GC12	12.6±4.2	-0.63±0.12	0.38±0.09	-0.28±0.08	-0.49	-0.21±0.07
GC17	11.9±2.0	-1.58±0.23	0.32±0.22	-1.28±0.07	-1.39	-1.87±0.08
GC18	15.0±3.8	-0.65±0.11	0.34±0.08	-0.33±0.08	-0.58	-0.33±0.08
GC19	10.6±1.8	-1.38±0.22	0.06±0.22	-1.33±0.08	-1.34	-1.16±0.09
GC28	15.0±6.6	-0.81±0.21	0.12±0.13	-0.70±0.18	-0.90	-0.81±0.09
GC29	15.0±7.3	-1.15±0.23	0.27±0.13	-0.90±0.17	-1.15	-1.22±0.09
GC30	15.0±3.1	-0.63±0.11	0.30±0.07	-0.35±0.07	-0.29	-0.53±0.09
GC37	12.6±2.9	-1.42±0.19	0.34±0.17	-1.10±0.09	-1.03	-1.10±0.09
GC38	8.9±2.0	-2.05±0.17	0.50±0.07	-1.58±0.16	-1.36	-1.91±0.10
GC45	15.0±7.1	-2.38±0.46	0.80±0.37	-1.63±0.40	(-1.44)	-0.95±0.11
GC47	15.0±3.8	-0.24±0.12	0.15±0.06	-0.10±0.09	-0.54	-0.37±0.08
GC60	10.6±2.1	-2.27±0.24	0.50±0.19	-1.80±0.16	(-0.79)	-1.79±0.10
GC74	13.3±4.3	-2.08±0.42	0.30±0.41	-1.80±0.18	-1.62	-1.84±0.11
GC78	10.6±4.1	-0.70±0.21	0.03±0.14	-0.68±0.14	-1.31	-0.85±0.11

2.3. On average, after all the exclusions, approximately 2/3 of the indices are used in the final fit. A major advantage of this method is that we are not reliant on Balmer indices (which can be contaminated by galaxy emission or strongly affected by BHBs). The errors given for the final derived parameters are statistical 1σ confidence intervals calculated by a Monte Carlo style method with 1000 realisations of the best-fit SSP.

2.4 Derived GC Ages, Metallicities and Alpha Abundances

The results of our fitting procedure are given in Table 2.4. We also present the metallicity estimates by the methods of BH90 and SB04. For GCs 45, 47 and 78, the SSP-derived parameters should be regarded with some caution as the final values are less reliable than those for the rest of the sample.

2.4.1 Age

The derived ages for our sample are given in Table 2.4. All GCs have ages of greater than 10 Gyr; the only exception is GC38, with an inferred age of 8.9 Gyr. Our previous discussion of the effects of BHBs on age estimation in Section 2.3.2 leads us to suggest that GC38, with the strongest BHB in our sample, is actually older than its inferred age. Assuming that the BHB in GC38 is stronger than modelled,

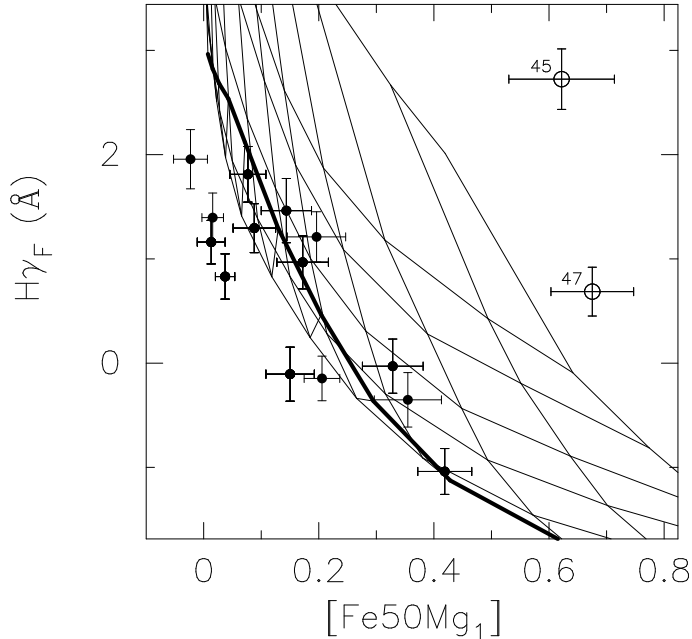


Figure 2.5: Index-index plot of $H\gamma_F$ vs $[Fe50Mg_1]$. Open circles indicate GCs for which one or more of the plotted indices are significantly affected by emission features in the index side-bands (i.e. GCs 45 and 47). Filled circles indicate GCs for which the three indices give fits similar to the full multi-index solution. The TMK04 grid lines shown are for $[E/Fe]=+0.3$ with metallicity in 0.25 dex steps from -2.25 to +0.5 (left to right) and ages of 1,2,3,5,8,12 and 15 Gyr (top to bottom), the heavier line is 15 Gyr. The GCs with reliable indices are consistent with old ages and a range of metallicities. Note that the ages used in this work are not derived from this plot.

then the true age and metallicity of this GC will be older and more metal-poor than given (although the BHB almost exclusively affects age-sensitive indices, age and metallicity are degenerate parameters in the SSP fitting process).

An index-index plot is presented in Figure 2.5 of $H\gamma_F$ vs $[Fe50Mg_1]$, where $[Fe50Mg_1] = Fe5015 \times Mg_1$. We have chosen this combination of Balmer and metal-sensitive lines as these indices appear to be the most accurate in our GC sample. The plot indicates that the GCs are consistent with being very old and covering a range of metallicity typical for GC systems. The GCs for which one of these two indices are not reliable, and hence not used in the best-fit solution, are also shown. These are GCs 45 and 47, for which $Fe5015$ and $H\gamma_F$ are affected by emission features in the index side-bands. These GCs have the most galactic background light due to their spatial positions (see Figure 2.2).

Figure 2.6 shows an age-metallicity plot for the GCs with values from Table 2.4. The GCs all have old ages for a large range in total metallicity ($[Z/H]$). The BHB GC38 has an arrow on it pointing in the direction corresponding to the age-metallicity 3:2 degeneracy (Worthey 1994).

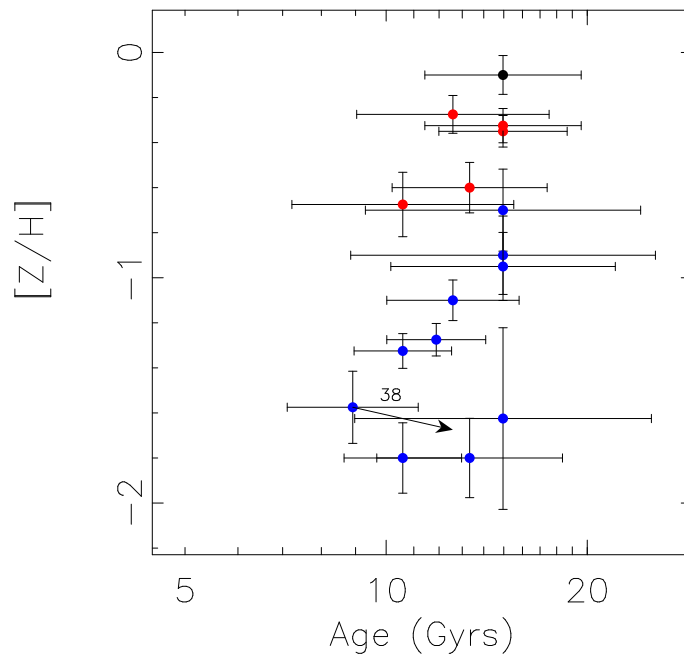


Figure 2.6: Age-metallicity distribution. The GCs are consistent with a coeval age of ~ 13 Gyr, and show a range of metallicities of ~ 2 dex. The arrow on GC38 indicates the direction it would shift towards assuming it is older than the SSP age indicates (due to the presence of a BHB artificially making it appear younger). In colour versions of this plot, the GCs are colour-coded according to their observed colour. The most metal-rich GC has an anomalously blue colour, otherwise the metal-poor GCs have blue colours and the metal-rich GCs are red.

2.4.2 Metallicity

A test of the reliability of the derived total metallicity $[Z/H]$ is obtained by plotting this measure against the empirical metallicity derived by the method of BH90 and that derived by the PCA method of SB04 (see Table 2.4). For the old ages of these GCs both methods are well-calibrated. Figure 2.7 shows there is generally good agreement between the different methods over a metallicity range of ~ 2 dex. The PCA metallicities appear to show somewhat better agreement than those of BH90 with $[Z/H]$ derived from SSP models.

As a further consistency check of our results we plot the observed B–V colour from Forbes *et al.* (2001b) versus total metallicity $[Z/H]$ in Figure 2.7. We can see that the metallicity correlates well with the observed colour and is consistent with the 12 Gyr isochrone of the TMK04 SSP models with BHBs. We believe GC47 to have an anomalous colour (see discussion in the following paragraph).

Finally, we compare the observed colours of these GCs with colours predicted from the SSP derived ages and total metallicities. For GCs with $[Z/H] \leq -1$ we use the BHB mass loss models and for $[Z/H] > -1$ we use the RHB models with no mass loss. This is consistent with the HB morphology suggested by the CaII index values. The predicted colour errors are indicative estimates only. Figure 2.8 shows that there is reasonable agreement between the predicted and observed colour. The main outlier is GC47. The colours measured for GC47 disagree with its inferred age and metallicity. Also, the spectra (see Figure 2.3) suggests that GC47 should have a colour similar to the reddest GC (i.e. GC12). Thus we suspect a systematic error in the observed colour for GC47.

2.4.3 Abundance Ratio

We show relationship between $[E/Fe]$ and $[Fe/H]_{SSP}$ in Figure 2.9. The sum of these two measures approximates the total metallicity $[Z/H]$ ($[Fe/H]_{SSP}$ is derived from the fitted value of $[Z/H]$). The plot shows that $[E/Fe]$ is consistent with a value of twice solar ($[E/Fe]=+0.3$), except perhaps at the lowest metallicities ($[Fe/H]_{SSP} < -2$) where the extrapolation of the SSP model to high $[E/Fe]$ is becoming unreliable. Such values are similar to those found for Galactic GCs (e.g Proctor *et al.* 2004).

2.5 Galaxy Spectrum

2.5.1 Long-slit Observations

On the same observing run (see Section 2.2) a 300s long-slit exposure along a P.A. = 60° centred on NGC 1052 itself was obtained. Standard reduction methods were used with IRAF software. Two dimensional distortions were measured on the arc lamp frames then removed using the task transform. The width for each aperture extracted increases with radius to achieve a signal-to-noise of ~ 30 at 5000 \AA for most of the apertures. The radial extent over which we can measure useful spectra is limited to $\sim 18''$ west-south-west of the galactic centre and $\sim 7.5''$ in the east-north-east direction.

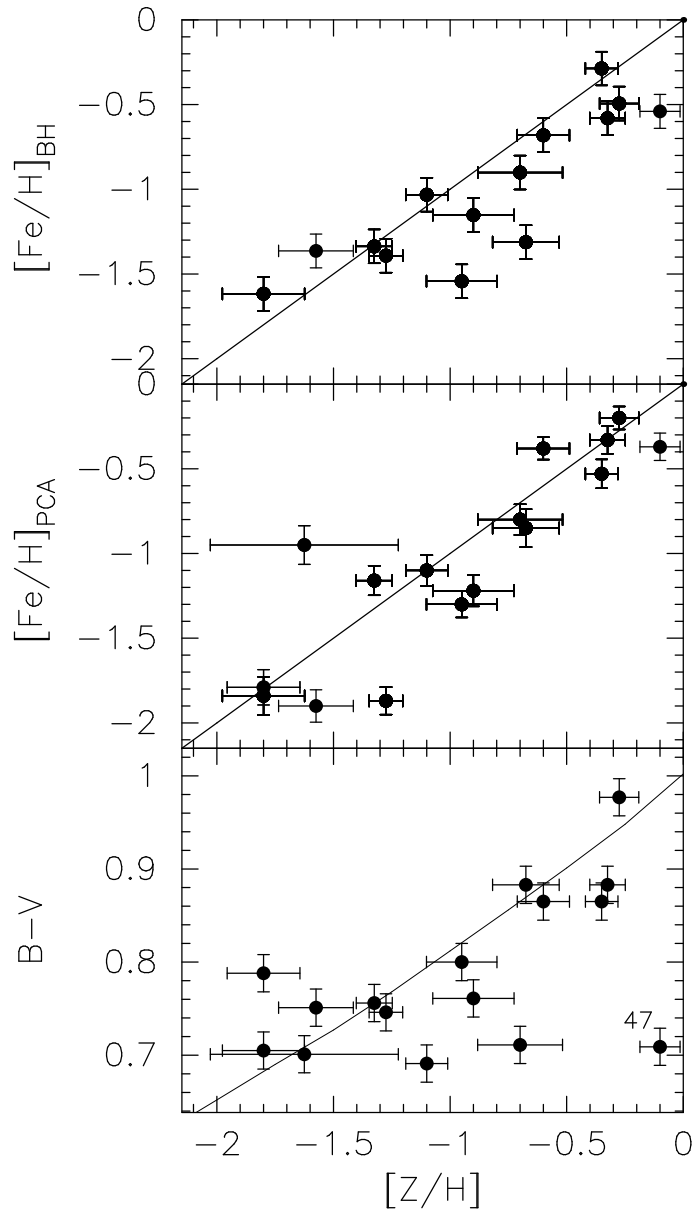


Figure 2.7: Comparison of empirical metallicities and observed colours with total metallicity. The top two plots show the metallicity from the method of BH90 ($[\text{Fe}/\text{H}]_{\text{BH}}$) and from SB04 ($[\text{Fe}/\text{H}]_{\text{PCA}}$). A one-to-one line is also shown. GCs 45 and 60 which have unreliable BH90 metallicities are not plotted. A good correlation is seen with points lying close to the one-to-one line for both empirical methods. The lower plot shows the observed $B-V$ colour from Forbes *et al.* (2001b) with $[\text{Z}/\text{H}]$. A reasonable agreement is found with the 12 Gyr isochrone from the TMK04 SSP models that include BHBs (solid line). The major outlier GC47 (which has an inexplicably blue colour) is labelled.

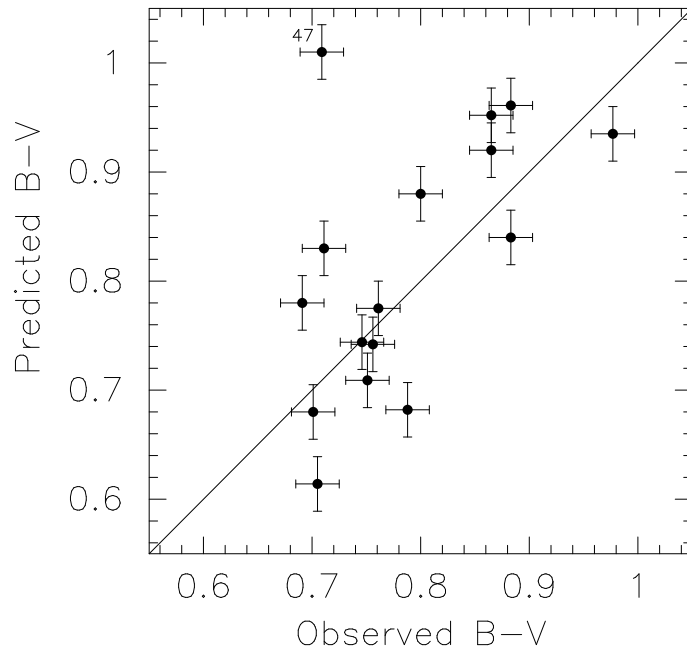


Figure 2.8: The B–V colour predicted from the inferred $[Z/H]$ and age is plotted against the observed B–V colour from Forbes *et al.* (2001b). The errors for the predicted colours are indicative only. GC47 which has an anomalous colour is labelled. For the other GCs there is good agreement between the predicted and observed colours.

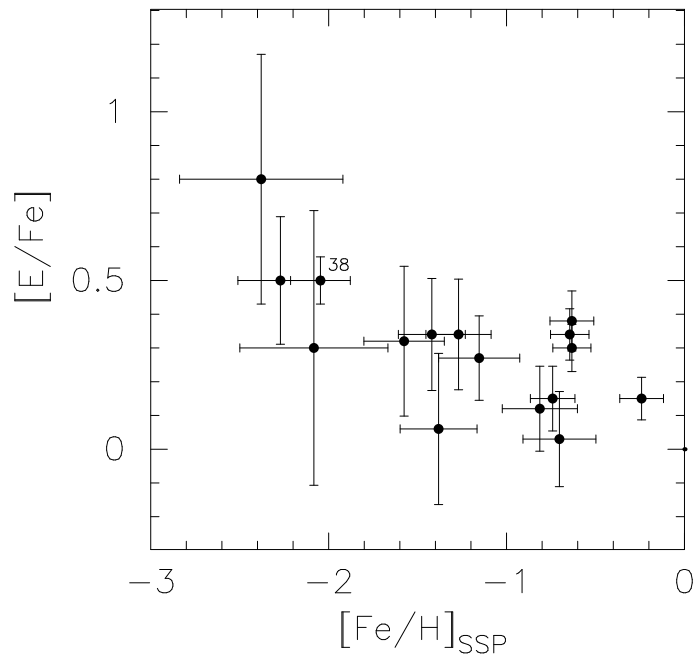


Figure 2.9: Abundance ratio against SSP derived iron metallicity. The GCs show a trend of decreasing $[E/Fe]$ with increasing $[Fe/H]_{SSP}$. However within errors a constant value of twice solar ($[E/Fe]=+0.3$) is consistent with the data.

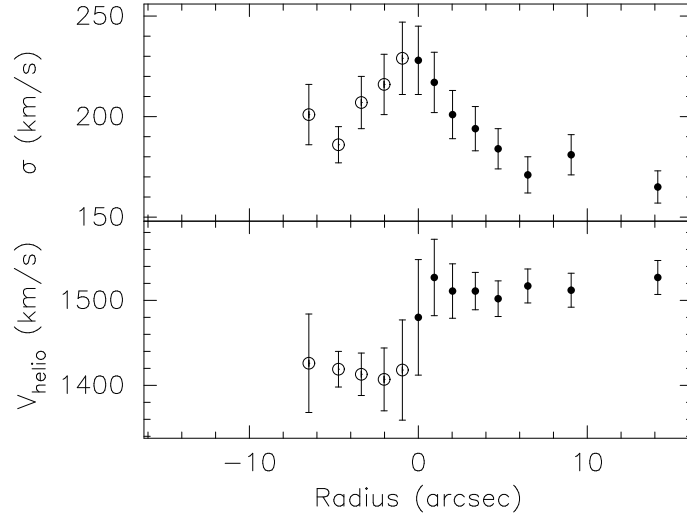


Figure 2.10: Recession velocity and velocity dispersion as functions of radius. Negative radii shown as open symbols indicate east-north-east of the galaxy centre, filled symbols indicate west-south-west. Rotation of order 50 km/s about the systemic velocity of 1470 km/s is clear from the lower panel. The velocity dispersion shown in the upper panel is peaked towards the galaxy centre.

For each spectrum, recession velocities were measured by cross-correlation using `fxcor` in IRAF. Velocity dispersions for the galaxy apertures were measured by cross-correlation with standard stars and comparison of the FWHM velocities with cross-correlations of the standard stars broadened by a range of velocity dispersions. These kinematic data are presented in Table 2.5.

2.5.2 Derived Parameters

Figure 2.10 shows that the galaxy rotates on the order of 50 km/s along our observed axis of P.A. = 60° . This rotation is consistent with that measured by Binney, Davies & Illingworth (1990), who find rotation of ~ 100 km/s along the major axis (P.A. = 120°) and none along the minor axis. Our observed axis is at an angle of 60° to the major-axis, therefore we expect the magnitude of rotation to be about $\cos(60^\circ) = 0.5$ of that found along the major-axis as observed. The velocity dispersion is centrally peaked, with a maximum value of ~ 230 km/s, as found by Binney *et al.* (1990).

Lick indices were measured for the galaxy at each radius and the same offset to the Lick system was applied as per the GC data. Denicolo *et al.* (2005) presents indices, measured along the major axis of NGC 1052, which are consistent with our observed values. Several indices show gradients with galactocentric radius. A sample of these are plotted in Figure 2.11, showing some clear radial trends. The metallicity and [E/Fe] sensitive indices (e.g., CN₂ and Mg₁) have a strong gradient towards higher values in the centre. A similar trend is observed for other [E/Fe] sensitive indices, e.g., Mgb. The Fe5270 line, which is primarily sensitive to iron metallicity [Fe/H], shows almost no gradient. Other Fe lines such as Fe4383, Fe4531 and Fe5406 also show no gradient with radius. These trends are also evident in the Denicolo *et al.* (2005) data. The galaxy therefore possesses strong gradients in

Table 2.5: Galaxy parameters. Radius is the centre of each aperture, where negative radii indicate east-north-east of the galaxy centre. 1σ errors are presented.

Radius (arcsec)	V_{helio} (km/s)	σ (km/s)	Age (Gyr)	[Fe/H] (dex)	[E/Fe] (dex)	[Z/H] (dex)
14.1	1527±20	165± 8	4.7±3.0	-0.08±0.22	0.42±0.07	0.32±0.21
9.1	1512±20	181±10	4.5±2.9	0.15±0.24	0.21±0.09	0.35±0.28
6.5	1517±20	171± 9	1.9±1.2	0.48±0.24	0.36±0.07	0.81±0.23
4.7	1502±21	184±10	1.8±0.9	0.65±0.17	0.42±0.06	1.05±0.19
3.4	1511±22	194±11	1.5±0.6	0.63±0.18	0.57±0.06	1.16±0.18
2.0	1511±32	201±12	2.1±1.0	0.65±0.13	0.51±0.05	1.13±0.15
1.0	1527±45	217±15	1.6±0.4	0.55±0.14	0.81±0.04	1.31±0.15
0.0	1480±68	228±17
-1.0	1418±59	229±18	1.8±0.4	0.65±0.11	0.84±0.05	1.44±0.12
-2.0	1407±37	216±15	1.6±0.4	0.65±0.11	0.69±0.04	1.30±0.12
-3.4	1413±25	207±13	1.9±0.7	0.63±0.13	0.51±0.05	1.11±0.15
-4.7	1419±21	186± 9	2.4±1.3	0.53±0.16	0.36±0.07	0.86±0.18
-6.5	1426±58	201±15	1.9±0.7	0.65±0.13	0.36±0.06	0.99±0.15

[E/Fe] sensitive indices, but no gradients in the [Fe/H] sensitive indices. The effect of central galactic emission is obvious in the $H\beta$ index plot, with large negative values at small radii. The other Balmer indices and Fe5015 are similarly affected by emission.

Due to the high total metallicity of the galaxy, we use the Fe– method from PS02 as opposed to the Trager *et al.* (2000a) method used earlier to calculate the [E/Fe]. This is necessary because the isochrone shape is driven by [Z/H] at low metallicity and [Fe/H] at high metallicity (see PS02 for a full explanation). Due to the high α -element abundance ratios present in the galaxy, we extrapolate the TMK04 models to [E/Fe]=+0.9. Figure 2.12 demonstrates the extremely high abundance ratios present in the central regions by showing a plot of $\langle Fe \rangle$ vs Mgb, where $\langle Fe \rangle = (Fe5270 + Fe5335)/2$.

To obtain reasonable fits to the TMK04 SSP models it was necessary to exclude several indices from all apertures during the fitting process. Galactic emission, which increases towards the centre, forces the removal of all the Balmer lines and Fe5015 from the fitting process. The index C4668 was also removed due to its systematic deviance from the best fit.

We also clipped individual deviant indices following a similar method to Section 2.3.3. This resulted in a total of 12% of the remaining indices being removed (mostly Mg₂, Ca4455 and Fe4383). We were unable to obtain reasonable fits for the central aperture, probably due to strong galactic emission, and do not present the fitted parameters for it. The values obtained for age, [Fe/H], [E/Fe] and [Z/H] are presented in Table 2.5 and also plotted against radius in Figure 2.13.

Figure 2.13 shows no strong radial gradient in either age or [Fe/H]. There is however a very strong gradient of decreasing [E/Fe] with increasing radius. In the central arc-second the estimated [E/Fe] of $\sim +0.8$ dex is unusually high.

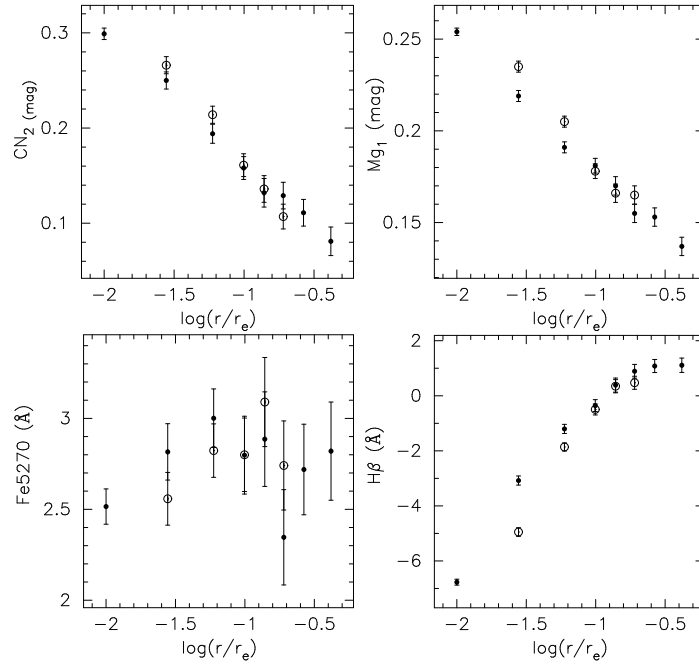


Figure 2.11: Representative plots of indices vs. \log radius in terms of the effective radius ($r_e=34''$). We have folded the data about the centre with points from the east-north-east marked with open symbols, filled symbols indicate west-south-west. The strong emission in $H\beta$ is clearly seen as negative values. This highlights the need to exclude the Balmer indices from our fitting process. The Mg_1 gradient when viewed in tandem with the Fe5270 lack of gradient implies that $[Fe/H]$ is roughly constant with radius and that the abundance ratio is much greater in the central region. The gradient in other α -element sensitive indices reinforces this picture.

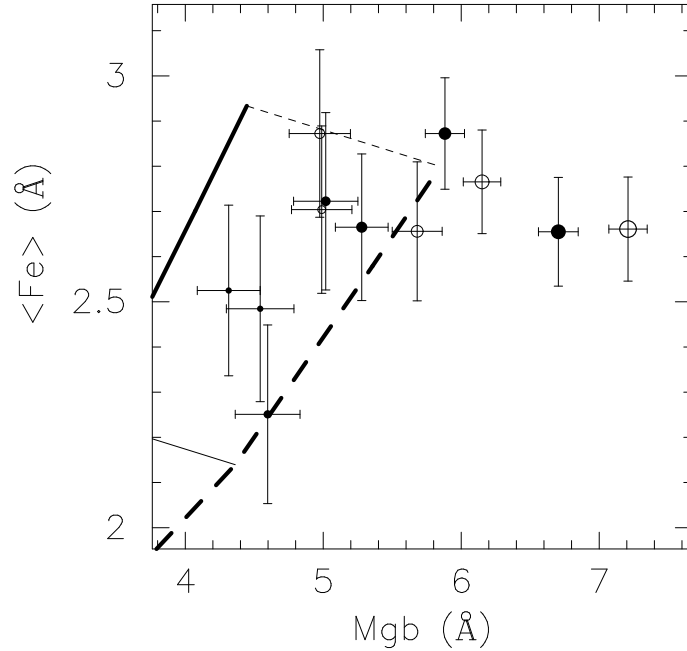


Figure 2.12: Plot of $\langle \text{Fe} \rangle$ vs Mgb indices. Bold lines show the 2 Gyr isochrones of $[\text{E}/\text{Fe}]=+0.3$ dex (solid) and $[\text{E}/\text{Fe}]=+0.6$ dex (dashed). The thin lines show $[\text{Fe}/\text{H}]=+0.0$ (solid) and $+0.4$ (dashed). Point sizes decrease with radius. The open symbols are the east-north-east apertures and the filled symbols indicate the apertures towards the west-south-west. The plot shows that the central apertures are the most α -element enhanced with abundance ratios above $+0.6$ dex.

2.6 Discussion

To summarise, we have obtained spectra for 16 GCs which sample both the blue and red sub-populations in NGC 1052. Ages, metallicities and abundance ratios for these GCs have been derived using the multi-line fitting technique of PS02 applied to the SSPs of TMK04. We find the blue GCs in NGC 1052 to be uniformly old ≥ 10 Gyr and metal-poor (with the exception of GC47 for which we strongly suspect an incorrect colour). The red GCs are similarly old but metal-rich. We do not find any young GCs associated with the recent merger event, even though we have sampled the expected colour and luminosity regime for young GCs.

We do, however, find evidence for young *galaxy* stars associated with the merger event. Our luminosity-weighted age of ~ 2 Gyr for the NGC 1052 stars is compatible with that estimated from the HI tidal tails and infalling HI gas of ~ 1 Gyr (van Gorkom *et al.* 1986).

The high central value and strong gradient observed for $[\text{E}/\text{Fe}]$ in NGC 1052 is unusual for an elliptical galaxy. For example, Mehlert *et al.* (2003) find negligible gradients in $[\text{E}/\text{Fe}]$ for 35 early-type galaxies in their sample of Coma galaxies. Proctor (2002), using the same method as this work, finds a maximum $[\text{E}/\text{Fe}] \simeq +0.4$ and no significant $[\text{E}/\text{Fe}]$ gradient in the bulges of 28 late and early-type galaxies.

The α -element abundance ratio for NGC 1052 is largely insensitive to the combination of indices we fit, unlike age and metallicity. Therefore, barring a major contamination of all the $[\text{E}/\text{Fe}]$ sensitive indices (which must also affect the observa-

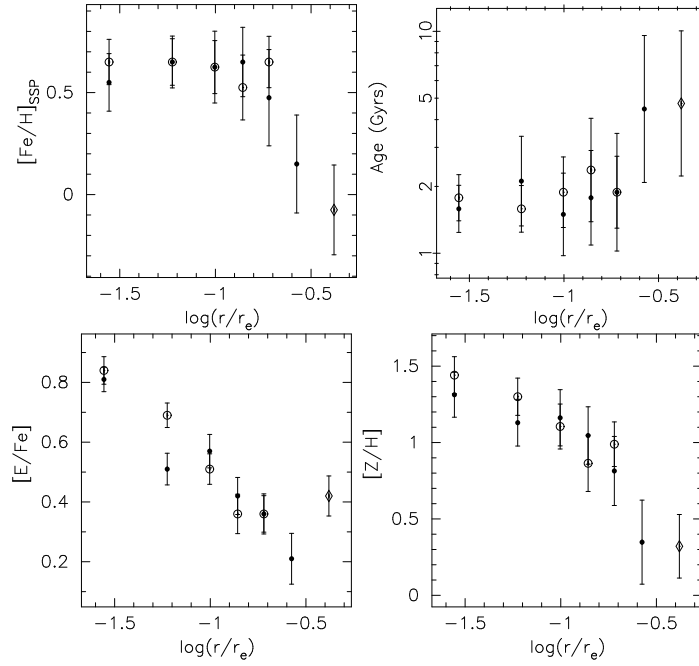


Figure 2.13: The derived stellar population parameters for the galaxy field stars are plotted with radius. We have folded the data about the galaxy centre with points from the east-north-east marked with open circles, filled symbols indicate west-south-west. The open diamonds indicate the aperture which has a less reliable fit. The central galaxy aperture is not shown. There is no strong gradient in either age or iron metallicity. There is a clear trend of α -element abundance ratio increasing towards the centre. Total metallicity shows a radial gradient.

tions of Denicolo *et al.* 2005), we can confidently say that the central galaxy starlight is more α -element enhanced than $\sim +0.6$ dex. Such α -element enhancements and the deduced high central metallicities ($[Z/H]=+1.3$ dex) are far beyond current SSP models. Therefore, it is impossible to pin down exact values for the central galaxy field stars. At $[Z/H]=+1.3$ the total metallicity would be 20 times that of the Sun, implying a metal content by mass of $\sim 40\%$. This value is unrealistically high, which suggests that our extrapolations beyond the current SSP models are unreliable.

van Gorkom *et al.* (1986) speculated that NGC 1052 had accreted a gas-rich dwarf galaxy about 1 Gyr ago. They find a total HI mass of $\sim 5 \times 10^8 M_\odot$ which seems consistent with this idea. Such a small quantity of gas could also explain why we have detected no GCs forming in this merger (even allowing for some cold gas to have been used up in field star formation and/or ionised). Even a small burst by mass will give a young age for the galaxy central stars (Terlevich & Forbes 2002).

Our results also indicate that the central merger-induced starburst involved very high metallicity and α -element enhanced gas. Such high metallicity gas is not usually associated with dwarf galaxies but massive spirals. The most obvious explanation for the high α -element enhancement is a high central concentration of Type II supernovae from the starburst. Inflows over any significant timescale are less likely, since no radial metallicity gradient is seen. A spiral galaxy with a small bulge and on-going star formation in the disk could produce the young central ages observed without star formation from the merger itself being the dominant luminosity source.

To better evaluate these possibilities we need stellar population information for the galaxy out to at least one effective radius. This will provide an age, metallicity and α -element abundance ratio for the assumed old (>10 Gyr) underlying population. With this information the next step would be to apply a chemo-gas code in an attempt to reproduce the observed properties.

In terms of the GC formation models described in Sections 1.2.2 and 2.1, the detection of old red and blue GC sub-populations in NGC 1052 is generally consistent with the predictions of both Forbes *et al.* (1997) and Cote *et al.* (1998). The ages are not yet accurate enough to determine whether the red GCs are a few Gyr younger than the blue ones as expected in Forbes *et al.* (1997). On the other hand, we find no evidence for GCs forming in the merger event, in contrast to the expectations of the merger model of Ashman & Zepf (1992).

There are now several examples of galaxies with spectroscopically confirmed *minor* contributions to their GC systems from recently formed GCs, while the vast bulk of their GCs appear to be very old. NGC 1399, a central cluster galaxy which is old and has no photometric indication of intermediate-age GCs, may have a small number of ~ 2 Gyr old GCs (Forbes *et al.* 2001a). Photometry of GCs in the merger remnant NGC 3610, which has a spectroscopic age of 1.6 ± 0.5 Gyrs (Denicolo *et al.* 2005), suggested the presence of an intermediate-age sub-population (Whitmore *et al.* 2002). However, spectroscopy of some of these candidate intermediate-age GCs indicates that only a small portion of these clusters are in fact ~ 2 Gyr old (Strader *et al.* 2004a).

Perhaps the best example of intermediate-age GCs in a merger remnant is NGC 1316; it has a similar age (~ 3 Gyrs) and lies at a similar distance (22.9 Mpc) as NGC 1052 (Goudfrooij *et al.* 2001). Figure 2.14 shows a comparison of the colour magnitude diagrams for the spectroscopically confirmed GCs of these two

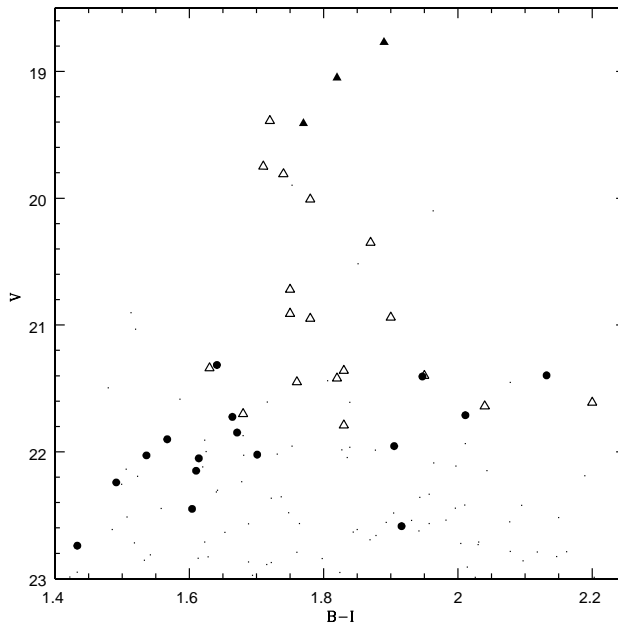


Figure 2.14: The colour magnitude diagram for spectroscopically confirmed GCs around NGC 1052 (filled circles). The small dots are GC candidates around NGC 1052 from the imaging of Forbes *et al.* (2001b). The triangles are spectroscopically confirmed GCs around NGC 1316 (Goudfrooij *et al.* 2001) with their magnitude’s adjusted to account for the distance modulus difference. Only the filled triangles had high enough S/N for ages and metallicities to be measured, the open triangles have measured velocities but not indices. Most of the NGC 1316 GCs have intermediate colours ($B-I \sim 1.8$) and are significantly brighter than the NGC 1052 GCs. Therefore we do not expect a similar sub-population of ~ 3 Gyr GCs in NGC 1052.

galaxies. Only the 3 brightest NGC 1316 GCs had high enough S/N to measure ages, and these are 2 magnitudes brighter in V than the brightest GCs for which we obtained spectra in NGC 1052. All three GCs were found to be ~ 3 Gyrs old and solar metallicity (Goudfrooij *et al.* 2001). The NGC 1316 GC colour distribution peaks at $B-I \sim 1.8$, which lies between the peaks of the NGC 1052 GC colour distribution. There is no significant population of NGC 1052 GCs in the same colour and magnitude parameter space as the young NGC 1316 GCs. Therefore we do not expect a similar sub-population of ≤ 3 Gyr GCs in NGC 1052.

2.7 Conclusions

We have obtained low-resolution spectra for 19 Globular Cluster (GC) candidates associated with the merger remnant elliptical NGC 1052. Of this sample, 16 are identified as *bona fide* GCs by their radial velocities.

Using the multi-index χ^2 fitting technique of Proctor & Sansom (2002), and the simple stellar population models of Thomas, Maraston & Korn (2004) we derive individual ages, metallicities and abundance ratios for the 16 confirmed GCs. We

find all of the GCs to be very old, i.e. ≥ 10 Gyr, with a range of metallicities. The predicted colours, based on the derived ages and metallicities, agree well with the observed GC colours. We find no evidence for young GCs associated with the likely minor merger event ~ 1 Gyr ago.

We also obtained a long-slit spectrum covering the central $\sim 15''$ of NGC 1052. No strong gradient in either age or metallicity was found. However, a large abundance ratio gradient exists. The stellar population in the central regions of NGC 1052 has a luminosity-weighted age of ~ 2 Gyr with $[\text{Fe}/\text{H}] \sim +0.6$ and a very high α -element abundance ratio of $\sim +0.8$ dex. The measurement of such high metallicities and abundance ratios requires extrapolation beyond the SSP models and so these measurements should be treated with caution. The recent central star formation episode was most likely induced by infalling gas associated with the recent merger. Thus, although NGC 1052 shows substantial evidence for a recent merger and an associated starburst, it appears that the merger did not induce the formation of many, if any, new GCs. As the formation of luminous star clusters appears to accompany most significant star formation events, the absence of young GCs and the high $[\text{E}/\text{Fe}]$ values in the centre of the galaxy (suggesting short star formation timescales) may indicate that a relatively small amount of star formation occurred in the merger. This interpretation is consistent with “frosting” models for the formation of early-type galaxies (e.g. Trager *et al.* 2000b).

Chapter 3

Gemini/GMOS Spectra of Globular Clusters in the Leo Group Elliptical NGC 3379

This chapter is based on upon Sections 1-3, 5 and 6 of Pierce et al. , 2006, MNRAS, 366, 1253.

3.1 Introduction

The Globular Cluster (GC) systems of numerous elliptical galaxies have been well-studied photometrically (e.g. Gebhardt & Kissler-Patig 1999; Kundu & Whitmore 2001; Larsen *et al.* 2001). Since the discovery of the bimodal colour distribution of GCs in elliptical galaxies (see Harris 1999 for a review), several models have been proposed to explain how these GC systems are formed.

Ashman & Zepf (1992) propose that some, or all, of the high-metallicity GCs will be formed during gas-rich merger events and therefore be of a similar age to those mergers. For the case of a series of minor gaseous mergers, a roughly monotonic increase in metallicity is expected with decreasing age.

The multi-phase collapse model of Forbes, Brodie & Grillmair (1997) proposes that the majority of GCs are native to their galaxy and formed during two, or more, proto-galactic collapse phases. Red, metal-rich, GCs are expected to be 2–4 Gyrs younger than their blue, metal-poor counterparts according to the semi-analytic GC formation model of Beasley *et al.* (2002).

Cote, Marzke & West (1998), invoke tidal capture of GCs from dwarf galaxies to account for the blue GC population of large elliptical galaxies. A higher fraction of blue, metal-poor, GCs is expected compared with spirals of a similar luminosity. Assuming that blue GCs form at the same time as their parent galaxy, “down-sizing” (Cowie *et al.* 1996; Kodama *et al.* 2005) suggests that blue GCs captured from dwarf galaxies should be younger than the native blue GCs.

Thus a key discriminant of the formation models is GC age. Unfortunately from photometry alone it is very difficult to determine the age and metallicity of individual GCs, due to the age-metallicity degeneracy (Brodie *et al.* 2005), therefore high quality spectra are required. The stellar population properties of individual

GCs can be measured accurately with low-resolution integrated spectra of sufficient signal-to-noise (≥ 30). The age-metallicity degeneracy can be broken by measuring spectral Lick indices (Worthey 1994), and comparing those indices to single stellar population (SSP) models. High signal-to-noise spectroscopic studies (i.e. those capable of determining ages for individual GCs) of elliptical galaxy GC systems are limited to around a dozen galaxies (e.g. NGC 1399 Forbes *et al.* 2001; NGC 1023 Larsen & Brodie 2002; NGC 1316 Goudfrooij *et al.* 2001; NGC 3610 Strader *et al.* 2003, 2004a; NGC 2434, NGC 3379, NGC 3585, NGC 5846 and NGC 7192 Puzia *et al.* 2004; NGC 5128 Peng, Ford & Freeman 2004; NGC 4365 Brodie *et al.* 2005; NGC 1052 Pierce *et al.* 2005). Except for Goudfrooij *et al.* and Peng *et al.*, these works find the majority of GCs to be old (>10 Gyrs) with a small fraction of young GCs for some galaxies.

In this work we report the analysis of Gemini/GMOS spectra of a sample of GCs in NGC 3379. This is a typical, nearby (10.8 ± 0.6 Mpc, Gregg *et al.* 2004) E0/1 elliptical galaxy. It is of intermediate luminosity ($M_V = -21.06$) with typical early-type colours, Mg₂ index and velocity dispersion (Davies *et al.* 1987) for its luminosity. There is no sign of any optical disturbance (Schweizer & Seitzer 1992). There is, however, a small nuclear dust ring at a radius of $1.5''$ (van Dokkum & Franx 1995) and some ionised gas that extends to a radius of $8''$ (Macchetto *et al.* 1996).

NGC 3379 is one of only a few elliptical galaxies to lie close enough that its stars can be resolved by the Hubble Space Telescope (HST). Resolved stellar population measurements using the *HST* NICMOS camera in the *J* and *H* bands have been made by Gregg *et al.* (2004). Measuring individual stellar magnitudes and colours to just below the Red Giant Branch (RGB) tip, they found the outer region stellar population to be old, with ages > 8 Gyr and a mean metallicity around solar. They noted similarities to the Galactic bulge. For the central region, Terlevich & Forbes (2002) used Lick indices to estimate an age of 9.3 Gyrs, $[\text{Fe}/\text{H}] = +0.16$ and $[\text{Mg}/\text{Fe}] = +0.24$. This suggests that radial age and metallicity variations are relatively small.

The *U*, *B*, *R*, *I* photometry of the GC system of this galaxy reveals the classic GC colour bimodality (Whitlock, Forbes & Beasley 2003). Whitlock *et al.* estimate a GC specific frequency of $S_N = 1.1 \pm 0.6$, which is low for an elliptical galaxy, although it is important to remember that NGC 3379 belongs to a relatively small group of galaxies (Leo) and, therefore, a low S_N is not unexpected (Bridges 1992). The *B*, *V*, *R* photometry of Rhode & Zepf (2004) indicates a similarly low S_N of 1.2 ± 0.3 and that approximately 70% of NGC 3379 GCs are blue.

To derive GC ages and metallicities we measure Lick indices from our GMOS spectra. We then apply the multi-index χ^2 -minimisation method of Proctor & Sansom (2002), which employs all the available Lick indices to break the age-metallicity degeneracy and simultaneously measure the α -element abundance ratios (see Proctor, Forbes & Beasley 2004 for an application to Galactic GCs and Chapter 2 for NGC 1052 GCs).

In this chapter we present our GMOS observations and data reduction of GC spectra in Section 3.2. An analysis of ages, metallicities and α -element abundance ratios derived from Lick indices is presented in Section 3.3. We discuss our results in Section 3.4 and present our conclusions in Section 3.5.

3.2 Observations and data reduction

The observations described below are part of Gemini program GN-2003A-Q-22. GC candidates were selected from Gemini North Multi-Object Spectrograph (GMOS; Hook *et al.* 2002) imaging, obtained during January 2003, for three fields around NGC 3379. The data reduction and GC candidate selection process is almost identical to that of Forbes *et al.* (2004) for NGC N4649, briefly, SExtractor (Bertin & Arnouts 1996) was used to select GC candidates based upon their Gemini zero point colours ($0.7 < g - i < 1.4$), magnitudes ($i < 24$) and structural properties (i.e. objects with stellarity index > 0.35). Interstellar reddening towards NGC 3379 is $E(B-V) = 0.024$ mag and is not taken into consideration (Schlegel *et al.* 1998). Spectroscopy of NGC 3379 globular clusters was obtained with GMOS on the Gemini North telescope in the months of February and April 2003. GMOS masks for three fields were designed, but only the central field was observed within the time allocation. Seeing was typically ~ 0.9 arcsec.

The GMOS CCDs consist of 3 abutted 2048×4608 EEV chips with a plate scale of 0.0727 arcsec/pixel (un-binned). For our set-up, we binned $4 \times$ in the dispersion direction, yielding 1.84 \AA per binned pixel, giving a final resolution of FWHM $\sim 4 \text{ \AA}$. The dispersion runs across the detectors in the GMOS instrument, resulting in two $\sim 20 \text{ \AA}$ gaps in the dispersion direction of the spectra. The B600_G5303 grating was used, with central wavelengths for successive exposures set alternately to 5000 \AA and 5025 \AA (in order to obtain full wavelength information across the gaps in the GMOS detectors). The effective wavelength range of each slit-let is a function of its position on the mask, but typically covered $3800 \text{ \AA} - 6660 \text{ \AA}$. A slit width of 1.0 arcsec was chosen to match the seeing and the minimum slit length was 6 arcsec, a compromise between maximising the number of slit-lets and allowing for reliable sky-subtraction. Exposures of 20×1800 s were taken, yielding a total of 10 hours on-source integration time. Bias frames, dome flat-fields and Copper-Argon (CuAr) arc exposures were taken as part of the Gemini baseline calibrations.

These data were reduced using the Gemini/GMOS packages in IRAF and a number of custom made scripts. From the CuAr arcs, wavelength solutions with typical residuals of 0.1 \AA were achieved. Objects and sky regions in the object spectra were manually identified in cross-sections of the two-dimensional images. The spectra were then extracted by tracing them in the dispersion direction. After some experimentation, optimal (variance) extraction was found to yield the best results since our data are over-sampled on the detector. In some cases, objects were too faint to trace individually and we therefore co-added several 2-d images, taken adjacent in time, to act as a reference for the extractions. We verified beforehand that flexure was minimal between the reference images. Finally, the extracted spectra were median combined and weighted by their fluxes with cosmic ray rejection.

In the absence of any velocity standard stars, the recession velocities were measured by using four Bruzual & Charlot (2003) model stellar energy distributions (SEDs) for old ages with metallicities $[\text{Fe}/\text{H}] = -2.25, -1.64, -0.64$ and -0.33 . The task FXCOR in IRAF was used and the average (weighted by the cross-correlation peak-height) was taken. Objects with recession velocities in the range 900 ± 400 km/s are potentially associated with NGC 3379. These are presented in Table 3.1. There was one foreground star and one background galaxy out of the 24 spectra obtained.

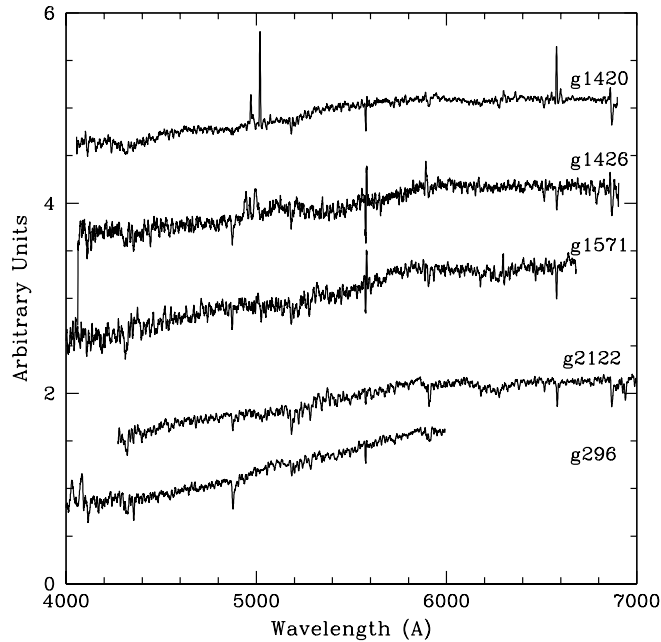


Figure 3.1: Normalised GC spectra which have been offset by one unit. These spectra have not been de-redshifted. These sample spectra show the wavelength range that the majority of our spectra cover and display the range of S/N and metallicity present. The spectrum of g1426 shows emission features around 5000 Å and 5890 Å of unknown origin. The PN hosting GC, g1420, is also plotted and the emission due to 4959 and 5007 Å [OIII] lines can be seen redshifted to 4971 and 5019 Å.

Our low contamination rate of 9% is due to good imaging and colour selection. We note that the spectrum of g1420 shows emission lines, most notably 4959 and 5007 Å [OIII], which we assume are due to a planetary nebula (see Fig. 3.1). Minniti & Rejkuba (2002) report a similar discovery for a GC in NGC 5128 and provide a discussion of the implications. Another GC, g1426, shows unexplained emission features around ~ 5000 Å.

A first-order flux calibration was carried out by normalising the spectra with a low-order polynomial. In order to measure Lick indices, we convolved our spectra with a wavelength-dependent Gaussian kernel to match the resolution of the Lick/IDS system (see Beasley *et al.* 2004b). Lick indices (Trager *et al.* 1998) were measured from our normalised spectra. Due to the variable wavelength ranges in these spectra, the same set of indices could not be measured for all spectra. However, all covered a wavelength range of 4500–5500 Å. Uncertainties in the indices were derived from the photon noise in the unfluxed spectra. No Lick standard stars were observed so we therefore cannot fully calibrate the GCs onto the Lick system. Consequently there are some systematic differences between some of the measured indices and those used in the SSP models. These issues are discussed further in Sections 3.3 and 3.4. Measured line indices and uncertainties are presented in Tables 3.2 and 3.3.

The final spectra have $S/N = 18\text{--}58 \text{ \AA}^{-1}$ at 5000 Å, giving errors in the $H\beta$ index

Table 3.1: Confirmed Globular Clusters around NGC 3379. Cluster ID, coordinates, g magnitude, $g-r$ and $g-i$ colours are from our GMOS imaging and are instrumental magnitudes only. Heliocentric velocities are from the spectra presented in this work.

ID	R.A. (J2000)	Dec. (J2000)	g (mag)	$g-r$ (mag)	$g-i$ (mag)	V_{helio} (km/s)
g1566	10:47:50.5	12:34:37.2	19.83	0.65	0.96	1071±18
g296	10:48:02.2	12:35:57.6	21.40	0.62	0.88	1022±52
g1940	10:47:48.2	12:35:45.3	21.42	0.74	0.90	875±25
g1550	10:47:53.6	12:34:54.6	21.47	0.71	1.09	1100±31
g2122	10:47:47.7	12:34:14.8	21.49	0.74	0.93	922±32
g1078	10:47:54.2	12:36:31.9	21.54	0.70	1.00	1000±24
g1420	10:47:50.7	12:35:32.3	21.54	0.62	0.90	764±38
g1540	10:47:53.5	12:35:04.9	21.68	0.58	0.83	790±41
g1617	10:47:50.4	12:33:47.8	21.88	0.62	0.96	650±37
g1588	10:47:49.7	12:34:10.2	22.32	0.60	1.10	546±45
g114	10:48:04.9	12:35:38.5	22.35	0.61	0.90	861±45
g1426	10:47:50.6	12:35:19.2	22.37	0.61	0.87	797±71
g1610	10:47:58.9	12:33:54.5	22.39	0.55	0.79	957±61
g1571	10:47:49.7	12:34:32.8	22.47	0.72	1.04	744±28
g1519	10:47:49.6	12:35:27.0	22.49	0.73	1.16	623±42
g1934	10:47:47.9	12:36:23.4	22.72	0.64	0.76	1004±65
g1580	10:47:54.2	12:34:21.6	22.84	0.71	1.09	1066±32
g219	10:48:01.8	12:37:22.0	23.04	0.57	0.85	868±95
g1893	10:47:45.1	12:37:53.0	23.26	0.86	1.21	804±43
g1630	10:47:50.5	12:36:11.8	23.65	0.77	1.21	1115±61
g1595	10:47:52.9	12:34:04.4	23.69	0.67	1.00	970±70
g230	10:48:01.2	12:37:06.9	23.93	0.80	1.28	1022±90

of 0.13–0.44 Å (we note that g1566 has an $H\beta$ error of ± 0.065 Å and $S/N=118$, however this is not representative as this GC is ~ 1.5 mags brighter than any other).

3.3 Ages, Metallicities and α -Element Abundance Ratios

In this section we describe how we derive ages, metallicities and α -element abundances. The resulting values are listed in Table 3.4.

We apply the χ^2 multi-index fitting technique of Proctor & Sansom (2002) for this analysis. This method involves the comparison of the measured Lick indices with SSP models (its application to extra-galactic GCs is described in Chapter 2). The SSP models of Thomas, Maraston & Korn (2004; hereafter TMK04) were chosen because they present the only set of models that include the effect of α -element abundance ratios on the Balmer lines.

We compare the measured Lick indices to the TMK04 SSPs and obtain a min-

Table 3.2: Globular Cluster indices $\lambda < 4600 \text{ \AA}$. Central index values (first line) and errors (second line). Indices in brackets are removed during the fitting process. Missing values are due to limited wavelength coverage.

ID	H δ_A (\AA)	H δ_F (\AA)	CN ₁ (mag)	CN ₂ (mag)	Ca4227 (\AA)	G band (\AA)	H γ_A (\AA)	H γ_F (\AA)	Fe4383 (\AA)	Ca4455 (\AA)	Fe4531 (\AA)
g1566	0.493	3.106	-0.962	0.896	2.365	0.591	2.008
	0.069	0.117	0.119	0.073	0.167	0.084	0.124
g296	(4.054)	(3.555)	(0.002)	(0.038)	0.481	2.887	-0.409	1.019	0.707	0.794	0.856
	(0.253)	(0.166)	(0.008)	(0.009)	0.138	0.237	0.238	0.148	0.353	0.173	0.266
g1940	3.256	-0.919	0.437	1.207	0.514	2.532
	0.235	0.237	0.151	0.342	0.169	0.243
g1550	1.302	(0.057)	(0.106)	0.681	4.005	(-4.947)	(-1.474)	3.992	(0.467)	3.044
	0.205	(0.008)	(0.010)	0.151	0.246	(0.273)	(0.173)	0.342	(0.179)	0.255
g2122	5.555	-5.405	-1.191	4.199	(0.866)	3.108
	0.251	0.295	0.184	0.363	(0.185)	0.266
g1078	0.865	1.694	(0.010)	(0.043)	0.588	3.866	-1.420	0.486	(1.280)	(0.285)	2.309
	0.291	0.195	(0.008)	(0.009)	0.146	0.241	0.249	0.157	(0.354)	(0.177)	0.250
g1420	(1.278)	(0.019)	(0.049)	(1.089)	2.719	-0.457	(0.541)	0.763	0.504	(0.770)
	(0.193)	(0.008)	(0.009)	(0.139)	0.254	0.249	(0.159)	0.366	0.178	(0.266)
g1540	3.926	2.973	(-0.057)	(-0.053)	0.439	2.091	0.367	(1.201)	0.877	0.477	0.846
	0.270	0.185	(0.008)	(0.009)	0.149	0.255	0.245	(0.155)	0.369	0.182	0.277
g1617	(0.724)	(-0.021)	(0.017)	(0.191)	3.743	-1.765	0.525	2.259	0.447	1.943
	(0.240)	(0.009)	(0.011)	(0.177)	0.292	0.302	0.188	0.415	0.209	0.305
g1588	1.192	4.292	(-4.894)	-0.283	3.098	0.837	3.327
	0.213	0.350	(0.386)	0.234	0.492	0.249	0.356
g114	(0.829)	2.917	(-0.079)	(-0.079)	(-0.314)	2.070	0.402	1.935	0.551	0.648	(-0.256)
	(0.432)	0.270	(0.012)	(0.014)	(0.221)	0.382	0.357	0.218	0.534	0.259	(0.398)
g1426	2.368	(-0.037)	(-0.008)	(-0.208)	4.122	0.267	0.525	0.860	0.051	1.447
	0.268	(0.011)	(0.013)	(0.218)	0.342	0.351	0.230	0.521	0.259	0.389
g1610	(4.667)	3.479	(-0.234)	(-0.232)	0.175	(-2.291)	-1.207	0.580	1.182	0.678	1.332
	(0.380)	0.261	(0.012)	(0.014)	0.215	(0.433)	0.363	0.229	0.520	0.250	0.390
g1571	(3.298)	(1.842)	(0.001)	(0.042)	0.859	(6.656)	(-8.418)	-1.715	6.113	2.101	2.561
	(0.439)	(0.315)	(0.013)	(0.015)	0.230	(0.350)	(0.448)	0.268	0.498	0.260	0.397
g1519	1.238	3.570	-2.920	0.183	3.012	0.952	2.863
	0.205	0.369	0.389	0.239	0.515	0.252	0.366
g1934	0.262	1.058	1.875	-0.069	0.517	-0.171
	0.427	0.384	0.238	0.606	0.300	0.462
g1580	-1.848	(-1.852)	(0.177)	(0.129)	(-1.926)	3.971	-5.028	-0.634	5.124	2.185	(0.530)
	0.659	(0.475)	(0.017)	(0.020)	(0.367)	0.487	0.526	0.323	0.631	0.308	(0.494)
g219	(-4.486)	(0.019)	(0.037)	(0.188)	(2.267)	-1.395	4.035	(1.342)	0.040	-0.334	-0.274
	(0.665)	(0.422)	(0.016)	(0.018)	(0.253)	0.613	0.473	(0.325)	0.767	0.385	0.559
g1893	2.245
	0.602
g1630	(-5.925)	(0.150)	(0.121)	(3.212)	5.462	-8.396	-1.286	6.183	(-1.965)	(5.771)
	(0.927)	(0.025)	(0.029)	(0.339)	0.650	0.851	0.487	0.960	(0.555)	(0.615)
g1595	(-0.313)	(-3.507)	(-0.182)	(-0.060)	-0.684	-2.792	2.502	(4.899)	(7.957)	(3.874)	(5.532)
	(1.160)	(0.986)	(0.030)	(0.034)	0.575	1.038	0.761	(0.414)	(0.961)	(0.498)	(0.773)
g230	(11.407)	2.689	(-0.644)	(-0.585)	(-3.332)	(-4.732)	2.696	(-3.572)	(-3.244)	-0.978	(6.999)
	(0.813)	0.766	(0.028)	(0.031)	(0.645)	(1.047)	0.726	(0.612)	(1.213)	0.556	(0.671)

Table 3.3: Globular Cluster indices $\lambda > 4600 \text{ \AA}$. Central index values (first line) and errors (second line). Indices in brackets are removed during the fitting process. Missing values are due to limited wavelength coverage.

ID	C4668 (\AA)	H β (\AA)	Fe5015 (\AA)	Mg ₁ (mag)	Mg ₂ (mag)	Mgb (\AA)	Fe5270 (\AA)	Fe5335 (\AA)	Fe5406 (\AA)	Fe5709 (\AA)	Fe5782 (\AA)
g1566	(1.474)	1.994	2.692	(0.039)	(0.110)	1.895	1.668	(1.606)	0.832	0.467	0.242
	(0.180)	0.065	0.139	(0.001)	(0.002)	0.064	0.070	(0.080)	0.059	0.044	0.042
g296	0.339	(2.679)	1.676	(-0.039)	(0.028)	(1.027)	1.194	0.819	(0.778)
	0.382	(0.132)	0.283	(0.003)	(0.003)	(0.130)	0.142	0.163	(0.119)
g1940	1.193	2.153	2.816	(0.008)	(0.093)	2.045	1.745	1.425	(1.250)	(0.772)	0.178
	0.362	0.131	0.279	(0.003)	(0.003)	0.128	0.142	0.161	(0.117)	(0.087)	0.084
g1550	(3.430)	(1.100)	3.697	(0.085)	(0.198)	2.810	2.206	1.687	1.354	0.727	0.391
	(0.369)	(0.139)	0.287	(0.003)	(0.003)	0.133	0.143	0.163	0.118	0.089	0.085
g2122	2.411	1.670	3.940	(0.065)	(0.200)	2.953	2.387	(2.850)	1.546	0.590	(0.346)
	0.394	0.144	0.304	(0.003)	(0.004)	0.139	0.150	(0.165)	0.123	0.093	(0.089)
g1078	(3.035)	2.147	(4.188)	(0.025)	(0.112)	2.118	1.495	1.113	1.115	0.685	0.314
	(0.366)	0.134	(0.280)	(0.003)	(0.003)	0.130	0.144	0.165	0.119	0.087	0.084
g1420	1.273	(0.938)	(-0.436)	(0.038)	(0.115)	1.418	1.153	1.115	0.694	0.250	0.302
	0.380	(0.143)	(0.296)	(0.003)	(0.003)	0.136	0.147	0.166	0.121	0.093	0.088
g1540	(-1.675)	2.934	(-0.446)	(0.016)	(0.056)	1.441	0.717	0.898	(0.973)	(-0.433)	-0.156
	(0.414)	0.139	(0.325)	(0.003)	(0.004)	0.144	0.163	0.184	(0.133)	(0.101)	0.095
g1617	1.517	(1.131)	2.076	(-0.032)	(0.076)	2.534	1.268	0.814	0.354	0.288	0.163
	0.448	(0.169)	0.352	(0.003)	(0.004)	0.155	0.176	0.203	0.148	0.112	0.106
g1588	(-0.540)	2.255	(-0.892)	(0.081)	(0.167)	2.413	(3.422)	1.600	(-0.020)	0.700	(0.002)
	(0.546)	0.187	(0.418)	(0.004)	(0.005)	0.185	(0.195)	0.226	(0.175)	0.121	(0.118)
g114	(2.781)	2.327	2.621	(0.001)	(0.051)	1.230	1.687	1.310	0.706
	(0.558)	0.197	0.426	(0.004)	(0.005)	0.196	0.212	0.245	0.180
g1426	0.957	2.962	(-0.001)	(-0.067)	(-0.005)	2.373	(-1.293)	-0.045	0.920	(-0.364)	0.161
	0.570	0.196	(0.433)	(0.004)	(0.005)	0.188	(0.240)	0.267	0.188	(0.143)	0.131
g1610	0.796	2.451	3.175	(0.024)	(0.075)	(0.797)	0.906	0.900	0.419
	0.576	0.207	0.441	(0.004)	(0.005)	(0.208)	0.222	0.252	0.189
g1571	1.771	0.976	(0.318)	(0.085)	(0.157)	2.159	2.677	2.220	(0.742)	(-0.124)	0.705
	0.578	0.214	(0.464)	(0.004)	(0.005)	0.207	0.221	0.249	(0.192)	(0.138)	0.126
g1519	0.895	(0.468)	(6.229)	(-0.003)	(0.189)	(4.168)	(3.613)	1.874	(-0.074)	(1.240)	0.362
	0.549	(0.213)	(0.406)	(0.004)	(0.005)	(0.180)	(0.190)	0.226	(0.173)	(0.129)	0.126
g1934	0.258	3.209	(-2.122)	(-0.023)	(-0.052)	(-3.180)	1.031	0.496	(0.961)	0.157	-0.198
	0.662	0.231	(0.533)	(0.005)	(0.006)	(0.260)	0.264	0.301	(0.216)	0.168	0.167
g1580	2.831	(3.334)	(7.071)	(0.042)	(0.166)	(3.601)	2.713	(0.901)	(0.421)	0.856	(-0.083)
	0.696	(0.246)	(0.518)	(0.005)	(0.006)	(0.236)	0.260	(0.306)	(0.225)	0.163	(0.161)
g219	(-2.680)	2.595	0.108	(-0.034)	(0.043)	1.345	0.930	-0.152	0.715
	(0.809)	0.274	0.614	(0.006)	(0.007)	0.271	0.299	0.346	0.246
g1893	7.066	(3.030)	7.438	(0.111)	(0.250)	5.102	(4.318)	2.351	2.286	1.414	(0.316)
	0.818	(0.305)	0.615	(0.006)	(0.007)	0.273	(0.293)	0.345	0.254	0.191	(0.182)
g1630	(1.358)	2.091	(0.673)	(0.145)	(0.238)	2.505	2.254	2.013	(-0.329)	1.568	1.053
	(0.979)	0.354	(0.827)	(0.007)	(0.009)	0.351	0.366	0.417	(0.322)	0.219	0.212
g1595	(12.186)	2.914	0.448	(0.043)	(0.066)	(3.838)	-0.352	(-2.982)	-0.690	(1.311)	-0.223
	(1.024)	0.396	0.897	(0.009)	(0.010)	(0.366)	0.451	(0.543)	0.386	(0.268)	0.268
g230	(9.738)	(0.763)	0.969	(-0.113)	(0.067)	0.724	(4.403)	1.941	(-1.199)
	(1.046)	(0.442)	0.856	(0.008)	(0.010)	0.405	(0.395)	0.466	(0.388)

Table 3.4: Derived Globular Cluster Properties. Age, [Fe/H], [E/Fe] and [Z/H] are derived from the χ^2 minimisation process, with errors derived by a Monte Carlo style method. [Fe/H]_{BH} is derived according to the method of Brodie & Huchra (1990) from a reduced sample of indices.

ID	Age (Gyr)	[Fe/H] (dex)	[E/Fe] (dex)	[Z/H] (dex)	[Fe/H] _{BH} (dex)
g1566	12.6±1.1	-1.17±0.05	0.15±0.05	-1.03±0.03	-1.15±0.06
g296	11.2±1.5	-1.82±0.11	0.71±0.10	-1.15±0.06	-1.84±0.26
g1940	11.9±2.1	-1.26±0.11	0.30±0.10	-0.98±0.06	-1.31±0.12
g1550	15.0±4.8	-0.69±0.11	0.15±0.07	-0.55±0.11	-0.52±0.18
g2122	15.0±2.0	-0.47±0.07	0.15±0.06	-0.33±0.04	-0.45±0.10
g1078	10.0±1.7	-1.05±0.09	0.24±0.09	-0.83±0.06	-1.17±0.06
g1420	10.0±1.4	-1.40±0.11	0.21±0.09	-1.20±0.06	-1.23±0.10
g1540	9.4±1.7	-2.09±0.18	0.68±0.17	-1.45±0.09	-1.64±0.04
g1617	11.2±1.9	-1.52±0.12	0.68±0.10	-0.88±0.08	-1.59±0.28
g1588	8.4±2.9	-0.57±0.14	0.15±0.09	-0.43±0.13	-0.33±0.16
g114	15.0±6.5	-1.14±0.16	-0.06±0.15	-1.20±0.14	-1.60±0.17
g1426	7.5±2.5	-1.58±0.13	0.80±0.07	-0.83±0.11	-2.37±0.44
g1610	10.6±2.1	-1.62±0.13	0.71±0.12	-0.95±0.09	-1.98±0.40
g1571	15.0±3.6	-0.10±0.08	-0.27±0.05	-0.35±0.08	-0.29±0.21
g1519	12.6±2.9	-0.72±0.13	-0.03±0.10	-0.75±0.09	-0.82±0.37
g1934	10.0±2.3	-2.31±0.31	0.65±0.29	-1.70±0.15	-2.27±0.21
g1580	9.4±2.5	-0.24±0.13	0.09±0.09	-0.15±0.09	-0.73±0.12
g219	12.6±1.8	-2.72±0.37	0.50±0.35	-2.25±0.13	-2.15±0.25
g1893	11.2±5.9	0.12±0.16	0.24±0.09	0.35±0.13	0.44±0.05
g1630	11.2±5.4	0.10±0.19	-0.24±0.08	-0.13±0.19	0.20±0.35
g1595	8.9±3.2	-3.00±0.49	0.80±0.41	-2.25±0.31	-2.08±0.42
g230	15.0±5.9	-1.52±0.30	-0.30±0.34	-1.80±0.23	-2.34±0.94

imum χ^2 fit. This fit is obtained using all the indices measured. Simultaneously a set of χ^2 minimisation fits are found with each of the indices omitted. From this set, we select the fit with the lowest total χ^2 , remove the necessary index and repeat until a stable fit is achieved with no highly aberrant ($> 3\sigma$) indices remaining. All GCs had some indices that were significant outliers to the fit and therefore removed during this process. For g1426 none of the indices potentially affected by the PN style emission lines are included in the final fit.

The molecular band indices Mg₁ and Mg₂ are systematically offset due to poor flux calibration and were excluded for all GCs (see Proctor *et al.* 2005). Similar to other GC studies (e.g. Beasley *et al.* 2004a) we find the CN indices to be enhanced relative to the models and therefore they were also removed.

An index-index plot of H γ_A vs Fe4383 is shown in Fig. 3.2. This pairing of indices was chosen as the combination of an age and a metallicity sensitive index that had the largest number of reliable points. This shows the majority of GCs lie near the 15 Gyr age line. Horizontal branch morphology is the apparent source of the offset to the left of the TMK04 15 Gyr age line seen in the majority of the low

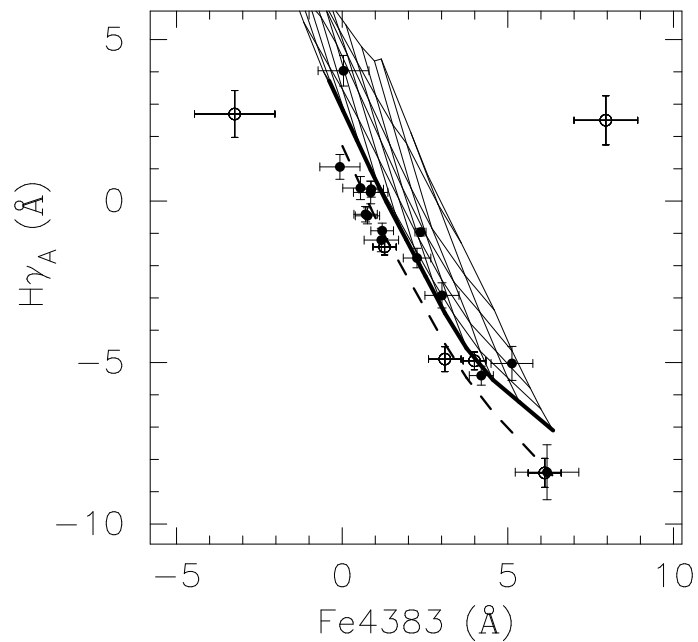


Figure 3.2: The indices $H\gamma_A$ vs $Fe4383$ are plotted against age-metallicity grids from TMK04. We show the grid for $[E/Fe]=+0.3$, with metallicity in 0.25 dex steps from from -2.25 (left) to $+0.5$ (right) and ages of 1,2,3,5,8,12 and 15 Gyrs (top to bottom); the bold line is 15 Gyrs and the dashed line is the red horizontal branch 15 Gyr isochrone from Thomas, Maraston & Bender (2003). Filled circles are shown for GCs where both indices are included in the fits; if either index is excluded then an open circle is plotted. A large number of the GCs fall near the maximum age line for the Thomas, Maraston & Bender (2003) red horizontal branch SSPs.

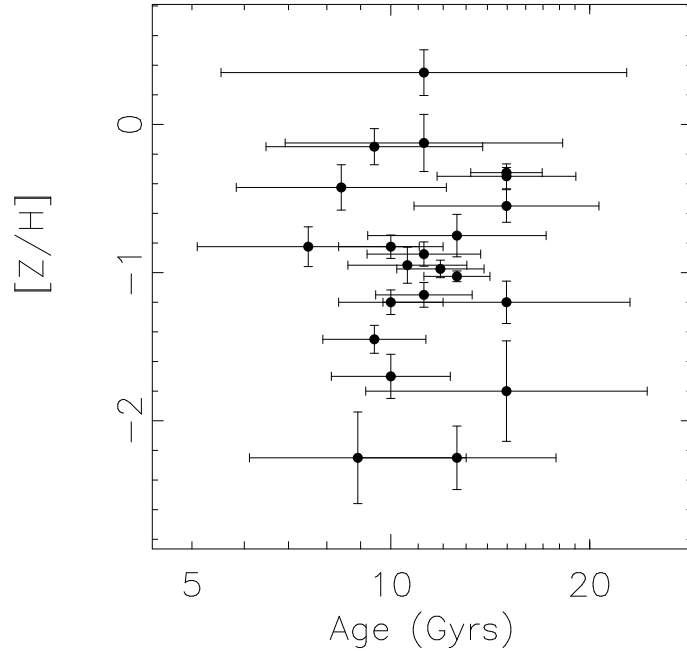


Figure 3.3: GC age-metallicity relation. The plot shows that the observed GCs are consistent with an old age and a wide range of metallicities.

metallicity GCs (see Section 2.3.2 for a brief discussion on the effect of horizontal branch morphology on GC χ^2 fitting). TMK04 models in this regime possess a predominantly blue horizontal branch whereas the red horizontal branch models from Thomas, Maraston & Bender (2003) pass directly through these points. There are a couple of clear outliers for which one or both index values have been excluded from the fitting process. However to derive values we use the results from the χ^2 fitting process.

From our quantitative χ^2 minimisation fits we find all of the GCs to be consistent with an old age (≥ 10 Gyrs) with a spread of metallicities from $[\text{Fe}/\text{H}] < -2$ to solar (Fig. 3.3). This is consistent with Fig. 3.2 and indeed the fitting procedure has identified clear outliers. The GC, g1426, with the youngest fit age of 7.5 Gyrs, is the GC with unexplained emission lines in its spectrum. It also has $[\text{E}/\text{Fe}] = +0.8$ which is at the maximum of the models. While none of the clearly affected indices were included in the fit, we suspect that the fit was still somewhat influenced by the emission source.

A test of SSP-derived metallicities is to compare them with those derived using the Brodie & Huchra (1990; hereafter BH) method. We were unable to use the full sample of metal-sensitive indices due to the poor sensitivity at shorter wavelengths. We therefore measured the G band, Fe52, MgH and Mg₂ BH indices using the method outlined in their paper. We define a Brodie-Huchra metallicity as the average of the empirically calibrated metallicity from these 4 indices, where the error quoted is the standard deviation. This metallicity is referred to as $[\text{Fe}/\text{H}]_{\text{BH}}$ in Table 3.4. Fig. 3.4 shows that the BH metallicities closely match those derived by χ^2 fitting to SSPs. The outliers at low metallicity are at the limits of the SSP models for either $[\text{Fe}/\text{H}]$ or $[\text{E}/\text{Fe}]$.

We compare the observed $g-i$ colours for the GCs with the predicted $g-i$ colours

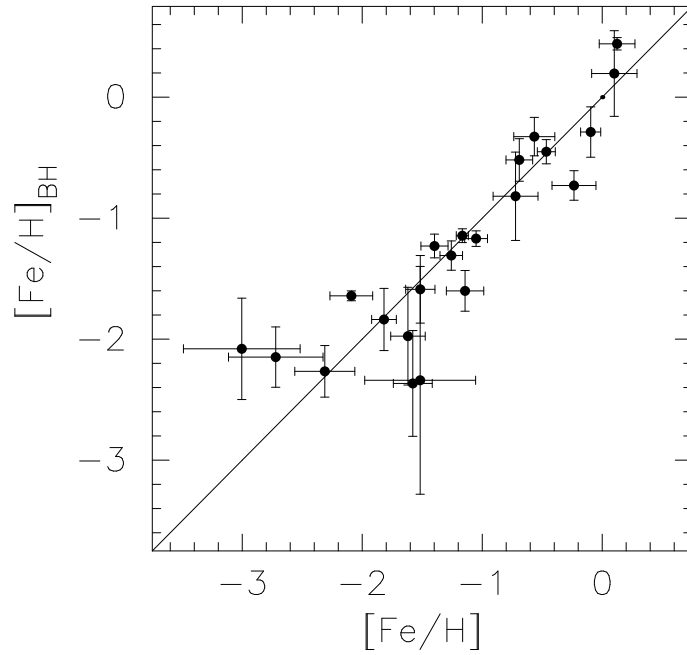


Figure 3.4: A comparison of Brodie-Huchra metallicity vs our derived metallicity. The four points with poor agreement at low metallicity (below $[\text{Fe}/\text{H}]_{BH} = -2$) all are at the limits of the SSP models.

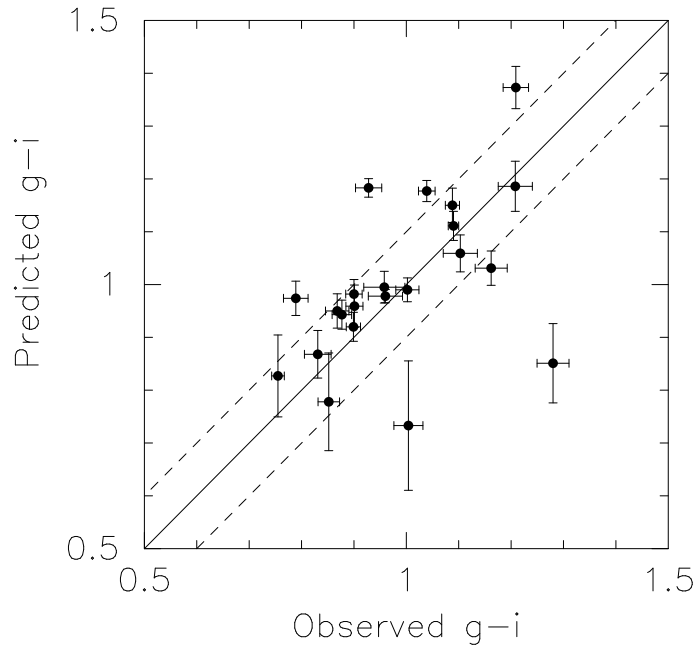


Figure 3.5: The predicted colour from stellar population fits vs observed $g-i$ colour. The outliers are GCs that are generally at the limits of the SSP models. The errors for both observed and predicted colours are lower limits and may be significantly underestimated. The dashed lines show the RMS scatter of ± 0.1 mag around the one-to-one solid line. A Spearman Rank test gives a probability of correlation of 99.2%.

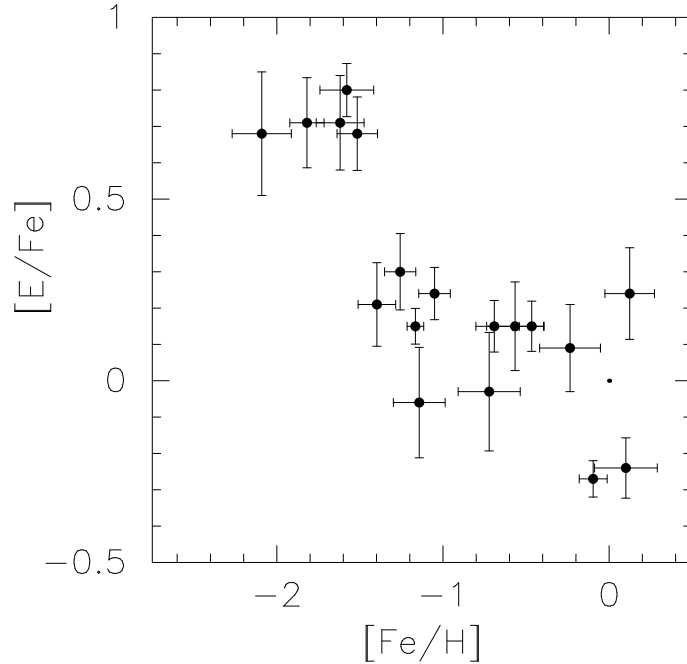


Figure 3.6: A plot of α -element ratio vs metallicity. The four GCs with poorly determined metallicities and α -element abundance ratios (i.e. $[E/Fe]$ errors >0.3) are not shown. The plot indicates a correlation in the sense of increased enhancement with decreasing metallicity.

from the Bruzual & Charlot (2003) SSPs, with the ages and metallicities from TMK04 SSPs in Fig. 3.5 (thus there could be some systematic offsets due to model differences). The use of Bruzual & Charlot (2003) colour models is necessary because the TMK04 SSPs do not include g and i magnitudes. There are several outliers in the colour-colour plot; these include the low metallicity GCs mentioned previously as well as a few others that are at the SSP model maximum age. A Spearman Rank test gives the probability of correlation as 99.2%. Overall the figure gives us confidence in the SSP-derived parameters.

TMK04 estimate α -element abundance ratios using the parameter $[E/Fe]$. A definition of $[E/Fe]$ for the SSP models used can be found in Thomas *et al.* (2004). Briefly, it includes α -elements, such as O, Ne, Mg, Si, S, Ar, Ca and Ti plus two non- α -elements N and Na. The $[E/Fe]$ vs. $[Fe/H]$ plot presented in Fig. 3.6 shows decreasing α -element abundance ratio with increasing metallicity, including two solar metallicity GCs with sub-solar α -element abundance ratios. The source of this trend is confirmed by the index-index plots of Fig. 3.7, in which high-metallicity GCs generally have α -sensitive indices that are consistent with $[E/Fe] < +0.3$. The lower metallicity GCs have α -element sensitive indices that are predominantly stronger than $[E/Fe] = +0.3$.

3.4 Discussion

The reliability of GC parameters derived from Lick indices and our χ^2 fitting method is affected by several factors, most importantly the stability of the fit when individual

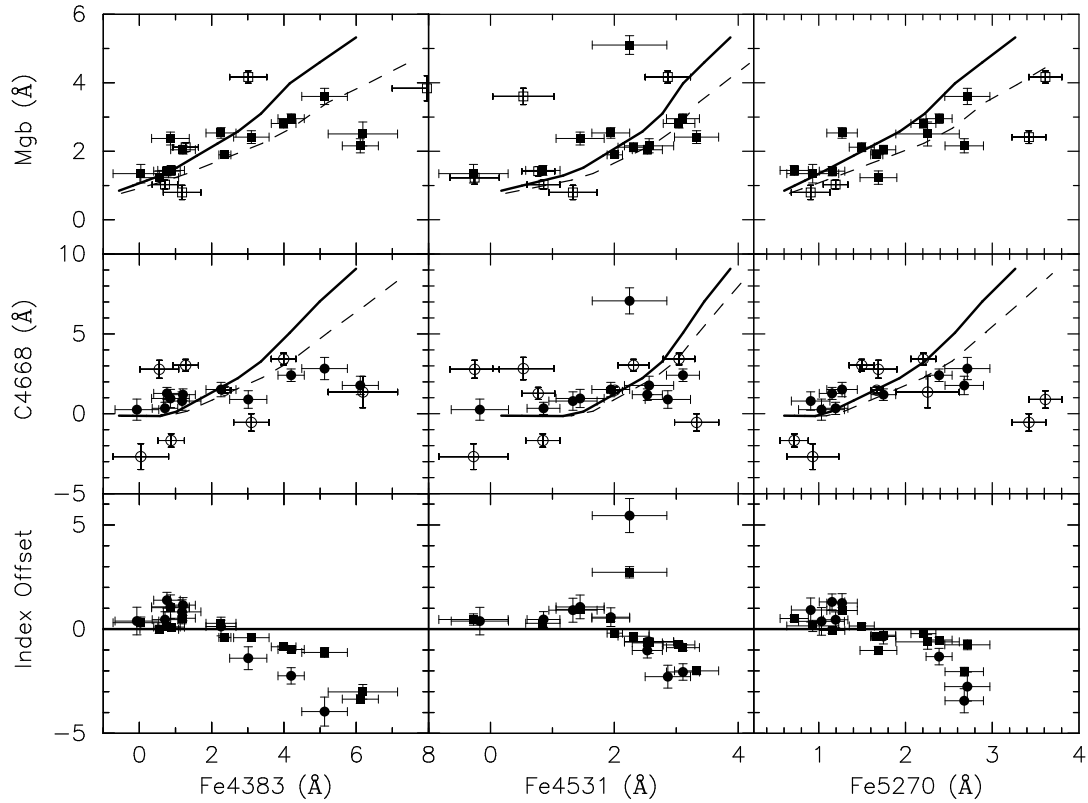


Figure 3.7: The upper row shows the α -element sensitive Mgb index vs three different Iron indices (Fe4383, Fe4531 and Fe5270). The middle row shows C4668 vs the same Iron indices. All six have TMK04 12 Gyr isochrones plotted with $[E/Fe]=+0.3$ as solid and $[E/Fe]=+0.0$ as dashed lines. Filled symbols show where both indices are included in the fit; if either of the indices are not included in the final fit then open symbols are shown. For several plots one or two highly aberrant indices fall outside the range plotted. All six plots show that the α -sensitive indices are above the $[E/Fe]=+0.3$ dex model at low Iron sensitive index values and are below for high Iron values. The bottom row of plots shows the index offset relative to the $[E/Fe]=+0.3$ dex model line, for included indices. Square symbols are Mgb and the circles C4668. A strong trend of decreasing α -element ratio with increasing Iron abundance is seen for both α -element sensitive indices relative to the $[E/Fe]=+0.3$ model expectation.

indices are excluded. For some GCs it is not possible to find a stable fit that includes a large number of indices (>10). This is often the case for the low S/N GCs. The large index errors of low S/N GCs mean that, within 3σ , the indices can be consistent with a wide range of ages and metallicities. In this situation the fit can be driven by a single index which is outside the range spanned by the models, leading to a fit at the extreme of the SSP models. When this occurs the Monte Carlo determined errors are large, reflecting the lower accuracy of these parameters.

To examine the effects of these factors we tested the reliability of the χ^2 fit metallicities by comparing them to Brodie-Huchra metallicities. Fig. 3.4 shows the good agreement between the two metallicity measures, with some divergence below $[\text{Fe}/\text{H}]=-2$ dex. We then used $g-i$ colour as a test of the derived age and metallicity. Model predictions for $g-i$ from BC03, for our χ^2 fit ages and metallicities (derived using TMK04 SSPs), are plotted against the observed $g-i$ colours in Fig. 3.5. We see reasonable agreement between the predicted and observed colours, with the outliers being those low S/N GCs that are at the limits of the models.

Having established the reliability of our χ^2 minimisation fits for age and metallicity, we find all of the GCs are consistent with an old age (≥ 10 Gyrs) within errors and a spread of metallicities is seen from $[\text{Fe}/\text{H}] < -2$ to solar (see Fig. 3.3). We see no discernible age structure.

We next consider the α -element abundance ratio parameter $[\text{E}/\text{Fe}]$. Due to the necessary exclusion of the Mg and CN indices (see Section 3.3), the only strongly α -element sensitive indices included in the fits are Mgb and C4668. However, all the plots of Mgb and C4668 against Fe sensitive indices (Fig. 3.7) display the same overall trend, of decreasing α -element ratio with increasing metallicity. This is highlighted by plotting the residuals of the model $[\text{E}/\text{Fe}]=+0.3$ line to these index pairings. This is also seen for $[\text{E}/\text{Fe}]$ derived from the χ^2 fitting process (Fig. 3.6). A similar trend is apparent for GCs in NGC 1052 (See Fig. 2.9) and is also noted in Puzia (*et al.* 2005). This contrasts with the findings of Carney (1996) for Galactic GCs in which $[\alpha/\text{Fe}]$ is largely constant for GCs of all metallicities. However, the Puzia *et al.* (2005), NGC 3379 and NGC 1052 results are derived from TMK04 models. These models were constructed using the results of Korn, Maraston & Thomas (2005) which included the effects of α -element variation on stars. The application of the Korn *et al.* (2005) models at low metallicity may therefore play a part in generating the observed trend of high α -element ratios for GCs at low metallicity. At such low metallicity we can see from Fig. 3.7 that the indices cannot offer much leverage to differentiate the $[\text{E}/\text{Fe}]$ values. The measurement of $[\text{E}/\text{Fe}]$ is discussed in Section 6.2.3.

However, we note that the α -element ratio trend extends up to the solar metallicity at which the Trippico & Bell (1995) models were calculated. Of particular interest are the two GCs with solar metallicity, $[\text{E}/\text{Fe}]\sim-0.25$ and ages greater than 10 Gyrs. While there is no obvious link, it is interesting to note that X-ray observations of hot gas in the centre of the NGC 5044 galaxy group reveal a similar abundance pattern, of a sub-solar α -element ratio at solar metallicity (Buote *et al.* 2003). A significant number of type Ia, rather than type II, supernovae are therefore necessary to produce enough Iron to explain this abundance pattern. Such a process must have occurred rapidly due to the old ages of the GCs.

3.5 Conclusions

We have obtained Gemini/GMOS spectra for 22 GCs around the elliptical galaxy NGC 3379. We present ages, metallicities and α -abundance ratios that were derived by applying the multi-index χ^2 minimisation method of Proctor & Sansom (2002) to the SSP models of Thomas *et al.* (2004). Metallicity estimates, derived according to the method of Brodie & Huchra (1990), agree closely with those from our χ^2 minimisation method. We also find good agreement between the observed colours and those predicted from our χ^2 minimisation method ages and metallicities. All the GCs are found to be consistent with old ages, i.e. ≥ 10 Gyr, with a wide range of metallicities. This is consistent with the resolved stellar population work of Gregg *et al.* (2004) who found the galaxy stars in the outer regions to be old. We find no evidence for a young GC sub-population. The α -abundance ratios appear to decrease with increasing metallicity, however interpretation of this trend is complex and requires further work.

Chapter 4

Gemini/GMOS Spectra of Globular Clusters in the Virgo Giant Elliptical NGC 4649

This chapter has been published as Pierce et al. , 2006, MNRAS, 368, 325.

4.1 Introduction

Accurately determined ages, metallicities and α -element abundances of globular cluster (GC) systems across the entire range of galaxy types can provide strong constraints for galaxy formation models. One example of such a constraint is the recently observed trend of decreasing α/Fe ratios with increasing metallicity for extra-galactic GC systems (Puzia *et al.* 2005; Chapter 2; Chapter 3). This trend restricts the allowable chemical enrichment histories, relative contribution of Type Ia vs Type II supernova, and star formation timescales for galaxies well beyond the Local Group, where there is little possibility of directly resolving stellar populations.

To accurately measure ages, metallicities and abundance ratios with Lick indices from low-resolution spectra requires a minimum S/N of ~ 30 per \AA , which corresponds to an $\text{H}\beta$ error of $\pm 0.3\text{\AA}$ (Cardiel *et al.* 2003). With an integration time of ~ 8 hours on an 8-metre class telescope it is possible to obtain multi-object spectra to this depth for the brightest GCs of a rich GC system for galaxies within ~ 20 Mpc of the Milky Way.

A major aim of most moderate to high S/N GC spectroscopy has been to measure ages and hence infer when GC formation occurred. Spectroscopic follow-up is a complementary approach to recent photometric results. Rhode, Zepf & Santos (2005) show that the mass-normalised number of blue GCs increases with host galaxy mass. This suggests that the formation of blue GCs is affected by the mass of the host halo. The observed “blue tilt” correlation between GC luminosity and colour of the blue, metal-poor, sub-population (Strader *et al.* 2005; Harris *et al.* 2005) requires significant spectroscopic follow-up to be both confirmed and understood. Another property of the blue sub-population to be studied is the correlation between host galaxy luminosity and mean blue GC sub-population colour (Strader, Brodie & Forbes 2004b), which implies a correlation between galaxy mass and blue

GC metallicity. This is another indication that the formation of blue GCs is affected by the mass of the host halo.

The majority of the most recent GC spectroscopy for large ellipticals has focused on group ellipticals (e.g. NGC 1052 Pierce *et al.* 2005; NGC 3379 Pierce *et al.* 2006a; NGC 3610 Strader *et al.* 2003,2004a; NGC 5128 Peng *et al.* 2004; NGC 2434, NGC 3379, NGC 3585, NGC 5846 and NGC 7192 Puzia *et al.* 2004).

From the literature there are several large ellipticals in clusters for which GC spectra have been analysed to measure ages and metallicities. Cohen, Blakeslee & Ryzhov (1998) present spectral indices for 150 of M87’s GCs. These vary in S/N, with a sizeable fraction of high enough quality to be useful. Co-adding GCs of similar metallicity, they find the GCs are generally old (≥ 10 Gyrs) with metallicities spanning from $[\text{Fe}/\text{H}]=-2$ to above solar. Cohen, Blakeslee & Cote (2003) measure metallicities for 47 GCs associated with NGC 4472 (M49). However the S/N is less than 30 for all of the spectra and therefore ages for individual GCs cannot be measured with any confidence. Beasley *et al.* (2000) co-added spectra for NGC 4472 GCs finding both the metal-rich and metal-poor sub-populations to be old.

For the Fornax cluster, Kissler-Patig *et al.* (1998) measured metallicities for 18 GCs around NGC 1399. Forbes *et al.* (2001) presented higher S/N spectra for 10 GCs and found two to be young (1-2 Gyrs). From the Goudfrooij *et al.* (2001) spectroscopic sample of NGC 1316, only the spectra of 3 exceptionally bright GCs have high enough S/N to measure ages. The Lick indices of all 3 bright GCs indicate a young age (~ 3 Gyrs) corresponding to the host galaxy’s recent merger event. The GC colour-magnitude plot for NGC 1316 is atypical in that there is a significant population of bright, intermediate-colour GCs.

One galaxy with what appears to be conflicting results is NGC 4365 in the Virgo cluster. Brodie *et al.* (2005) present spectroscopic results for NGC 4365 GCs and find some GCs previously thought to belong to an intermediate age sub-population (Larsen *et al.* 2003; Puzia *et al.* 2002), are in fact an intermediate metallicity sub-population with old ages. Kundu *et al.* (2005) present HST NIC3 H-band data and find that these agree with earlier claims of a GC sub-population with intermediate ages 2-8 Gyrs. There appears to be no consensus yet for the GC population of this galaxy, unlike other systems. We return to this galaxy for further discussion in Section 5.2.2.

While possessing a larger GC population, cD and brightest cluster galaxies have the additional complication of GCs potentially associated with the cluster potential. The Virgo cluster elliptical NGC 4649 (M60) is a worthy target for GC spectroscopy as a non-central, giant, cluster elliptical.

NGC 4649 (M60) is luminous, $M_V=-22.38$, and relatively nearby at $D=16.8$ Mpc. UV data for the galaxy light suggests a major old population, plus minor on-going star-formation (Magris & Bruzual 1993). However, from optical spectra, Terlevich & Forbes (2002) measure Lick indices and obtain an age of 11 Gyr, metallicity of $[\text{Fe}/\text{H}]=+0.3$ and $[\text{Mg}/\text{Fe}]=+0.3$ for the central regions of the galaxy. The Chandra X-ray observations of Randall *et al.* (2004) find some structure in the diffuse gas.

The GC imaging study of Forbes *et al.* (2004) found the standard colour bimodality and $S_N=4.1$. Assuming the two sub-populations have similar mass functions, this suggests a similar formation age. NGC 4649 is one of the galaxies with the observed “blue-tilt” (Strader *et al.* 2005). Recently Spitler *et al.* (2006) have

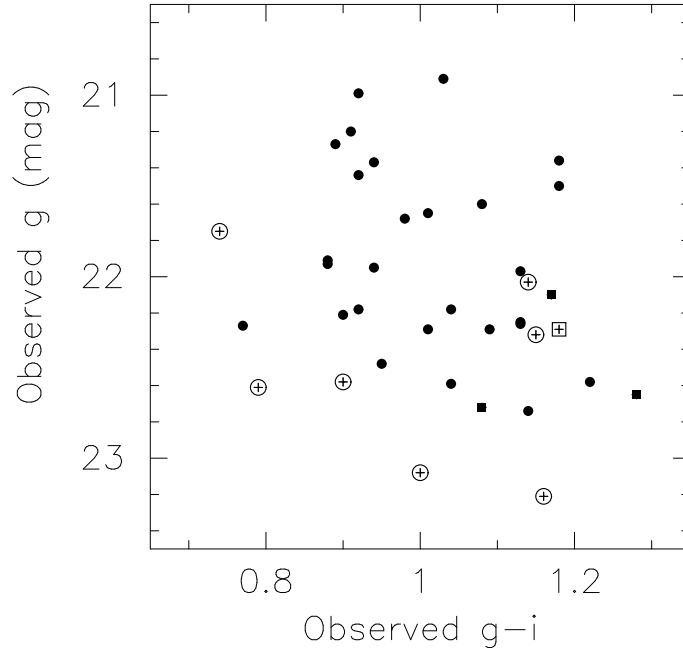


Figure 4.1: NGC 4649 GC colour magnitude diagram from the GMOS imaging. GCs with uncertain fits are shown as open points and young, very metal-rich GCs are shown as squares. The young GCs are all red, but are not amongst the brightest sampled.

shown that the “blue-tilt” is present amongst the GC population of a nearby spiral galaxy, the Sombrero. Unfortunately our spectroscopic sample does not sample far enough down the luminosity function to adequately test hypotheses regarding the “blue-tilt”. We propose observations in Section 5.2.4 to test several “blue-tilt” hypotheses.

4.2 Observations and data reduction

The observations described below are part of Gemini program GN-2002A-Q-13. GC candidates were selected from Gemini North Multi-Object Spectrograph (GMOS; Hook *et al.* 2002) imaging, obtained during 2002 April, for three fields around NGC 4649. The data reduction and GC candidate selection process is described in Forbes *et al.* (2004) and Bridges *et al.* (2006). The colour magnitude diagram of the spectroscopically confirmed GCs is shown in Fig. 4.1.

GMOS masks for three fields were designed, but only the central field was observed within the time allocated. Spectra of NGC 4649 globular clusters were obtained with GMOS on the Gemini North telescope during 2003 on May 31, June 1, June 4 and June 27. Seeing ranged from 0.65–0.9 arc-seconds over the four nights. Exposures of 16×1800 s were taken, yielding a total of 8 hours on-source integration time. Bias frames, dome flat-fields and Copper-Argon (CuAr) arc exposures were taken as part of the Gemini baseline calibrations. From the CuAr arcs, wavelength solutions with typical residuals of 0.1 \AA were achieved.

These data were reduced using the Gemini/GMOS packages in IRAF and a

number of custom made scripts (see Bridges *et al.* 2006 for details). After some experimentation, optimal (variance) extraction was found to yield the best results since our data are over-sampled on the detector. In some cases, objects were too faint to trace individually and we therefore co-added several 2-d images, taken adjacent in time, to act as a reference for the extractions. We verified beforehand that flexure was minimal between the reference images. Finally, the extracted spectra were median combined and weighted by their fluxes with cosmic ray rejection.

In the absence of any velocity standard stars, the recession velocities were measured by using six Bruzual & Charlot (2003) model stellar energy distributions (SEDs) for 14 and 5 Gyr ages with metallicities $[\text{Fe}/\text{H}] = -1.64, -0.33$ and $+0.1$. The task FXCOR in IRAF was used and the average was taken. Objects with recession velocities in the range 1100 ± 600 km/s are potentially associated with NGC 4649. These are presented in Table 4.1. There was one background object (a QSO at $z \sim 0.5$) out of the 39 spectra obtained. Our low contamination rate of 2.5% is due to good imaging and colour selection.

In order to measure Lick indices, we convolved our spectra with a wavelength-dependent Gaussian kernel to match the resolution of the Lick/IDS system (see Beasley *et al.* 2004b). Lick indices (Trager *et al.* 1998) were measured from our spectra. Due to the variable wavelength ranges in these spectra, the same set of indices could not be measured for all spectra. However, all covered a wavelength range of 4500–5500 Å. Uncertainties in the indices were derived from the photon noise in the unfluxed spectra. No Lick standard stars were observed so we therefore cannot fully calibrate the GCs onto the Lick system (see Section 3.2; Pierce *et al.* 2006a). Consequently there are some small systematic differences between some of the measured indices and those used in the SSP models. These issues are discussed further in Sections 4.3 and 4.4. Measured line indices are presented in Tables 4.2 and 4.4. Line index uncertainties are presented in Tables 4.3 and 4.5. The final spectra have $S/N = 5\text{--}21 \text{ \AA}^{-1}$ at 5000 Å, giving errors in the $H\beta$ index of 0.12–0.38 Å. A sample are shown in Fig. 4.2.

4.3 Ages, Metallicities and α -Element Abundance Ratios

In this section we describe the measurement of ages, metallicities and α -element abundances which are presented in Table 4.6. We apply the χ^2 multi-index fitting technique of Proctor & Sansom (2002) for this analysis. This method involves the comparison of the measured Lick indices with SSP models (its application to extra-galactic GCs is described fully in Sections 1.3.2, 2.3.3 and 3.3). The SSP models of Thomas, Maraston & Korn (2004; hereafter TMK04) were chosen because these include the effect of α abundance ratios on the Balmer lines, unlike the models of Bruzual & Charlot (2003) and Vazdekis (1999).

We compare the measured Lick indices to the TMK04 SSPs and obtain a minimum χ^2 fit. This fit is initially sought using all the indices measured. Simultaneously, a set of χ^2 minimisation fits are found with each of the indices omitted. From this set, we select the fit with the lowest total χ^2 , remove the necessary index and repeat until a stable fit is achieved with no highly aberrant ($> 4 \sigma$) indices

Table 4.1: Confirmed globular clusters around NGC 4649. Cluster ID, coordinates, g magnitude and $g-i$ colours are from our GMOS imaging and are instrumental magnitudes only. Heliocentric velocities are from the spectra presented in this work.

ID	R.A. (J2000)	Dec. (J2000)	X (pixels)	Y (pixels)	g (mag)	$g-i$ (mag)	V_{helio} (km/sec)	V_{err} (km/sec)
89	190.983978	11.536740	1324.96	478.67	22.72	1.08	1199.2	43.4
124	190.981033	11.536771	1339.40	621.02	21.91	0.88	833.4	59.6
68	190.986160	11.539418	1447.41	362.65	22.58	1.22	649.3	33.6
148	190.977036	11.545153	1769.64	777.98	22.74	1.14	1184.8	46.8
175	190.974426	11.531744	1120.73	961.31	22.29	1.18	852.3	37.6
183	190.972626	11.538513	1461.97	1019.24	22.26	1.13	1299.4	35.8
158	190.971558	11.589099	3957.80	853.95	23.21	1.16	1261.0	46.0
360	190.949738	11.594447	4316.58	1883.79	21.20	0.91	1270.1	40.1
329	190.957642	11.538593	1531.35	1741.23	21.93	0.88	1511.2	65.3
277	190.962753	11.548118	1978.06	1454.03	22.59	1.04	1299.1	46.5
251	190.960129	11.599953	4542.24	1358.58	22.29	1.09	1099.7	43.9
298	190.960342	11.551459	2153.17	1556.03	22.58	0.90	1063.0	52.5
318	190.959274	11.536565	1424.30	1671.14	23.08	1.00	1173.4	48.6
606	190.936737	11.548500	2110.58	2706.89	21.36	1.18	627.0	39.6
558	190.938461	11.555140	2430.02	2595.52	21.75	0.74	1087.8	50.8
434	190.949310	11.528630	1077.12	2185.82	22.18	1.04	925.9	36.6
462	190.947189	11.532343	1269.20	2272.22	22.18	0.92	1112.8	45.4
517	190.942352	11.539107	1623.47	2476.30	22.03	1.14	857.2	56.3
412	190.945847	11.582625	3751.32	2121.39	22.48	0.95	483.6	47.5
502	190.942627	11.559628	2632.89	2375.35	22.10	1.17	688.6	43.5
640	190.931168	11.586047	3984.06	2815.36	22.61	0.79	1015.5	104.5
740	190.932129	11.529132	1176.86	3012.11	21.68	0.98	962.1	44.8
806	190.929291	11.538971	1673.81	3107.00	21.50	1.18	1197.4	46.2
899	190.927261	11.533805	1428.31	3227.10	21.44	0.92	1372.0	42.7
975	190.924591	11.539021	1696.82	3333.25	20.99	0.92	1052.2	42.3
1063	190.920807	11.535969	1563.10	3529.46	21.37	0.94	953.9	47.3
1011	190.918243	11.596663	4563.36	3393.26	21.95	0.94	1135.0	45.7
1037	190.919540	11.564267	2962.26	3469.39	21.97	1.13	1017.1	42.6
1145	190.916580	11.532989	1434.77	3745.73	21.60	1.08	926.8	47.3
1252	190.910614	11.544307	2018.25	3985.40	21.27	0.89	1134.2	47.0
1384	190.906281	11.550952	2364.45	4165.70	20.91	1.03	1122.0	58.2
1126	190.918457	11.526026	1083.67	3685.07	22.21	0.90	1346.1	47.9
1298	190.909515	11.536103	1619.00	4073.00	22.25	1.13	1324.5	38.0
1211	190.912033	11.544750	2033.87	3914.83	22.29	1.01	889.3	69.3
1098	190.914841	11.581110	3812.20	3623.63	22.27	0.77	1305.2	39.3
1182	190.911743	11.562973	2932.52	3850.43	22.32	1.15	1454.0	45.1
1574	190.896591	11.602605	4950.56	4411.99	21.65	1.01	703.0	53.9
1443	190.904984	11.551611	2402.56	4225.51	22.65	1.28	667.9	63.4

Table 4.2: Globular cluster indices $\lambda < 4600$ Å. Indices in brackets are removed during the fitting process. Missing values are due to limited wavelength coverage. Index errors are presented in Table 3.

ID	H δ_A (Å)	H δ_F (Å)	CN ₁ (mag)	CN ₂ (mag)	Ca4227 (Å)	G band (Å)	H γ_A (Å)	H γ_F (Å)	Fe4383 (Å)	Ca4455 (Å)	Fe4531 (Å)
89	(-8.936)	(-0.154)	(0.125)	(0.165)	0.448	5.290	-1.691	0.944	2.259	1.085	1.939
124	3.226	2.950	(-0.008)	(0.035)	0.621	(3.662)	1.155	2.004	1.883	0.008	1.310
68	(2.165)	(3.963)	(0.033)	(0.101)	1.045	5.253	-5.858	-0.766	(8.650)	2.139	(5.030)
148	(-10.481)	(-3.591)	(0.295)	(0.357)	1.440	(2.541)	(-3.292)	(0.473)	6.518	0.823	3.553
175	(-2.707)	(-0.900)	(0.168)	(0.173)	1.016	2.234	-2.255	-0.180	2.729	2.310	3.974
183	0.270	0.831	(0.083)	(0.051)	-0.004	5.785	-3.500	-0.165	4.196	1.225	2.247
158	-3.139	-0.488	(0.180)	(0.151)	0.882	6.213	-1.419	0.893	3.112	1.406	3.244
360	0.865	3.528	-1.488	0.556	2.904	1.068	2.187
329	1.989	1.520	(-0.085)	(-0.078)	0.305	(1.784)	-0.260	0.830	2.898	0.702	0.928
277	(0.415)	(2.965)	(-0.070)	(-0.041)	0.614	4.777	-6.229	-2.614	4.175	0.609	2.223
251	6.561	-4.919	-1.155	2.320	(0.087)	2.617
298	3.471	(-1.123)	(-0.137)	(-0.142)	(-1.050)	0.375	(3.654)	(3.162)	1.359	(1.426)	0.426
318	(-6.529)	(-2.985)	(0.181)	(0.190)	1.187	4.917	0.321	1.237	-1.053	0.943	(6.004)
606	-0.875	0.697	(0.145)	(0.197)	(0.401)	5.062	-5.650	-1.572	4.103	1.209	3.229
558	3.361	2.874	(-0.061)	(-0.030)	0.183	(3.782)	1.268	(3.135)	(3.474)	0.382	1.311
434	-0.600	-0.655	(0.027)	(0.060)	0.182	6.155	-4.006	-1.522	(0.478)	0.618	2.909
462	0.503	2.451	(0.096)	(0.122)	1.444	5.113	-3.244	-0.350	0.392	0.793	2.908
517	(4.415)	(4.534)	(0.043)	(0.033)	(-0.051)	4.880	-3.174	-0.156	2.425	1.193	2.759
412	0.235	0.859	(-0.054)	(-0.072)	(-0.867)	4.880	-3.487	0.392	2.514	1.509	1.864
502	(-4.873)	(-1.419)	(0.209)	(0.225)	1.121	5.483	-4.837	-0.666	4.282	(0.933)	4.245
640	(1.353)	(1.588)	(0.035)	(0.052)	(2.221)	0.728	(6.237)	3.149	-4.268	1.415	0.314
740	2.822	3.308	(0.011)	(0.027)	0.617	3.172	-0.098	1.478	2.720	0.625	1.785
806	(-5.422)	(-1.911)	(0.302)	(0.361)	1.077	(3.982)	-6.102	-0.699	6.163	1.663	3.206
899	1.250	1.462	(0.024)	(0.068)	0.831	4.754	-2.170	0.321	2.233	0.133	2.367
975	3.233	2.390	(-0.030)	(0.022)	0.478	3.632	-0.767	0.980	1.782	0.150	2.049
1063	0.349	1.798	(0.028)	(0.057)	0.076	2.937	-1.370	1.176	3.206	0.733	1.619
1011	(5.206)	-1.727	(1.520)	3.486	(-0.183)	2.550
1037	-0.260	-1.406	(0.148)	(0.202)	(0.405)	(1.864)	(-2.044)	-0.808	3.080	0.460	4.094
1145	-0.414	0.605	(0.083)	(0.107)	0.635	5.077	-3.217	-0.668	2.842	1.186	2.451
1252	1.541	2.265	(0.048)	(0.076)	0.694	3.673	-1.594	0.725	2.029	0.125	1.823
1384	(-0.236)	(1.215)	(0.068)	(0.092)	0.618	3.596	-1.039	0.727	1.054	0.569	2.381
1126	(-1.003)	(1.215)	(0.078)	(0.105)	0.032	(2.886)	1.166	2.330	(5.764)	1.223	0.288
1298	(-3.213)	(1.650)	(0.131)	(0.179)	0.643	5.052	-3.889	-0.447	4.607	1.422	2.993
1211	(-2.832)	(0.173)	(0.222)	(0.245)	1.118	4.989	-2.369	0.862	2.320	0.751	1.741
1098	2.101	1.964	(0.002)	(0.018)	(-1.346)	3.909	1.203	1.692	-0.399	-0.643	1.470
1182	-1.099	0.500	(0.204)	(0.231)	0.705	3.754	-4.786	-0.178	5.309	0.547	1.187
1574	0.443	2.740
1443	(-8.897)	(-2.203)	(0.250)	(0.350)	1.441	3.752	-4.720	-0.683	5.693	(-1.506)	(0.000)

Table 4.3: Globular cluster indices errors $\lambda < 4600 \text{ \AA}$. Missing values are due to limited wavelength coverage. Index errors are derived from photon noise in the unfluxed spectra.

ID	H δ_A (\AA)	H δ_F (\AA)	CN $_1$ (mag)	CN $_2$ (mag)	Ca4227 (\AA)	G band (\AA)	H γ_A (\AA)	H γ_F (\AA)	Fe4383 (\AA)	Ca4455 (\AA)	Fe4531 (\AA)
89	0.822	0.472	0.017	0.020	0.322	0.500	0.539	0.328	0.731	0.356	0.530
124	0.375	0.253	0.011	0.013	0.204	0.341	0.336	0.208	0.494	0.252	0.368
68	0.594	0.365	0.017	0.019	0.305	0.492	0.572	0.345	0.616	0.326	0.466
148	0.851	0.554	0.018	0.021	0.309	0.551	0.566	0.336	0.686	0.369	0.519
175	0.606	0.413	0.015	0.018	0.261	0.472	0.458	0.293	0.610	0.281	0.420
183	0.515	0.353	0.014	0.016	0.271	0.399	0.455	0.281	0.571	0.284	0.418
158	0.989	0.649	0.024	0.028	0.436	0.656	0.729	0.459	0.971	0.478	0.667
360	0.160	0.273	0.281	0.175	0.383	0.188	0.280
329	0.397	0.279	0.011	0.013	0.212	0.367	0.351	0.223	0.494	0.245	0.371
277	0.597	0.368	0.016	0.019	0.304	0.505	0.579	0.381	0.692	0.353	0.515
251	0.433	0.524	0.331	0.673	0.332	0.459
298	0.499	0.421	0.015	0.017	0.321	0.493	0.429	0.263	0.692	0.325	0.514
318	0.730	0.504	0.018	0.021	0.325	0.562	0.582	0.366	0.888	0.428	0.570
606	0.384	0.257	0.010	0.012	0.181	0.284	0.323	0.204	0.389	0.193	0.277
558	0.364	0.246	0.011	0.012	0.201	0.328	0.321	0.187	0.454	0.236	0.351
434	0.514	0.378	0.013	0.015	0.248	0.371	0.438	0.286	0.599	0.286	0.403
462	0.488	0.310	0.013	0.015	0.220	0.383	0.424	0.267	0.581	0.279	0.406
517	0.496	0.312	0.014	0.016	0.267	0.387	0.428	0.266	0.569	0.278	0.394
412	0.561	0.386	0.015	0.018	0.318	0.460	0.519	0.312	0.690	0.328	0.485
502	0.625	0.414	0.014	0.017	0.248	0.401	0.458	0.283	0.557	0.278	0.391
640	0.579	0.400	0.016	0.018	0.263	0.522	0.424	0.279	0.798	0.351	0.560
740	0.362	0.235	0.010	0.012	0.194	0.318	0.317	0.195	0.448	0.228	0.332
806	0.469	0.313	0.011	0.013	0.187	0.309	0.346	0.206	0.399	0.206	0.302
899	0.336	0.231	0.009	0.011	0.167	0.276	0.298	0.186	0.404	0.204	0.291
975	0.257	0.179	0.007	0.009	0.137	0.226	0.232	0.144	0.331	0.169	0.242
1063	0.333	0.219	0.009	0.010	0.170	0.278	0.280	0.169	0.382	0.194	0.287
1011	0.366	0.404	0.238	0.540	0.284	0.392
1037	0.503	0.381	0.013	0.015	0.245	0.412	0.405	0.264	0.542	0.272	0.370
1145	0.401	0.274	0.010	0.012	0.189	0.302	0.334	0.214	0.435	0.212	0.313
1252	0.302	0.200	0.008	0.010	0.151	0.255	0.266	0.165	0.372	0.191	0.276
1384	0.276	0.184	0.007	0.009	0.135	0.227	0.228	0.143	0.324	0.159	0.231
1126	0.491	0.321	0.013	0.015	0.248	0.403	0.387	0.234	0.521	0.273	0.429
1298	0.572	0.340	0.014	0.016	0.259	0.410	0.458	0.285	0.568	0.283	0.421
1211	0.574	0.376	0.014	0.016	0.243	0.403	0.441	0.267	0.595	0.295	0.438
1098	0.473	0.323	0.013	0.016	0.282	0.416	0.407	0.255	0.627	0.326	0.460
1182	0.562	0.376	0.015	0.017	0.262	0.441	0.479	0.289	0.579	0.310	0.437
1574	0.230	0.327
1443	0.828	0.524	0.017	0.020	0.298	0.520	0.560	0.347	0.667	0.389	0.532

Table 4.4: Globular cluster indices $\lambda > 4600 \text{ \AA}$. Indices in brackets are removed during the fitting process. Missing values are due to limited wavelength coverage. Index errors are presented in Table 5.

ID	C4668 (\AA)	H β (\AA)	Fe5015 (\AA)	Mg ₁ (mag)	Mg ₂ (mag)	Mgb (\AA)	Fe5270 (\AA)	Fe5335 (\AA)	Fe5406 (\AA)	Fe5709 (\AA)	Fe5782 (\AA)
89	3.089	(0.060)	6.110	(0.022)	(0.140)	3.582	1.318	2.239	1.677
124	-0.554	2.540	2.414	(-0.023)	(0.055)	1.740	1.433	1.686	0.771
68	3.689	1.188	(2.959)	(0.030)	(0.207)	3.641	2.867	(3.201)	1.719
148	4.343	1.559	5.026	(0.021)	(0.125)	3.140	2.632	1.258	1.386
175	6.261	1.336	4.277	(0.079)	(0.209)	3.148	2.794	2.074	1.612
183	0.592	2.337	4.266	(0.021)	(0.149)	3.265	2.208	1.830	1.233
158	2.391	0.326	3.733	(0.010)	(0.147)	3.022	2.638	1.438	1.376	0.823	1.039
360	2.034	2.574	3.346	(0.011)	(0.093)	2.057	1.726	1.386	1.017	0.549	0.248
329	1.044	2.401	3.422	(-0.018)	(0.059)	1.844	1.085	0.730	0.342
277	1.967	0.693	3.140	(0.047)	(0.148)	3.575	2.039	1.968	1.142
251	3.537	1.213	5.896	(0.060)	(0.221)	4.205	1.952	2.026	1.621	0.600	0.666
298	-0.013	2.302	2.896	(0.019)	(0.037)	1.072	(1.647)	1.052	1.083
318	(-5.908)	0.490	-1.582	(-0.032)	(0.093)	2.665	-0.015	2.098	1.380
606	4.089	1.486	4.178	(0.102)	(0.242)	3.531	(1.912)	(2.670)	(1.665)
558	-1.369	2.326	2.665	(0.010)	(0.044)	(0.671)	1.889	1.503	0.607
434	2.491	1.878	2.343	(0.025)	(0.123)	2.506	2.118	1.852	0.903
462	2.792	1.203	(2.264)	(0.023)	(0.104)	2.234	2.104	0.806	0.988
517	4.152	(1.208)	4.771	(0.080)	(0.201)	3.094	(3.386)	1.581	1.391
412	3.400	(0.110)	3.138	(0.041)	(0.106)	2.258	(0.861)	2.101	1.017	0.451	0.812
502	7.967	2.025	6.563	(0.107)	(0.287)	5.055	2.396	3.027	1.513	0.555
640	2.724	2.310	0.315	(-0.055)	(-0.067)	(-0.753)	-0.508	1.176	(-0.343)	0.189	(0.752)
740	0.912	1.340	(4.897)	(0.010)	(0.109)	2.759	1.770	1.713	0.935
806	4.799	0.995	(2.748)	(0.076)	(0.282)	(5.771)	2.819	2.265	1.744
899	1.132	1.847	2.220	(0.002)	(0.090)	2.692	1.416	(1.844)	0.903
975	0.648	2.222	3.512	(-0.004)	(0.083)	2.330	1.691	1.420	0.711
1063	2.715	2.109	3.420	(-0.008)	(0.086)	1.769	1.693	1.530	0.959
1011	3.098	1.602	2.698	(0.072)	(0.135)	(1.685)	1.984	0.972	1.159	0.508	0.430
1037	(5.808)	1.082	5.031	(0.078)	(0.233)	3.307	2.351	1.509	(-0.189)	(-0.008)	0.410
1145	3.328	1.800	5.140	(0.041)	(0.182)	3.746	2.080	1.744	1.449
1252	0.854	2.480	4.032	(-0.016)	(0.084)	(1.908)	1.484	1.480	0.726
1384	(4.074)	1.862	2.771	(0.059)	(0.150)	2.590	1.839	1.390	(1.181)
1126	0.487	2.999	1.284	(-0.013)	(0.065)	1.288	0.919	0.772	0.099
1298	1.132	1.634	2.884	(0.014)	(0.141)	3.575	1.882	1.781	0.972
1211	1.910	1.433	2.478	(0.036)	(0.192)	(2.128)	2.149	(2.962)	(1.666)
1098	-1.524	(0.813)	2.016	(-0.038)	(0.041)	2.144	1.139	0.298	-0.282	0.883	0.180
1182	5.486	1.656	5.991	(0.103)	(0.257)	(5.120)	1.632	2.840	1.048	(1.795)	0.985
1574	0.993	1.899	3.024	(0.031)	(0.109)	(2.388)	1.254	0.543	1.067	0.395	0.328
1443	6.813	1.976	(8.367)	(0.028)	(0.217)	(5.264)	(0.929)	(1.110)	2.288

Table 4.5: Globular cluster indices errors $\lambda > 4600 \text{ \AA}$. Missing values are due to limited wavelength coverage. Index errors are derived from photon noise in the unfluxed spectra.

ID	C4668 (\AA)	H β (\AA)	Fe5015 (\AA)	Mg $_1$ (mag)	Mg $_2$ (mag)	Mgb (\AA)	Fe5270 (\AA)	Fe5335 (\AA)	Fe5406 (\AA)	Fe5709 (\AA)	Fe5782 (\AA)
89	0.746	0.284	0.535	0.006	0.006	0.245	0.283	0.309	0.222
124	0.539	0.186	0.393	0.004	0.005	0.179	0.199	0.224	0.165
68	0.702	0.261	0.527	0.005	0.006	0.231	0.247	0.273	0.206
148	0.743	0.277	0.566	0.006	0.007	0.253	0.278	0.324	0.234
175	0.595	0.224	0.453	0.005	0.005	0.207	0.221	0.250	0.183
183	0.615	0.213	0.443	0.004	0.005	0.201	0.220	0.251	0.182
158	1.010	0.384	0.756	0.007	0.009	0.335	0.358	0.416	0.301	0.223	0.206
360	0.405	0.144	0.307	0.003	0.004	0.139	0.153	0.173	0.127	0.095	0.090
329	0.533	0.189	0.400	0.004	0.005	0.183	0.206	0.235	0.172
277	0.734	0.272	0.558	0.005	0.006	0.239	0.266	0.302	0.223
251	0.652	0.247	0.487	0.005	0.006	0.218	0.243	0.272	0.198	0.152	0.140
298	0.737	0.257	0.549	0.005	0.006	0.254	0.272	0.319	0.229
318	0.984	0.348	0.751	0.007	0.008	0.309	0.363	0.391	0.282
606	0.406	0.149	0.311	0.003	0.004	0.140	0.152	0.166	0.123
558	0.523	0.181	0.389	0.004	0.004	0.182	0.194	0.222	0.163
434	0.584	0.209	0.446	0.004	0.005	0.201	0.221	0.249	0.184
462	0.591	0.222	0.455	0.005	0.005	0.207	0.227	0.265	0.190
517	0.563	0.212	0.422	0.004	0.005	0.190	0.199	0.232	0.169
412	0.707	0.279	0.547	0.005	0.006	0.246	0.276	0.303	0.225	0.170	0.156
502	0.548	0.209	0.424	0.004	0.005	0.192	0.215	0.235	0.174	0.131
640	0.774	0.283	0.621	0.006	0.007	0.285	0.316	0.349	0.262	0.188	0.173
740	0.482	0.174	0.350	0.004	0.004	0.162	0.181	0.206	0.151
806	0.433	0.164	0.341	0.003	0.004	0.141	0.160	0.180	0.131
899	0.428	0.154	0.322	0.003	0.004	0.144	0.163	0.183	0.135
975	0.354	0.125	0.262	0.003	0.003	0.118	0.132	0.150	0.110
1063	0.412	0.149	0.310	0.003	0.004	0.144	0.156	0.177	0.129
1011	0.566	0.213	0.444	0.004	0.005	0.203	0.214	0.247	0.179	0.135	0.127
1037	0.530	0.206	0.414	0.004	0.005	0.185	0.198	0.223	0.169	0.125	0.115
1145	0.446	0.164	0.330	0.003	0.004	0.150	0.168	0.190	0.137
1252	0.402	0.138	0.290	0.003	0.003	0.136	0.150	0.171	0.126
1384	0.323	0.118	0.253	0.002	0.003	0.114	0.127	0.142	0.103
1126	0.607	0.203	0.455	0.004	0.005	0.208	0.230	0.262	0.193
1298	0.617	0.223	0.458	0.004	0.005	0.198	0.224	0.252	0.186
1211	0.624	0.226	0.464	0.005	0.005	0.220	0.230	0.253	0.188
1098	0.686	0.255	0.510	0.005	0.006	0.226	0.258	0.299	0.221	0.158	0.155
1182	0.608	0.232	0.456	0.005	0.005	0.197	0.226	0.245	0.186	0.133	0.129
1574	0.483	0.174	0.369	0.004	0.004	0.166	0.185	0.213	0.150	0.114	0.106
1443	0.692	0.263	0.504	0.005	0.006	0.230	0.280	0.311	0.218

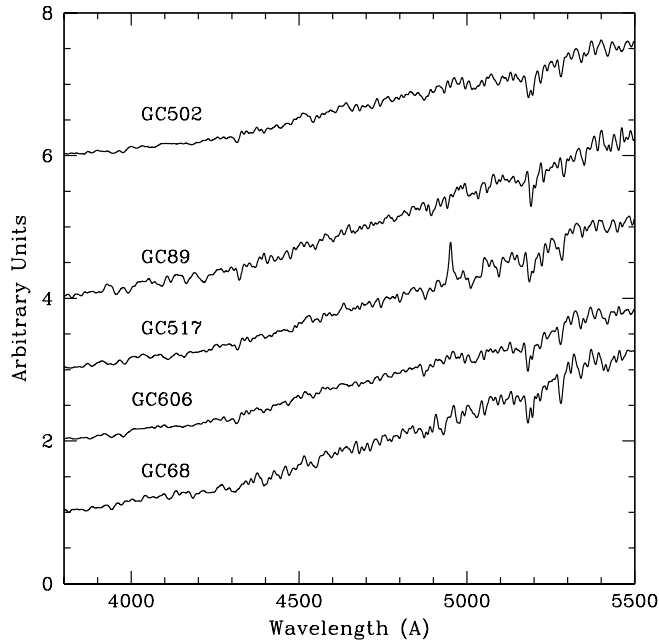


Figure 4.2: Sample GC spectra for NGC 4649. These spectra have not been de-redshifted. These sample spectra display a range of S/N and age. The top two are found to be young, GC517 in the middle has an uncertain, but potentially intermediate, age and the bottom two GCs are examples of old GCs.

remaining. All GCs had some indices that were significant outliers to the fit and therefore removed during this process. The errors given for the derived parameters are statistical 1σ confidence intervals calculated by a Monte Carlo style method (see Proctor *et al.* 2004 and Section 2.3.3 for details).

The molecular band indices Mg_1 and Mg_2 are systematically offset due to a number of calibration issues and were excluded for all GCs (see Proctor *et al.* 2005; Section 3.2). Similar to other GC studies (e.g. Beasley *et al.* 2004a) we find the CN indices to be enhanced relative to the models and therefore they were also removed.

From our sample of 38 GCs, 8 had poor or uncertain fits. We will identify these with open symbols in all figures. In particular, GC 640 is found to be very metal-poor. We find a Brodie-Huchra metallicity of -2.6 dex, which is 0.85 dex lower than any other GC in this sample. Many of the metal sensitive indices are below the values spanned by the SSP grids. One consequence of the low $[Fe/H]$ is a high $[E/Fe]$ uncertainty.

For GC 1443 there exists a conflict between the indices Fe4531, Fe5270 and Fe5335 which suggest a low metallicity and Fe4383, C4668, Fe5406, Fe5015 and Mgb which suggest the GC has super-solar metallicity. We find the more compelling fit is for a young and super metal-rich GC, however, this result is uncertain. Neither the Brodie-Huchra metallicity nor the photometric colours offer any strong constraint.

Low S/N makes a stable fit difficult for GCs 158 and 318. The inclusion or exclusion of single indices that are well below any clipping threshold can change the resulting fit. GC 318 is potentially part of the so-called “H” GC sub-population noted by Strader *et al.* (2005) of intermediate colour GCs, at approximately the

Table 4.6: Derived globular cluster properties. Age, [Fe/H], [E/Fe] and [Z/H] are derived from the χ^2 minimisation process, with errors derived by a Monte Carlo style method. [Fe/H]_{BH} is derived according to the method of Brodie & Huchra (1990) from a reduced sample of indices.

ID	Age (Gyr)	[Fe/H] (dex)	[E/Fe] (dex)	[Z/H] (dex)	[Fe/H] _{BH} (dex)	Notes
89	2.4±0.6	-0.29±0.15	0.36±0.07	0.05±0.11	-0.86	
124	15±6.0	-1.23±0.16	0.00±0.20	-1.23±0.12	-1.60	
68	15±4.4	-0.29±0.13	0.12±0.11	-0.18±0.08	-0.53	
148	14.1±5.1	-0.34±0.13	0.12±0.10	-0.23±0.09	-1.13	
175	2.4±0.4	0.04±0.11	0.12±0.09	0.15±0.09	-0.51	
183	8.9±2.7	-0.63±0.12	0.32±0.10	-0.33±0.11	-0.73	
158	7.9±3.6	-0.45±0.21	0.18±0.18	-0.28±0.17	-0.78	Low S/N
360	7.1±2.1	-0.87±0.11	0.21±0.07	-0.68±0.11	-1.32	
329	11.9±2.1	-1.47±0.15	0.42±0.15	-1.08±0.09	-1.55	
277	15±2.7	-0.50±0.12	0.24±0.10	-0.28±0.07	-0.75	
251	15±2.7	-0.58±0.10	0.46±0.08	-0.15±0.07	-0.34	
298	15±6.5	-1.14±0.22	-0.30±0.18	-1.43±0.15	-1.74	NGC 6171 Analog
318	12.6±4.4	-1.75±0.20	0.80±0.14	-1.00±0.17	-1.41	Low S/N
606	15±2.4	-0.45±0.10	0.24±0.07	-0.23±0.05	-0.33	
558	15±6.1	-1.02±0.15	-0.30±0.15	-1.30±0.11	-1.25	Stripped Dwarf?
434	12.6±2.6	-0.60±0.12	0.21±0.08	-0.40±0.09	-0.63	
462	12.6±3.7	-1.03±0.13	0.46±0.09	-0.60±0.12	-0.90	
517	5.6±1.7	-0.46±0.15	0.30±0.10	-0.18±0.10	-0.70	
412	7.9±3.2	-0.57±0.16	0.18±0.13	-0.40±0.16	-1.07	
502	3.0±0.8	0.17±0.11	0.38±0.05	0.53±0.11	-0.39	
640	13.3±4.6	-2.83±0.40	0.80±0.38	-2.08±0.25	-2.60	Very low metallicity
740	15±5.4	-1.33±0.14	0.40±0.10	-0.95±0.12	-1.14	
806	11.2±2.1	-0.10±0.09	-0.03±0.11	-0.13±0.08	-0.13	
899	11.9±2.1	-1.25±0.11	0.53±0.10	-0.75±0.08	-1.13	
975	15±4.7	-1.32±0.09	0.42±0.08	-0.93±0.06	-1.19	
1063	7.5±2.4	-0.72±0.13	-0.09±0.12	-0.80±0.10	-1.22	
1011	15±4.1	-1.01±0.14	0.36±0.24	-0.68±0.18	-0.66	
1037	15±2.9	-0.58±0.12	0.30±0.09	-0.30±0.07	-0.43	
1145	8.4±1.8	-0.53±0.09	0.38±0.06	-0.18±0.06	-0.69	
1252	8.4±2.3	-1.08±0.11	0.30±0.10	-0.80±0.10	-1.53	
1384	15±5.2	-1.26±0.14	0.46±0.08	-0.83±0.12	-0.95	
1126	8.9±2.5	-2.18±0.28	0.59±0.24	-1.63±0.19	-1.63	
1298	15±3.5	-0.82±0.12	0.42±0.10	-0.43±0.09	-0.89	
1211	15±4.8	-1.18±0.17	0.56±0.19	-0.65±0.14	-0.74	
1098	15±2.6	-2.00±0.13	0.80±0.12	-1.25±0.08	-1.72	
1182	5.3±1.4	-0.07±0.12	-0.06±0.14	-0.13±0.09	-0.73	
1574	11.9±2.6	-1.33±0.14	0.40±0.24	-0.95±0.15	-1.23	
1443	2.1±0.6	0.57±0.16	-0.21±0.10	0.38±0.17	-1.06	Complex metal lines

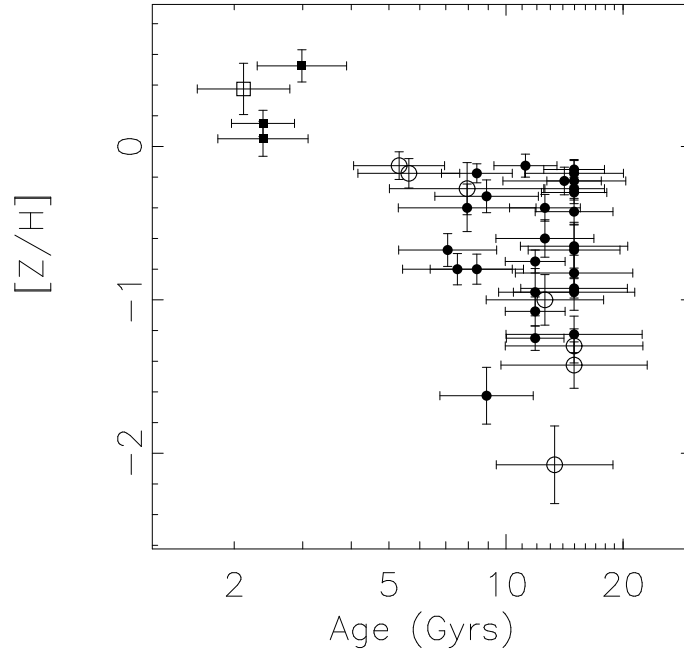


Figure 4.3: SSP fit metallicities and ages. GCs with uncertain fits are shown as open points. The majority of GCs are old (≥ 10 Gyrs) with a small number of young, very metal-rich GCs (shown as squares) and several GCs with potentially intermediate ages.

turn-over magnitude. GC 158 is in the magnitude range as well, but is too red to be considered a part of this sub-population.

For GC 298, $H\beta$ and $H\gamma$ suggest different ages (similar to the Galactic GC NGC 6171, see Proctor *et al.* 2004). The metal sensitive indices suggest that this GC is metal-poor and therefore more likely to be older than 5 Gyrs.

The ACS images (Proposal 9401, see Bridges *et al.* 2006) show GC 558 is extended and therefore is possibly a stripped dwarf. The χ^2 fit for 558 gives an old, metal-poor population with an apparently negative $[E/Fe]$. If this really is a stripped dwarf we do not necessarily expect to be able to fit it with a single stellar population due to potential stellar population gradients. We note that there are complex issues with sky subtraction around Mgb for this object on some nights, therefore Mgb is not included in the fit for this object.

We find two GCs, 517 and 1182, which appear to be of intermediate age ~ 5 Gyrs. Both are around solar metallicity ($[Z/H] \sim 0$), but with differing $[E/Fe]$ ($+0.3$ vs -0.06). It is not clear whether these GCs are in fact intermediate aged or if the age-metallicity degeneracy is not broken effectively in these cases.

The three clearly young and metal-rich GCs are 89, 175 and 502; these will be shown as squares on all plots. Their α -element abundance ratios are all $[E/Fe] \sim 0.3$ within errors. These α -element abundances are approximately 0.3 dex higher than for the old GC population at solar metallicity, tentatively suggesting a chemical enrichment history involving substantial star-formation and recent SN type II. It is interesting to note that these GCs are not amongst the brightest objects in our sample (Fig. 4.1). All three are observed to be photometrically red. See Section 4.4 for more on the young GCs.

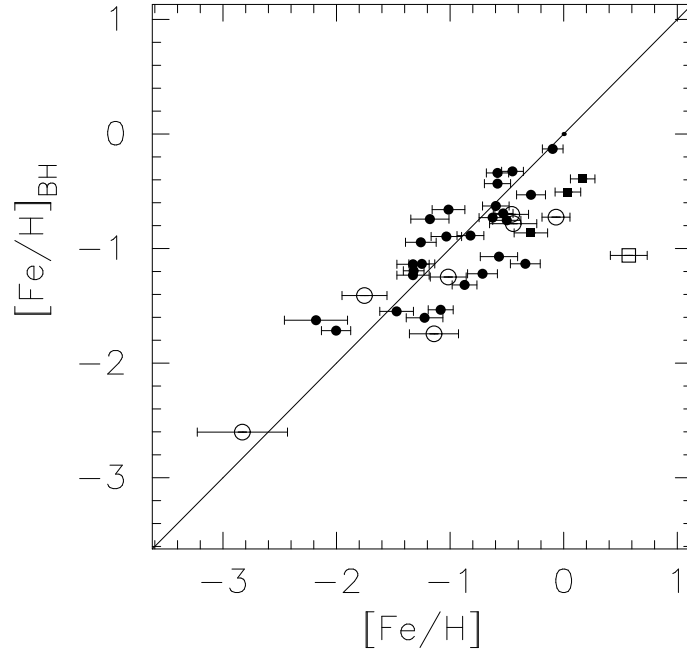


Figure 4.4: Brodie-Huchra metallicity is shown against SSP metallicity. The open points are GCs for which the χ^2 fits are uncertain. This plot shows a general trend of agreement for the majority of GCs. Young GCs are shown as square symbols. The clear outlier is GC 1443 where there are both strong and weak metal indices present in the spectrum.

In summary, within errors, we find that the majority of GCs are consistent with an old age (≥ 10 Gyrs). There are two GCs with potentially intermediate ages ~ 5 Gyrs, three GCs that are definitely young (2-3 Gyrs) and another GC that is most likely young.

One means to test our SSP-derived metallicities is to compare them with those derived by the Brodie & Huchra (1990; BH) method, which was originally calibrated to old stellar populations. Fig. 4.4 shows good agreement for the SSP-derived metallicities of old GCs and estimates from the BH method. One would expect the BH method to give lower metallicities for young stellar populations. However, the “young” objects (ages < 5 Gyrs), while systematically offset from the one-to-one line by ~ 0.5 dex, are within the scatter of the full sample.

A clear trend of decreasing $[E/Fe]$ with increasing $[Fe/H]$ is seen in Fig. 4.5. For GCs associated with NGC 3379, Pierce *et al.* (2006a) used the index-index plots to confirm the suggestion of a trend in the χ^2 fit α -element abundances. Similar index-index plots for NGC 4649 GCs do not show the trend that is seen in the fitted parameters. In the case presented here there is the added complication of age differences between GCs, whereas the NGC 3379 GCs in Chapter 3 were found to be universally old. It should be noted that we find no trend of α -element abundance ratios with age.

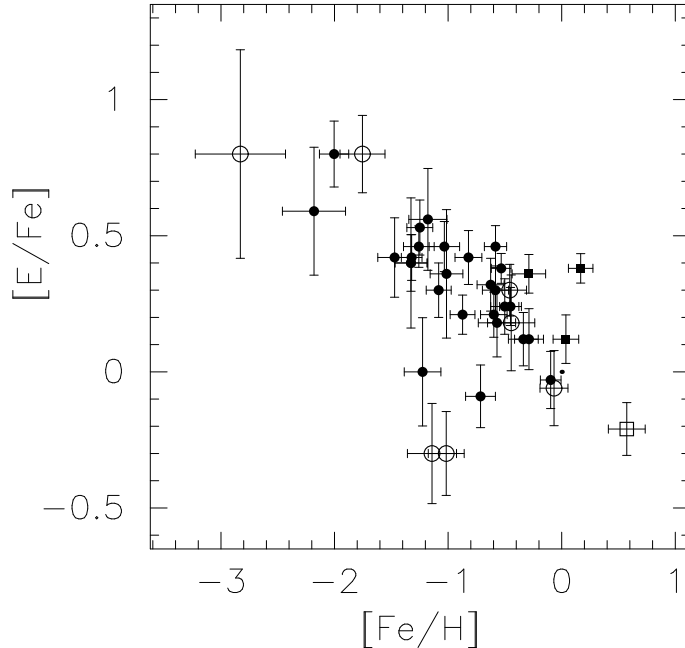


Figure 4.5: Alpha element abundance ratio vs metallicity. The open points are GCs for which the χ^2 fits are uncertain and the squares are young GCs. There appears to be a strong trend of decreasing $[E/Fe]$ with increasing $[Fe/H]$. However the significance of this trend is highly dependent on the low metallicity GCs ($[Fe/H] < -1.5$) for which $[E/Fe]$ is very difficult to determine.

4.4 Discussion

One of the more important factors for the χ^2 fitting analysis used in this work is the determination of errors. Uncertainties in the background subtraction of sky and galaxy light introduces Lick index errors in addition to the easily quantifiable Poisson noise. The relative effect of these errors increases for fainter GCs, so in reality not only do fainter GCs have larger index errors, but also those errors are increasingly underestimated.

Assuming Gaussian errors due to photon noise, 95% of measurements should be within 2σ . For most objects we measure ~ 16 indices, which means that when we apply a 2σ clip, only 1 index measurement should be excluded on average per object. For the application of χ^2 fitting to extragalactic GCs this is clearly not the case as we are often forced to exclude 3-7 indices at greater than 3σ before a stable result is obtained. Here we are also assuming that the SSP models are perfect. Both flux calibration and calibration to the Lick system introduce further errors and uncertainties.

The main manifestation of these unaccounted for errors is the increased difficulty in constraining ages and α -element abundance ratios for fainter GCs. In general, metallicities are less susceptible to these effects because of the large number (>10) of predominantly metallicity sensitive indices available. By contrast, there are only 3 primarily age indicators (i.e. the $H\beta$, $H\gamma$ and $H\delta$ lines) and only a few strongly α -element sensitive indices.

This underestimation of errors probably occurs in all extra-galactic GC samples.

For example, the large and homogeneous sample of Puzia *et al.* (2004) has index errors that appear underestimated by up to a factor of 2 based on the scatter in index-index plots. The χ^2 fitting method we apply is immune to this effect as long as the errors are uniformly underestimated by the same factor across all indices. However, it is unlikely this is the case as sky subtraction and galaxy light subtraction could affect every index differently. Despite these uncertainties, the χ^2 fitting method applied in this work appears to be robust to problems with individual indices. GCs strongly affected by error underestimation are easily identified during the fitting process. Modelling errors including horizontal branch morphology and α -element abundance prescriptions are also factors in the imperfect matching of observed data to the SSPs.

At least 3, and possibly 4, GCs are found to be young (2-3 Gyrs old) out of our sample of 38. This proportion is similar to the 2 young GCs from a sample of 10 found by Forbes *et al.* (2001) for NGC 1399, another large cluster elliptical with no signs of recent star formation. A 2-3 Gyr old central burst of star-formation that is approximately 10% by mass of the underlying old 10-14 Gyr population will cause a significant change to the spectral indices of the galaxy (e.g. Proctor *et al.* 2005). This has not been reported for the NGC 4649 galaxy light itself. Indeed, Terlevich & Forbes (2002) find the central stellar population of NGC 4649 to be ~ 11 Gyrs old. There are no observations to suggest a significant recent burst of star-formation in NGC 4649 (the UV SED work of Magris & Bruzual (1993) suggest minor on-going star-formation). Do these young GCs suggest that some of the GCs associated with large cluster gEs are not formed in that galaxy? Two of the young GCs (87 and 175) are at large projected galacto centric radii (see Fig. 4.6). These GCs are on the opposite side of NGC 4649 from the nearby companion spiral NGC 4647 (see Fig. 1 of Bridges *et al.* 2006).

This result raises several possibilities. Firstly that there was minimal galaxy star formation when these young GCs were formed and therefore GCs do not trace star formation particularly well. This would be contrary to what is commonly observed in other systems. Secondly, that our sampling is not representative of the overall GC population. This possibility is difficult to rule out. Thirdly, that GC accretion is a common enough process for large ellipticals that the GC system is “contaminated” by GCs formed in other galaxies and therefore the GC system is a complex trace of a combination of star-formation and galaxy assembly. More accurate ages and α -element abundance ratios are necessary to distinguish between local formation of the young GCs in massive ellipticals or accretion from nearby galaxies with more recent star-formation.

Our plot of α -element ratio with metallicity (Fig. 4.5) is the most visually compelling indication of a trend of decreasing $[E/Fe]$ with increasing $[Fe/H]$ in the literature to date. A similar trend is seen less clearly in Fig. 2.9 for NGC 1052 GCs, Puzia *et al.* (2005) for a sub-sample of bright GCs from 5 galaxies and Fig. 3.6 for NGC 3379 GCs.

Not all observers find the same trend in α -element ratios. Strader *et al.* (2004a) examine NGC 3610 GCs and appear to find an inverse trend to that presented in our Fig. 4.5. Based on a comparison of Mgb vs $\langle Fe \rangle$ they find the majority of GCs to have solar or sub-solar α -element ratios. Four of the metal-rich GCs appear to have abundance ratios of +0.3 dex; interestingly two of these are old and two are

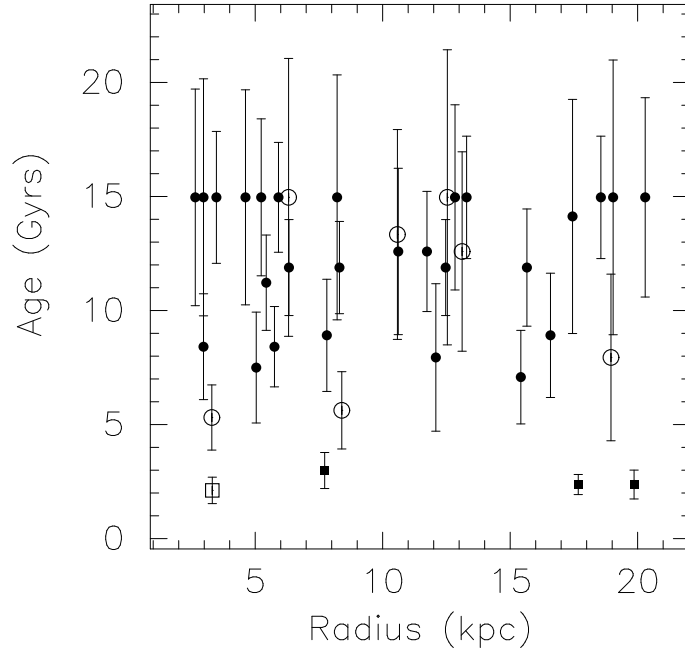


Figure 4.6: A plot of age vs projected galactocentric radii. The open points are GCs for which the χ^2 fits are uncertain and the squares are young GCs. There is no obvious trend with radius. Of interest are the two young GCs at large projected galactocentric radii ~ 17 – 20 kpc.

young.

Olsen *et al.* (2004), with a sample of 6 GCs associated with Sculptor group galaxies, find 4 metal-poor ($[\text{Fe}/\text{H}] < -1$) GCs with abundance ratios around $[\alpha/\text{Fe}] = -0.3$ and 2 metal-poor GCs with approximately solar abundances (see Fig. 8 of Olsen *et al.* 2004). This is derived from the ratio of $\text{Mgb}/\langle \text{Fe} \rangle$. We suggest, based on their Fig. 6, that the calibration to the Lick system of Mgb and $\text{Fe}5335$ for their data may be a problem.

It is worth noting that α -element abundance ratios are poorly constrained for low metallicities and it is therefore possible to argue that within errors the current larger samples, our three galaxies, NGC 1052, NGC 3379 and NGC 4649, and Puzia *et al.* (2005), are consistent with a universal value of $[\text{E}/\text{Fe}] = +0.3$ (consistent with Galactic α/Fe measures). The majority of GCs with well constrained α -element abundance ratios are relatively consistent with this value within errors. The trend seen in all 3 data sets may then be attributed to modelling effects in the Thomas *et al.* (2004) models used for all these cases. We discuss this issue in Section 6.2.3.

A rough order of magnitude estimate can be made of the S/N required to differentiate the α -element abundance ratios of metal-poor GCs. The expected difference in Mgb between solar abundance and $[\text{E}/\text{Fe}] = +0.3$, for a 10 Gyr $[\text{Fe}/\text{H}] = -1$ TMK04 model, is 0.237 \AA . To be able to observe a difference of this magnitude spectra with S/N corresponding to $\text{H}\beta$ errors of $\sim 0.13 \text{ \AA}$ are required. For the sample presented here, only two GCs are sufficiently bright to reach that accuracy. Calibration to the Lick system and accurate flux calibration are necessary to make possible the detailed exploration of α -element abundance effects at low metallicities. To completely resolve the differences in α -element abundance ratios currently measured, spectra of

substantially higher S/N than the current samples are required.

Considering index and index error uncertainties discussed at the beginning of this section we suggest that further work will be necessary to confidently determine if the metallicity α -element abundance ratio trend we observe is real or if it is an artefact of SSP modelling, χ^2 fitting, and observation calibrations, both flux and to the Lick system.

4.5 Conclusions

We present ages, metallicities and α -element abundance ratios for 38 GCs around NGC 4649 based on our Gemini/GMOS spectra. These were derived by applying the multi-index χ^2 minimisation method of Proctor & Sansom (2002) to the SSP models of Thomas *et al.* (2004). Close agreement is found with metallicity estimates derived according to the Brodie & Huchra (1990) method, with the young GCs systematically offset by a small amount (~ 0.5 dex) as expected. We find 3, possibly 4, GCs with ages of approximately 2 Gyrs, two of these are at large galactocentric radii (17–20 kpc). The α -element abundance ratio decreases with increasing metallicity.

The young GC fraction ($\leq 10\%$) is consistent with the picture presented by “frosting” models of recent minor star formation in ellipticals (Trager *et al.* 2000). In this particular case, noting the large galactocentric radii of 2 of the young GCs and the lack of evidence for recent star formation in the galaxy itself, it is quite possible that the young sub-population was not formed natively, but instead has been accreted.

Chapter 5

Future Directions

High quality imaging, especially from the HST/ACS, has raised some interesting new questions about GC systems (see Section 1.2.3.3). Two major topics that require confirmation and explanation are the “blue-tilt” observed as a GC luminosity-colour relationship for the blue sub-population of some, but not all, massive galaxies and the Yoon *et al.* (2006) SSP models which suggest that GC systems with bi-modal colours could be uni-modal in metallicity. These are issues that can best be tackled by high S/N integrated spectroscopy. This is because the galaxies for which the “blue-tilt” has been observed are too distant for resolved stellar population imaging (CMD studies) and a much larger sample of reliable spectroscopic metallicities are required to test the Yoon *et al.* (2006) models across the full metallicity range.

5.1 Stellar Population Models and Measurements

Flux and Lick calibrations are important to accurately measure stellar population parameters, especially α -element abundances (see Section 6.2.3). There are several inherent problems with the Lick/IDS system, on which current SSP models are based. These include the lack of flux calibration, variable spectral resolution and general inaccuracies in the stellar library due to instrumental vagaries. A major improvement to SSP models and the measurements of parameters could be made by using modern flux calibrated stellar libraries. This direction is being taken to produce new SSP models. Vazdekis (2006) has preliminary SSP models based on the MILES library (Sanchez-Blazquez *et al.* 2006) and Schiavon (2006) has produced SSPs models that use the Jones (1999) stellar library. These more recent stellar libraries have been observed on modern spectrographs and include more stars and better coverage of parameter space.

In the following subsections we suggest four improvements to SSP models that could be made within the next couple of years. These are the modelling of horizontal branch morphology as an independent parameter, modelling the effect of dynamic evolution of GC evolution, modelling individual element abundances for the common α -elements and increasing the number of indices modelled.

5.1.1 Horizontal branch morphology as a parameter

Horizontal branch (HB) morphology can affect many of the observed properties of GCs, including the photometric colours and spectral index strengths. Variations in horizontal branch morphology for galactic GCs of similar metallicity (van den Bergh 1967; Sandage & Willey 1967), and presumably age, have led to the suggestion that a second parameter, other than metallicity, is necessary to explain HB morphology. This effect is observed for pairs of Galactic GCs with very similar metallicities and ages, however with current SSP models we are unable to test this effect with integrated spectra of extra-galactic GCs or allow for HB morphology variation in our χ^2 fitting process.

For the GC systems we have studied, we find several cases where a few individual GCs appear to possess a larger contribution from blue HB stars than is included in the models. For example, GC 38 from NGC 1052 shows strong CaII inversion, indicative of a large blue HB contribution, and we find a much younger χ^2 fit age than for other GCs with similar metallicities (see Section 2.4.1). It is important to realise that we are most sensitive to the detection of anomalously blue HBs at low metallicity. In this case we find a younger age for that GC than the other GCs of similar metallicity, which is unexpected at low metallicity. For GCs with metallicity close to solar we assume that young age fits are genuinely young, rather than the possibility of HB effects, because we do not expect a strong blue HB contribution at high metallicity. Since GCs commonly match the oldest ages modelled, an especially red HB will probably not be noticed by an observer (see Section 3.3).

From integrated stellar populations it is difficult to accurately determine the HB morphology. There may be some fraction of GCs that have bluer or redder morphologies, for their metallicity, than the Milky Way system. Horizontal branch morphology can affect age measurements by up to ~ 0.3 dex and integrated colours by 0.1 mag.

One key aspect of SSP models is the HB morphology prescription and the rate that it changes with metallicity. In future models a broad range of giant branch mass-loss (or HB morphology) should be included as parameter spanning a range broader than is likely to be observed (in the same way that α -element abundance ratios are modelled to span a large range). However, there will be calibration difficulties since the metallicity-mass loss parameter space is not spanned by real GCs.

If modelled correctly, we should be able to use extra-galactic GC systems to test if the Milky Way metallicity-HB morphology relationship is universal, or if the relationship relies on local conditions (such as density or tidal field strength). We should also be able to resolve the difficulties in fitting GCs in the situation where the Balmer lines individually predict very different ages (several occurrences can be found in Chapters 1, 2 and 3).

5.1.2 The effect of dynamical processes on globular cluster evolution

When we measure the stellar populations of a GC, we compare it to an SSP model with a standard IMF. This implicitly assumes that dynamical evolution is not important. However, we know that GCs are tidally stripped and disrupted by their

host galaxy and that eventually they can be destroyed. Simulations of star cluster evolution in galactic potentials predict that tidal stripping will be significant over a Hubble time (e.g. Gnedin & Ostriker 1997). Observationally, there are several cases of tidal tails associated with Galactic GCs, indicating that tidal stripping of the more loosely bound stars does occur (Belokurov *et al.* 2006; Lee *et al.* 2004; Koch *et al.* 2004).

Mass segregation, the dynamical process by which more massive stars transfer kinetic energy to less massive stars, is observationally (Albrow, De Marchi & Sahu 2002; Lee *et al.* 2004; Koch *et al.* 2004) and theoretically well established (Fregeau *et al.* 2002). A feature of mass segregation is that higher mass stars are preferentially located in the core of star clusters and lower mass stars are preferentially located in the outer regions of the cluster. Therefore the lower mass stars are less tightly gravitationally bound to the star cluster. The combined effect of mass segregation and tidal stripping is the preferential loss of lower mass stars, which affects the cluster stellar mass function (Baumgardt & Makino 2003). After a few Gyrs, the assumption that a star cluster is an SSP, with its original mass function, is no longer valid. It is important to note that the fraction of primordial stellar binaries included in an N-body star cluster simulation affects the strength of the other dynamical processes (Hurley *et al.* 2005).

Lamer, Anders & de Grijs (2006) predict how these factors will affect the observed photometric colours of GCs. A key prediction is that in the middle of the clusters' lifetimes (in the period between 40 and 80% of the dynamical age) they become bluer due to the loss of low-mass stars and after 80% of the total lifetime it will rapidly become redder. This will result in an underestimate of the age of clusters during the period of 0.4 to 0.8 of its total lifetime and overestimate of the age after 0.8. While these predictions are for photometric colours and estimates of age, it would be interesting to see similar predictions for Lick index based estimates. Hurley (2006 priv. comm.) also suggests that dynamical evolution is significant for observable cluster characteristics. He finds that the observed colours of GCs are significantly bluer after 15 Gyrs (0.5 mag in V-K) when dynamical evolution is included.

Lamer *et al.* (2006) suggest that the loss of low-mass stars might explain the presence of old (~ 13 Gyr) clusters in NGC 4365 which are photometrically suggested to be intermediate-age clusters (2-5 Gyr). This may require that the tidal field of NGC 4365 is stronger than other large ellipticals where such a population is not observed. Another factor to consider when gauging the strength of tidal stripping is the GC orbit (Vesperini *et al.* 2003). If the orbits of the NGC 4365 GCs are significantly more radial than those of GCs in other similar ellipticals then tidally stripping of low-mass stars could be a possible explanation for the photometry that suggests intermediate-ages.

We expect that the preferential tidal stripping of low-mass stars will affect lower mass GCs more strongly than high mass GCs. This is because stars are less tightly bound to a lower mass host and therefore a similar tidal field will more effectively strip the less strongly bound low mass GCs. This is a possible mechanism to explain the observed "blue-tilt" in metal-poor GC colours observed for some galaxies. Assuming that blue GCs of different magnitudes possess similar metallicity distributions, but as their mass decreases they are increasingly tidally stripped and will become bluer due to the loss of low-mass (red) stars.

Another possible contribution to the “blue-tilt” is the ejection of less massive stars by binaries, in three and four body interactions. This is a well established dynamical process (Hut *et al.* 1992) and the effect is much larger for lower mass GCs because they have a weaker overall gravitational field and are less tightly bound compared with higher mass GCs. However, ejection of low-mass stars by binaries cannot explain the variation in the slope of the tilt with galacto-centric radius reported by Spitler *et al.* (2006) and Mieske *et al.* (2006b).

We suggest that it should be possible to construct SSP models based on the outputs of N-body star cluster simulations that include the effects of primordial binaries, mass-segregation and a variety of tidal stripping prescriptions. Isochrones of stellar luminosity and temperature can be extracted from the current generation of simulations and could be used in the place of the current Padova and Yale isochrones when constructing SSP model predictions of both photometric colours and spectral indices.

With sufficiently accurate models plus observations and employing the multi-dimensional χ^2 minimisation, it is plausible to measure the effects of dynamical evolution on the cluster stellar population and to improve the accuracy of stellar population parameter determinations. Without the creation of dynamically evolved SSP models it is difficult to quantify the expected magnitude of the various effects on individual spectral indices. However, based on the Lamer *et al.* (2006) and Hurley (2006 priv. comm.) work on photometric colours, we anticipate that the effect is non-negligible.

5.1.3 Modelling of elemental abundances

There is a lack of consensus regarding how to interpret Lick index measured α -element abundances. In particular, it is not always clear what [E/Fe] measures. Does it mostly trace oxygen or magnesium abundance? There is evidence amongst Galactic stars that elements classically considered to be α -element, which we expect to track each other, do not entirely correlate with each other and show different abundance trends with metallicity. For example in Jonsell *et al.* (2005), they measure the abundances of stars and Fig. 3 shows that the abundances of O and Mg differ significantly above solar metallicity.

Another question that could be tackled is the CN abundance anomalies observed for different GC systems (Burstein *et al.* 1984; Beasley *et al.* 2004a). In GCs the CN indices are usually found to be enhanced relative to iron and α -element sensitive indices. However, other comparable integrated stellar populations, such as elliptical galaxies, do not usually show CN enhancement.

SSPs which model each of the α -elements separately would allow us to fit individual abundances such as [C/Fe], [N/Fe], [Mg/Fe] and [O/Fe]. This would allow significantly more detailed interpretation of abundance variations and anomalies. Schiavon (2006) begins to do this.

5.1.4 Improving the index system

As a general principle, including the most information possible is beneficial for the χ^2 fitting method. This method also effectively includes all the information

incorporated in the indices in the fitting process and is in theory able to fit for any number of parameters simultaneously. Increasing the number of indices measured and modelled is crucial if we are to attempt to fit more parameters, as suggested in the previous sections, and to be confident that we are finding non-degenerate solutions. In the idealised case we need at least the same number of input values as free parameters to find a unique solution. For our situation, measuring stellar populations, there are several degenerate parameters, therefore we require a large number of indices to be confident of our results.

Extending the spectral coverage of the index definition system will allow additional leverage, especially indices in the near-UV that are sensitive to age and α -elements. In the future, stellar population measurements of galaxies at any significant redshift will require models for rest-frame UV indices. This is because the features we currently measure in the wavelength range (4000-5500 Å) are red-shifted to wavelengths contaminated with large numbers of skylines. Expanding the set of commonly modelled indices to wavelengths just blue-ward of 4000 Å would also significantly increase the leverage on all stellar populations parameters by including features such as CaII H+K, CNB and H η .

Another avenue to increasing the number of indices is to define and include indices for narrower and weaker absorption features. The Lick system was originally defined with a view to measuring stellar populations of galaxies. Due to the velocity dispersion of galaxies generally being in the range of 100-300 km/s, which corresponds to a wavelength resolution of approximately 1.7-5.1 Å, narrower features were not included in the Lick system index definitions. However, GC velocity dispersions are of order 10 km/s, corresponding to 0.17 Å, therefore for GCs it is possible to measure narrower spectral features with observations at adequate spectral resolution.

Serven, Worthey & Briley (2005) propose the use of some weaker spectral features, which require S/N > 100 spectra, to measure the abundances of individual elements. High S/N is required because for an index to provide leverage in constraining stellar population parameters it must have a useful dynamic range, where the dynamic range is the range of index values spanned divided by the typical index measurement error, including all calibration errors. Before such indices become useful, it will be necessary to greatly reduce the uncertainties in index measurement due to flux calibration, correction to Lick, sky subtraction and photon noise.

5.2 Globular Cluster Observations

There are many GC systems that could be observed in detail. Here we suggest a few possibilities with distinct purposes.

5.2.1 Studying a young globular cluster population

As mentioned previously in the Introduction Chapter (Section 1.2.3.4), there are no large spectroscopic samples of young GCs from a single early-type galaxy. Currently the largest sample of ~15-20 GCs is associated with NGC 5128 (Beasley *et al.* 2006). This sample of young GCs spans a large range in age and metallicity. A large sample

of young GCs with a uniform age, indicating formation in a similar event, would allow us to explore the properties of their formation in detail. An analysis of age or α -element abundance with galacto-centric radius can give an indication of how the star-formation event, during which the young GCs formed, occurred. A kinematic analysis of the young GC population against that of the old GCs can offer an insight into the formation mechanisms of the two populations (e.g. if the young population shows rotation or significantly lower velocity dispersion).

The Fornax cluster galaxy NGC 1316 is a prime target for possessing a large population of young GCs. Goudfrooij *et al.* (2001) present spectroscopic ages for the 3 highest S/N GCs in their sample and find all 3 to be ~ 3 Gyrs old. Further photometric studies by Goudfrooij *et al.* (2004) indicate that a substantial young GC population exists around NGC 1316. The GC system of NGC 1316 is distant enough that a large aperture telescope is necessary to obtain high S/N spectra. As a southern hemisphere galaxy, the best instruments to obtain optical spectra of its GC system are VIMOS/FORS/GMOS.

5.2.2 Resolving the NGC 4365 near-IR photometry controversy

In Section 1.2.3.3 of the Introduction Chapter we briefly discussed the use of near-IR photometry in combination with optical photometry as a method for breaking the age-metallicity degeneracy. There are conflicting opinions and results regarding the accuracy of stellar population ages derived from this method. Most of the controversy is centred on the GC system of NGC 4365 and whether there is a substantial population of intermediate age (2-8 Gyrs) GCs.

Davies *et al.* (2001), based on SAURON IFU spectroscopy of the centre of the galaxy, claim the galaxy stars are old and that NGC 4365 formed through a series of dissipative mergers >12 Gyrs ago. Puzia *et al.* (2002), using near-IR photometry of GCs, claims to find a 2-8 Gyr old sub-population of metal-rich GCs. Larsen *et al.* (2003) obtained fairly low S/N spectra of several GCs and find the Balmer indices consistent with ages of 2-5 Gyrs. Brodie *et al.* (2005) obtained much higher S/N spectra of 22 GCs, including overlap with some “young” GCs in the Larsen *et al.* (2003) sample, and find that all of the GCs they observe are old and that there is an intermediate metallicity sub-population. Larsen, Brodie & Strader (2005) present new K-band imaging and compare their spectroscopically observed colour-metallicity relation with model relations. They find an offset for the metal-rich GCs with observed colours being ~ 0.2 mags too red in V-K and ~ 0.05 mags too blue in V-I. Kundu *et al.* (2005) present H-band photometry which can be explained by an intermediate age population, but requires a large metallicity range ($[\text{Fe}/\text{H}] = -0.7$ to $+0.4$) for the intermediate age GCs.

Observations of GCs around NGC 4365, when compared to current SSP models such as Thomas *et al.* (2004) and Maraston (2005), seem to give conflicting results. There are some uncertainties regarding the modelling of near-IR colours which may resolve these conflicts. Lamer *et al.* (2006) suggest that dynamical evolution can potentially affect GC colours to photometrically disguise old (13 Gyr) GCs as intermediate-age clusters (2-5 Gyr). Salaris & Cassisi (2006) show that the modelling of the horizontal branch is crucial and that differences in morphology can

produce a GC system that emulates an age bi-modality of 8 Gyrs when observed through a combination of optical and near-IR filters. The modelling of asymptotic giant branch stars (AGB) and upper-AGB stars is important for IR colours and SSPs, especially intermediate age populations (Bressan, Granato & Silva 1998).

To resolve the current controversy of whether optical and near-IR photometry can identify intermediate age GCs, NGC 4365 needs a large (100+ GCs) high S/N > 30 spectroscopic follow-up. A detection, or strong non-detection, of a significant population of intermediate age GCs should resolve this issue.

5.2.3 Are Ultra-Compact Dwarfs galaxies or globulars?

The more recent studies of Ultra-Compact Dwarfs (UCDs) suggest that they are much more closely related to GCs than the initial works claimed (Drinkwater 2006 priv. comm.). Mieske *et al.* (2006a) measure several properties for a sample of compact objects in the Fornax cluster. They find a break in properties at a luminosity of $M_V = -11$ and a mass of $\sim 3 \times 10^6 M_\odot$.

Measuring the stellar population details of UCDs would offer a strong indicator of whether they are very massive GCs or the tidally stripped nuclei of dwarf galaxies. One chemical indicator that could be used to differentiate between the scenarios is the CN abundance, which is elevated in GCs relative to galaxies.

To test the difference or similarity between UCDs and GCs, a large homogeneous high S/N spectroscopic sample - encompassing the parameter space where these two object types are thought to overlap - would be beneficial. Corresponding samples from the Virgo and Fornax Clusters would help determine the environmental impact on the stellar populations of these compact objects.

5.2.4 Globular clusters across the luminosity function

As a parallel or follow-up to the study of bright compact objects around large ellipticals, it would be worthwhile to sample in detail GCs from both red and blue sub-populations to magnitudes at least as faint as the luminosity function turn-over. Ideally this sample should be as large as possible. We suggest obtaining around 500 high S/N spectra should allow us to answer many of the pressing issues. Homogeneously sampling the magnitude range $M_V = -11$ to -7 , and colour range $V-I = 0.7$ to 1.3 , and binning by magnitude in intervals of 0.5 mags and in colour by 0.05 mags, leads to 48 bins which should ideally contain at least 10 GCs each.

Such a sample would allow us to address several major points of interest. Firstly, the sampling in colour space, coupled to spectroscopically determined metallicities, will allow us to test the suggestions of Yoon *et al.* (2006) claiming that GC systems may have colour bi-modality but not metallicity bi-modality.

Secondly, we should be able to test whether the “blue-tilt” is due to a mass-metallicity relationship, dynamical evolution or some other effect. Part of the motivation for such a large sample is so that we can separate by galacto-centric radius and compare with the observations of Spitler *et al.* (2006) and Mieske *et al.* (2006b).

Thirdly, in such a large sample we are likely to obtain spectra of a reasonable number of young GCs (up to 10% which is approximately 50). With such a sample we can compare the luminosity function of young GCs with the older sub-populations.

It would also be informative to compare the luminosity function of young GCs associated with massive elliptical with no recent formation signs, for which the GCs may have been accreted (see Section 4.4), with those of a merger remnant such as NGC 1316 where the young GCs are expected to form locally in a large star-formation burst.

The prime targets to observe such a large sample are the most populous nearby GC systems, M87 in the Virgo Cluster and NGC 1399 in the Fornax Cluster. Both of these galaxies have distance moduli of approximately 31 mags. At those distances we suggest sampling GCs to $V=20-24$.

Due to the large magnitude range spanned, we suggest that due to integration time considerations the sample should be split into at least two and possibly more luminosity sub-samples. The brighter GCs with $V=20-22$ can be observed spectroscopically to good S/N in $\sim 2-4$ hours with an 8 metre telescope. In the southern hemisphere IMACS on the Magellan telescope, with its wide field of view, could be the best instrument to use for the brighter GCs. High S/N spectra of fainter GCs ($V=22-24$) are much more time consuming to obtain and would require 8+ hours of observation with an 8-10 metre telescope.

A large comprehensive sample such as we propose would enable thorough testing and comparison of the SSP modelling improvements suggested in Section 5.1. Many of the weaker effects, such as tidal stripping or the “blue-tilt”, require a large high quality sample to quantify with any statistical significance and to verify whether including extra parameters offers a real improvement in the stellar population fits.

Chapter 6

Conclusions

6.1 Individual galaxies

We have obtained spectra of GC systems around three galaxies. We measure the age, metallicity and α -abundance ratio of individual GCs by comparing their measured Lick indices with simple stellar population models.

- NGC 1052

NGC 1052 is a merger remnant elliptical galaxy with several indications of a recent merger and star formation. These include HI tidal tails, kinematical decoupling of gas and stars and a young stellar age in the centre of the galaxy. Therefore we expect a sub-population of young GCs to have been formed at the time of the merger (1-2 Gyrs ago). We find no young GCs amongst our sample of 16. To maximise S/N, we sample only the brightest GCs which, assuming similar mass functions for young and old GCs and lower mass-to-light ratios for young stellar populations, are most likely to contain any young population. However, we do not adequately sample small galactocentric radii, where young GCs are more likely to be formed in a merger. [E/Fe] with metallicity suggests a trend of decreasing α -element abundance ratio with increasing metallicity.

- NGC 3379

The GC system of NGC 3379 was selected as an observational target primarily because of the Planetary Nebulae kinematic measurements presented by Romanowsky *et al.* (2003), which were interpreted as an absence of dark matter. It is a moderate luminosity galaxy in the Leo group with no signs of recent interaction, merger or accretion. We find that all of the 22 observed GCs are old. This matches our expectations as there are no signs of recent star-formation activity in this galaxy. A trend of decreasing α -element abundance with increasing metallicity is seen for the fitted parameters. We see the α -element abundance trend reflected in various combinations of metallicity and α -element sensitive indices, confirming that the trend we find in the fitted parameters is present in the data.

- NGC 4649

NGC 4649 is a massive elliptical galaxy ($M_V = -22.38$) in the Virgo cluster. Optical spectroscopy of the centre of the galaxy indicates an old central age and super-

solar metallicity. We obtained spectra of 38 GCs and measured ages, metallicities and α -element abundance ratios. There are two GCs with formal age fits of ~ 5 Gyrs, however the χ^2 fits for these two GCs are uncertain and the age-metallicity degeneracy may not have been broken. We find four GCs which are definitely young (2-3 Gyrs). Two of the young GCs lie at large projected radii (18-20 kpc), which means they are less likely to have formed natively and are possibly accreted from dwarf galaxies. The young GCs have the highest metallicities of the entire sample with metallicities above solar. Similar to NGC 3379, we find a trend of decreasing α -element abundance with increasing metallicity. Of the three galaxies we have studied the α -element abundance trend is clearest for NGC 4649.

6.2 Stellar Population Parameters

Here we briefly discuss our conclusions for each of the stellar parameters derived, including in our analysis some results from the literature.

6.2.1 Metallicities

GC metallicities are of interest because they place constraints on the formation histories of galaxies. In particular, if the metallicity is bi-modal for elliptical galaxies, then two formation mechanisms or episodes are required.

The observationally simplest way to measure a statistically significant sample of GC metallicities is by using photometric colours, either in the optical or near-IR. Deep multi-band imaging containing hundreds of GCs can be obtained for Virgo distance galaxies in an hour, whereas spectroscopy of tens of objects can take up to 8 hours. Measuring metallicities for GCs from photometric colours, assuming they are old, requires a robust transformation of colour to metallicity.

In light of the recent suggestion of Yoon *et al.* (2006), the distribution of GC metallicities associated with elliptical galaxies is of renewed interest. They question the long standing assumption that the observed bi-modal colour distribution of elliptical galaxies GC systems indicates a bi-modal distribution in the metallicity. However, this has not been studied spectroscopically in a uniform, detailed manner for any individual galaxy, except NGC 5128, due to limited sample sizes and selection bias.

The age-metallicity degeneracy of stellar populations means that it is necessary to measure ages to be confident of the metallicity determined. Empirical metallicity calibrations such as Brodie & Huchra (1990) or the PCA method of Strader & Brodie (2004) require that an old age is assumed for the GC. For old GCs there is very good agreement between the empirical calibrations and χ^2 fit metallicities. However, for the young GCs associated with NGC 4649, we find their Brodie-Huchra metallicities to be 0.5-1 dex too low. This demonstrates the importance of simultaneous age and metallicity determinations.

For each of the GC systems we have studied, the metallicity distributions reflect the colour distributions sampled. However, there is substantial scatter in the colour-metallicity relationship, of the order 0.5 dex in metallicity (0.2 mag in V-I or g-i). This scatter could be due to dust reddening, photometric errors, horizontal branch

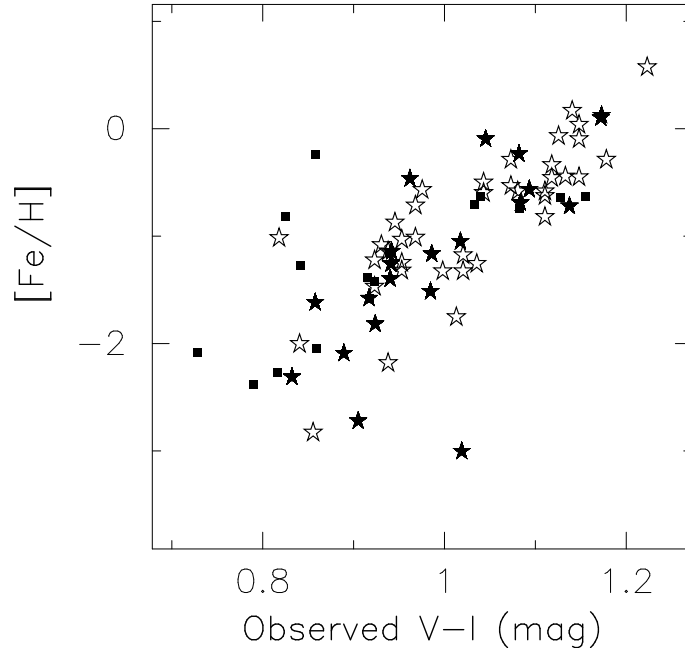


Figure 6.1: Comparison of the observed colour vs metallicity for the three galaxies studied. NGC 1052 points are solid squares, NGC 3379 points are stars and NGC 4649 points are open stars. The underlying relationship is clear but the scatter is quite substantial.

morphology or age variations. We cannot confidently comment on the exact shape of the colour-metallicity relationship, whether it requires multiple components or if there is an inflexion point, as suggested by the Yoon *et al.* (2006) models. In Sections 5.2.2 and 5.2.4 we propose some observations that could help resolve this uncertainty.

In Fig. 6.1 we plot the observed colour against the metallicity for the GCs from the three galaxies studied. We have converted the observed $g-i$ to $V-I$ for NGC 3379 and NGC 4649. The spread of points in the region of $V-I=1$ and $[Fe/H]=-1$ make any detection of bi-modality difficult.

Compared to many literature samples, our three studies include GCs of lower metallicity. This is because we sample an even colour distribution, rather than focusing on the most likely colours of a young metal-rich sub-population. For all three galaxies we have observed GCs with metallicities below $[Fe/H]=-2.25$. Most alternative high quality samples do not include GCs of such low metallicity (e.g. Kuntschner *et al.* 2002; Brodie *et al.* 2005; Puzia *et al.* 2005). Our large metallicity range is important for measuring correlations of other properties with metallicity, such as colour and $[E/Fe]$, because we sample a longer baseline in metallicity and we can test the correlations at lower metallicity.

6.2.2 Age distributions

Our interest in GC ages is based upon using them as a tracer of star formation events. The various models of GC system formation, in the context of elliptical galaxies, make differing predictions about their ages (Section 1.2.2). To discriminate

between the models we need to know at which times GCs formed, what fraction of GCs are young and whether the young GCs formed in distinct events or are spread over time.

The age distributions we find for our GC systems, and those reported in the literature, are not always entirely consistent with expectations based upon the host galaxy properties. For almost every extra-galactic GC system measured spectroscopically the overwhelming majority ($>80\%$) of GCs are old. For old GCs the standard age errors are usually ~ 2 Gyrs, therefore it is difficult to determine if there is any age sub-structure amongst them. Also, due to uncertainties in the effect of horizontal branch morphology on age measurements, we cannot confidently state whether there is an age difference between the metal-rich and metal-poor sub-populations.

We are therefore currently prevented by the accuracy of SSP models and the S/N of observations from studying old GCs ages in detail and cannot confidently discriminate between the different GC system formation models. Instead we turn our attention to another facet of GC system age distributions which is of great interest. Where do young GCs (<8 Gyrs) reside?

There are at least two cases where young GCs are found around massive, old, cluster galaxies with no signs of recent star-formation: NGC 4649 (Chapter 3) and NGC 1399 (Forbes *et al.* 2001).

There are some galaxies where we expect to find a young population, such as the merger remnant NGC 1052 (Chapter 2) or NGC 3115 (Kuntschner *et al.* 2002), which has several characteristics commonly associated with more recent star-formation: it is a low mass S0 with a young central age and resides in a low density environment. However, both of these galaxies are found to have only old GCs amongst those sampled. Another merger remnant NGC 3610 (Strader *et al.* 2003, 2004a) is found to have a significant population of young GCs. NGC 5128, a galaxy with several signs of recent merger and star-formation activity, has been well sampled by Beasley *et al.* (2006) and they find approximately 10% of their ~ 180 GCs are younger than 8 Gyrs.

The disjuncture between our expectations of where young GC populations should reside and where we actually find them is puzzling. This result may be due to small numbers and poor S/N, or may indicate that GC formation is not strongly tied to field star formation, contrary to the expectations of many authors (e.g. Brodie & Strader 2006).

6.2.3 Alpha element abundance ratios

The abundance of α -elements is a tracer of the contribution of different supernovae types. Therefore the abundance of α -elements relative to Iron, $[E/Fe]$, is commonly interpreted as a star-formation timescale indicator. The change in α -element abundance with metallicity is one means of tracking the chemical enrichment of a galaxy. In this sub-section we restate some results and raise some caveats when measuring $[E/Fe]$.

For each of our three globular cluster system samples we note a trend of decreasing α -element abundances $[E/Fe]$ with increasing metallicity $[Fe/H]$. Fig. 6.2 shows a comparison of the $[E/Fe]$ trend with $[Fe/H]$ for our three studied galaxies. While they show the same general trend, our data are not of sufficient quality to make a

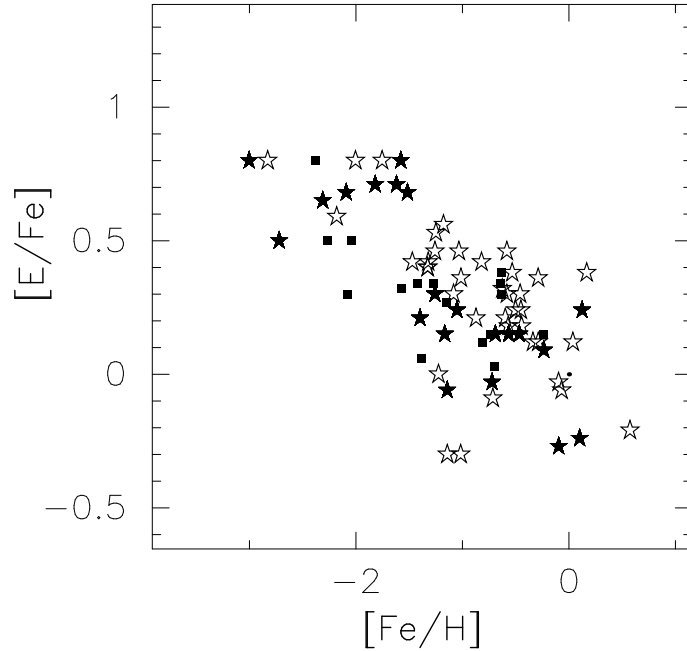


Figure 6.2: Comparison of Alpha element abundance ratio vs metallicity for the three galaxies studied. NGC 1052 points are solid squares, NGC 3379 points are stars and NGC 4649 points are open stars. All three galaxies show a similar trend of decreasing $[E/Fe]$ with increasing $[Fe/H]$.

conclusive comparison.

However, it is noteworthy that amongst the literature different trends are apparent for different galaxies' GC systems, even though the majority of recent publications have compared index measurements to the same set of SSP models. Either there are observational systematics or large elliptical galaxies have quite different chemical enrichment histories.

For most extra-galactic GC samples it is difficult to determine if there is any trend or not. This is because observers have often sampled limited metallicity ranges. For example, the Brodie *et al.* (2005) NGC 4365 sample spans $[Fe/H]=-1.3$ to -0.3 , whereas our NGC 4649 GCs span $[Fe/H]=-2$ to $+0.5$. Given the inherent scatter of ~ 0.2 dex due to Poisson errors for $[E/Fe]$ measurements, a metallicity baseline of ~ 2 dex is very beneficial when trying to determine whether there is a trend in $[E/Fe]$ with metallicity. If such a trend exists it appears to be of order $\Delta[E/Fe]=0.3$ dex per dex in $[Fe/H]$.

When we examine the literature, $[E/Fe]$ estimates are commonly based on index-index plots of $\langle Fe \rangle$ vs Mgb or Mg_2 . Several samples including Strader *et al.* (2003,2004a; NGC 3610), Brodie *et al.* (2005; NGC 4365), Cenarro *et al.* (2006; NGC 1407) and Olsen *et al.* (2004; Sculptor group galaxies) show either constant or increasing $[E/Fe]$ with metallicity. Our three galaxies, NGC 1052, 3379 and 4649, and the high S/N GCs in the Puzia *et al.* (2005) analysis, however, show a strongly decreasing $[E/Fe]$ with increasing metallicity.

The α -element abundance pattern is well known for Galactic GCs from high-resolution spectra of individual giant stars (Carney 1996; Pritzl *et al.* 2005). This abundance pattern is $[E/Fe]=+0.3$ for GCs with metallicity below $[Fe/H]=-1$ and

decreases to $[E/Fe]=+0.2$ at solar metallicity. A simple scenario is that the abundance pattern for elliptical galaxy GCs is similar to that of the Milky Way and therefore that at low metallicity the SSP models are not well calibrated.

Regardless of the calibration of the models at low metallicity there is still a variation in the trend reported for different samples of GCs. We suggest the differences between samples indicate that both Lick system and flux calibration are of particular importance when measuring α -element abundances, as compared to age or metallicity. This is because in many studies the measured α abundances are based on a small number of sensitive indices, usually the Mg indices, Mgb, Mg_1 and Mg_2 . The molecular band Mg_1 and Mg_2 indices are highly sensitive to flux calibration and therefore can easily give spurious results. Another factor is that to determine α -element abundance ratios, for low metallicity GCs, to an accuracy better than ~ 0.2 dex requires spectra of much higher S/N than have commonly been observed for extra-galactic GCs (see Section 4.4). To accurately measure α -element abundance ratios at metallicities below $[Z/H]=-1$ requires spectra with $H\beta_{Err} < 0.13$.

If the trend of decreasing α -element ratio with increasing $[Fe/H]$ we observe is real then, after initial enrichment to high $[E/Fe]$ by type II SN at low $[Fe/H]$, type Ia SN should be the major contributors to the metallicity enrichment. In a simple closed box scenario we would expect an age difference between the metal-poor, high $[E/Fe]$ and the metal-rich, low $[E/Fe]$ GCs, because type Ia SN do not contribute to the chemical enrichment of the gas associated with galaxy for approximately 1 Gyr. Even then the contribution is gradual and not instantaneous and so we might expect a measurable timescale for enrichment. However, while we do not measure an age difference between metal-poor and metal-rich GCs, it is possible within errors, both statistical and systematic, for an age difference of a few Gyrs to be difficult to detect. This is an unresolved problem and suggests that either GCs' α -element abundances or ages are not accurately measured.

6.3 Summary

GC spectra should enable us to measure the stellar populations of the stars forming during epochs of rapid star-formation through a galaxy's history. However we find this link is more tenuous than expected. There is an increasing wealth of GC observational data that are difficult to interpret in a coherent fashion. High quality, high S/N, well calibrated data is essential to avoid adding more "noise" to the picture.

Disentangling the contribution to the observed spectra of age, metallicity, α -element abundance, horizontal branch morphology, dynamic evolution and other element abundance anomalies requires improvements to the stellar population models, some of which are described in Section 5.1. Currently, we cannot probe the stellar population parameters to accuracies better than $\sim 0.1-0.2$ dex. Discriminating between measurement scatter and intrinsic spread amongst the many parameters, in particular age, is of great interest, but will require improved models and observations.

Bibliography

- [1] Albrow, M.D., De Marchi, G., Sahu, K.C., 2002, ApJ, 579, 660
- [2] Ashman, K.M., Zepf S.E., 1992, ApJ, 384, 50
- [3] Barmby, P., Huchra, J.P., Brodie, J.P., Forbes, D.A., Schroder, L.L., Grillmair, C.J., 2000, AJ, 119, 727
- [4] Baugh, C.M., 2006, Reports on Progress in Physics, astro-ph/0610031
- [5] Baugh, C.M., Cole, S., Frenk, C.S., 1996, MNRAS, 283, 1361
- [6] Baumgardt, H., Makino, J., 2003, MNRAS, 340, 227
- [7] Beasley, M.A., *et al.* , 2006, in prep.
- [8] Beasley, M.A., Baugh, C.M., Forbes, D.A., Sharples, R.M., Frenk, C.S., 2002, MNRAS, 333, 383
- [9] Beasley, M.A., Brodie, J.P., Strader, J., Forbes, D.A., Proctor, R.N., Barmby, P., Huchra, J.P., 2004a, AJ, 128, 1623
- [10] Beasley, M.A., Forbes, D.A., Brodie, J.P., Kissler-Patig, M., 2004b, MNRAS, 347, 1150
- [11] Beasley, M.A., Sharples, R.M., Bridges, T.J., Hanes, D.A., Zepf, S.E., Ashman, K.M., Geisler, D., 2000, MNRAS, 318, 1249
- [12] Bekki, K., 2005, ApJ, 626, L93
- [13] Bekki, K., Beasley, M.A., Brodie, J.P., Forbes, D.A., 2005, MNRAS, 363, 1211
- [14] Bekki, K., Forbes, D.A., 2006, A&A, 445, 485
- [15] Bekki, K., Forbes, D.A., Beasley, M.A., Couch, W.J., 2003, MNRAS, 344, 1334
- [16] Bell, E., *et al.* , 2005, ApJ, 625, 23
- [17] Belokurov, V., Evans, N. W., Irwin, M. J., Hewett, P. C., Wilkinson, M. I., 2006, ApJ, 637, 29
- [18] Bertin, E., Arnouts, S., 1996, A&AS, 117, 393
- [19] Binney, J.J., Davies, R.L., Illingworth, G.D., 1990, ApJ, 361, 78

- [20] Bower, R.G., Benson, A.J., Malbon, R., Helly, J.C., Frenk, C.S., Baugh, C.M., Cole, S., Lacey, C.G., 2006, MNRAS, 370, 645
- [21] Bressan, A., Granato, G.L., Silva, L., 1998, A&A, 332, 153
- [22] Bridges, T.J., 1992, PhD Thesis, Queens University, Kingston, Ontario
- [23] Bridges, T.J. *et al.*, 2003, in Bridges, T., Forbes, D., eds., 25th IAU General Assembly, JD6, Extragalactic Globular Clusters and their Host Galaxies. Astron. Soc. Pac., San Francisco, in press (astro-ph/0310324)
- [24] Bridges, T.J. *et al.*, 2006, MNRAS, in press
- [25] Brodie, J.P., Huchra J.P., 1990, ApJ, 362, 503 (BH)
- [26] Brodie, J.P., Strader, J., Denicolo, G., Beasley, M.A., Cenarro, A.J., Larsen, S.S., Kuntschner, H., Forbes, D.A., 2005, AJ, 129, 2643
- [27] Brodie, J.P., Strader, J., 2006, ARA&A, 44, 193
- [28] Brown, T.M., Ferguson, H.C., Smith, E., Kimble, R.A., Sweigart, A.V., Renzini, A., Rich, R.M., VandenBerg, D.A., 2003, ApJ, 592, L17
- [29] Brown, J.A., Wallerstein, G., 1992, AJ, 104, 1818
- [30] Bruzual, A.G., Charlot, S., 2003, MNRAS, 344, 1000
- [31] Buote, D.A., Lewis, A.D., Brighenti, F., Mathews, W.G., 2003, ApJ, 595, 151
- [32] Burstein, D., Faber, S.M., Gaskell, C.M., Krumm, N. 1984, ApJ, 287, 586
- [33] Butcher H., Oemler A., 1978, ApJ, 219, 18
- [34] Cannon, R., *et al.*, 2006, MNRAS, 372, 537
- [35] Capaccioli, M., Held, E.V., Lorenz, H., Vietri, M., 1990, AJ, 99, 1813
- [36] Capaccioli, M., Vietri, M., Held, E.V., Lorenz, H., 1991, ApJ, 371, 535
- [37] Cardiel, N., Gorgas, J., Sanchez-Blazquez, P., Cenarro, A.J., Pedraz, S., Bruzual, G., Klement, J., 2003, A&A, 409, 511
- [38] Carlson, M.N., *et al.*, 1998, AJ, 115, 1778
- [39] Carney, B.W., 1996, PASP, 108, 900
- [40] Cenarro *et al.*, 2006, in prep.
- [41] Cohen, J.G., Blakeslee, J.P., Cote, P., 2003, ApJ, 592, 866
- [42] Cohen, J.G., Blakeslee, J.P., Ryzhov, A.J., 1998, ApJ, 496, 808
- [43] Cohen, J.G., Briley, M.M., Stetson, P.B., 2002, AJ, 123, 2525
- [44] Cohen, J.G., Briley, M.M., Stetson, P.B., 2005, AJ, 130, 1177

- [45] Cote, P., Marzke, R. O., West, M. J., 1998, ApJ, 501, 554
- [46] Cote, P., McLaughlin, D.E., Hanes, D.A., Bridges, T.J., Geisler, D., Merritt, D., Hesser, J.E., Harris, G.L.H., Lee, M.G., 2001, ApJ, 559, 828
- [47] Cowie, L.L., Songaila, A., Hu, E.M, Cohen, J.G., 1996, AJ, 112, 839
- [48] Davies, R.L., Burstein, D., Dressler, A., Faber, S.M., Lynden-Bell, D., Terlevich, R.J., Wegner, G., 1987, ApJS, 64, 581
- [49] Davies, R.L., *et al.* , 2001, ApJ, 548, L33
- [50] Denicolo, G., Terlevich, R., Terlevich, E., Forbes, D., Terlevich,A., Carrasco, L., 2005, MNRAS, 356, 1440
- [51] De Lucia, G., Springel, V., White, S.D.M., Croton, D., Kauffmann, G., 2006, MNRAS, 366, 499
- [52] de Vaucouleurs, G., de Vaucouleurs, A., Corwin, H.G., Buta, R.J., Paturel, G., Fouque, P., 1991, Sky & Telescope, 82, 821
- [53] Durrell, P. R., Harris, W. E., Geisler, D., Pudritz, R., 1996, AJ, 112, 972
- [54] Elmegreen, B.G., Efremov, Y.N., 1997, ApJ, 480, 235
- [55] Fagiolini, M., Raimondo, G., Degl’Innocenti, S., 2006, A&A accepted, astro-ph/0609162
- [56] Fall, S.M., Zhang, Q., 2001, ApJ, 561, 751
- [57] Ferreras, I., Pasquali, A., de Carvalho, R.R., de la Rosa, I.G., Lahav, O., 2006, MNRAS, 370, 828
- [58] Ferraro, F.R., Mucciarelli, A., Carretta, E., Origlia, L., 2006, ApJ, 645, L33
- [59] Forbes, D.A., 2005, ApJ, 635, L137
- [60] Forbes, D.A., Beasley, M.A., Brodie, J.P., Kissler-Patig, M., 2001a ApJ, 563, 143
- [61] Forbes, D.A., Brodie, J.P., Grillmair, C.J., 1997, AJ, 113, 1652
- [62] Forbes, D.A., Faifer, F.R., Forte, J.C., Bridges, T., Beasley, M.A., Gebhardt, K., Hanes, D.A., Sharples, R., Zepf, S.E., 2004, MNRAS, 355, 608
- [63] Forbes, D.A., Georgakakis, A. E., Brodie, J.P., 2001b, MNRAS, 325,1431
- [64] Forbes, D.A., Ponman, T.J., Brown, R.J.N., 1998, ApJ, 508, L43
- [65] Forbes, D.A., Sparks, W., Macchetto, F.D., 1990, In *Paired and Interacting Galaxies, p 431, ed J. Sulentic, W. Keel, C. Telesco, NASA.*
- [66] Forbes, D.A., Strader, J., Brodie, J.P., 2004, AJ, 127, 3394

- [67] Freeman, K., Bland-Hawthorn, J., 2002, *ARA&A*, 40, 487
- [68] Fregeau, J.M., Joshi, K.J., Portegies Zwart, S.F., Rasio, F.A., 2002, *ApJ*, 570, 171
- [69] Fukugita, M., Hogan, C.J., Peebles, P.J.E., 1998, *ApJ*, 503, 518
- [70] Gebhardt, K., Kissler-Patig, M., 1999, *AJ*, 118, 1526
- [71] Genzel R., Baker A.J., Tacconi L.J., Lutz D., Cox P., Guilleaume, S., Omont, A., 2003, *ApJ*, 584, 633
- [72] Genzel R., Cesarsky C., 2000, *ARA&A*, 38, 761
- [73] Gnedin, O.Y., Ostriker, J.P., 1997, *ApJ*, 474, 223
- [74] Goudfrooij, P., Gilmore, D., Whitmore, B.C., Schweizer, F., 2004, *ApJ*, 613, L12
- [75] Goudfrooij, P., Mack, J., Kissler-Patig, M., Meylan, G., Minniti, D., 2001, *MNRAS*, 322, 643
- [76] Grebel, E.K., 2001, *ApSSS*, 277, 231
- [77] Gregg, M.D., Ferguson, H.C., Minniti, D., Tanvir, N., Catchpole, R., 2004, *AJ*, 127, 1441
- [78] Hanes, D.A., 1976, PhD Thesis, University of Toronto
- [79] Hanes, D.A., 1977a, *MNRAS*, 179, 331
- [80] Hanes, D.A., 1977b, *MNRAS*, 180, 309
- [81] Hanes, D.A., 1979, *MNRAS*, 188, 901
- [82] Harris, W.E., 1991, *ARA&A*, 29, 543
- [83] Harris, W.E., 1996, *AJ*, 112, 1487
- [84] Harris, W.E., 1999, *Ap&SS*, 267, 95
- [85] Harris, W.E., 2001, in *Saas-Fee Advanced School on Star Clusters*, ed. L. Labhardt & B. Binggeli (course 28) (New York: Springer)
- [86] Harris, W.E., Harris, G.L.H., 2002, *AJ*, 123, 3108
- [87] Harris, W.E., Pudritz, R.E., 1994, *ApJ*, 429, 177
- [88] Harris, W.E., van den Bergh, S., 1981, *AJ*, 86, 1627
- [89] Harris, W.E., Whitmore, B.C., Karakla, D., Okon, W., Baum, W.A., Hanes, D.A., Kavelaars, J.J., 2006, *ApJ*, 636, 90
- [90] Heggie, D.C., Hut, P., 1996, *IAUS*, 174, 303

- [91] Hook, I., *et al.*, 2002, SPIE, 4841, Power Telescopes and Instrumentation into the New Millennium
- [92] Hughes, J., Wallerstein, G., van Leeuwen, F., Hilker, M., 2004, AJ, 127, 980
- [93] Hurley, J.R., Pols, O.R., Aarseth, S.J., Tout, C.A., 2005, MNRAS, 363, 293
- [94] Hut, P., *et al.*, 1992, PASP, 104, 981
- [95] Israel, F.P., 1998, A&ARV, 8, 237
- [96] Ivans, I.I., Sneden, C., Kraft, R.P., Suntzeff, N.B., Smith, V.V., Langer, G.E., Fulbright, J.P., 1999, AJ, 118, 1273
- [97] Jones, L.A., 1999, PhD Thesis, University of North Carolina
- [98] Jonsell, K., Edvardsson, B., Gustafsson, B., Magain, P., Nissen, P. E., Asplund, M., 2005, A&A, 440, 321
- [99] Jordan, A., *et al.*, 2006, ApJ, 651, L25
- [100] Kauffmann, G., 1996, MNRAS, 281, 487
- [101] Kauffmann, G., Charlot, S., 1998, MNRAS, 294, 705
- [102] Kauffmann, G., White, S.D.M., Guiderdoni, B., 1993, MNRAS, 264, 201
- [103] Kawata, D., Gibson, B.K., 2003, MNRAS, 346, 135
- [104] Kazantzidis, S., Kravtsov, A.V., Zentner, A.R., Allgood, B., Nagai, D., Moore, B., 2004, ApJ, 611, L73
- [105] Kissler-Patig, M., 2000, In Reviews in Modern Astronomy 13: New Astrophysical Horizons, ed. R.E. Schielicke, p.13. Hamburg, Germany: Astronomische Gesellschaft
- [106] Kissler-Patig, M., Gebhardt, K., 1999, AGM, 15, E01
- [107] Knapp, G.R., Kerr, F.J., Williams, B.A., 1978, ApJ, 222, 800
- [108] Kodama, T., *et al.*, 2005, PASJ, 57, 309
- [109] Kobayashi, C., 2004, MNRAS, 347, 740
- [110] Koch, A., Grebel, E.K., Odenkirchen, M., Martinez-Delgado, D., Caldwell, J.A.R., 2004, AJ, 128, 2274
- [111] Kravtsov, A.V., Gnedin, O.Y., 2005, ApJ, 623, 650
- [112] Kundu, A., *et al.*, 2005, ApJ, 634, L41
- [113] Kundu, A., Whitmore, B.C., 2001, AJ, 121, 2950
- [114] Kuntschner, H., Ziegler, B.L., Sharples, R.M., Worthey, G., Fricke, K.J., 2002, A&A, 395, 761

- [115] Lamers, H.J.G.L.M., Anders, P., de Grijs, R., 2006, *A&A*, 452, 131
- [116] Larsen, S.S., Brodie, J.P., 2002, *AJ*, 123, 1488
- [117] Larsen, S.S., Brodie, J.P., Beasley, M.A., Forbes, D.A., Kissler-Patig, M., Kuntschner, H., Puzia, T.H., 2003, *ApJ*, 585, 767
- [118] Larsen, S.S., Brodie, J.P., Huchra, J.P., Forbes, D.A., Grillmair, C.J., 2001, *AJ*, 121, 2974
- [119] Larsen, S.S., Brodie, J.P., Strader, J., 2005, *A&A*, 443, 413
- [120] Larsen, S.S., Richtler, T., 2000, *A&A*, 354, 836
- [121] Larson, R.B., 1975, *MNRAS*, 173, 671
- [122] Lee, K.H., Lee, H.M., Fahlman, G.G., Sung, H., 2004, *AJ*, 128, 2838
- [123] Lee, H.-C., Yoon, S.-J., Lee, Y.-W., 2000, *AJ*, 120, 998
- [124] Lee, Y.-W., Joo, J.-M., Sohn, Y.-J., Rey, S.-C., Lee, H.-C., Walker, A.R., 1999, *Nature*, 402, 55
- [125] Leep, E.M., Wallerstein, G., Oke, J.B., 1986, *AJ*, 91, 1117
- [126] Lilly, T., Fritze-v. Alvensleben, U., 2006, *A&A*, 457, 467
- [127] Lintott, C.J., Ferreras, I., Lahav, O., 2006, *ApJ*, 648, 826
- [128] Macchetto, F., Pastoriza, M., Caon, N., Sparks, W.B., Giavalisco, M., Bender, R., Capaccioli, M., 1996, *A&A*, 120, 463
- [129] Magris, C.G., Bruzual, A.G., 1993, *ApJ*, 417, 102
- [130] Matteucci, F., Panagia, N., Pipino, A., Mannucci, F., Recchi, S., Della Valle, M., 2006, *MNRAS*, 372, 265
- [131] Maraston, C., Greggio, L., Thomas, D., 2001a, *Ap&SS*, 276, 893
- [132] Maraston, C., Kissler-Patig, M., Brodie, J. P., Barmby, P., Huchra, J. P., 2001b, *A&A*, 370, 176
- [133] McCrady, N., Gilbert, A.M., Graham, J.R., 2003, *ApJ*, 596, 240
- [134] McLaughlin, D.E., 1999, *AJ*, 117, 2398
- [135] McLaughlin, D.E., Pudritz, R.E., 1996, *ApJ*, 457, 578
- [136] Mehlert, D., Thomas, D., Saglia, R.P., Bender, R., Wegner, G., 2003, *A&A*, 407, 423
- [137] Mendel, J.T., Proctor, R.N., Forbes, D.A., 2006, *MNRAS*, submitted
- [138] Meylan, G., Sarajedini, A., Jablonka, P., Djorgovski, S.G., Bridges, T., Rich, R.M., 2001, *AJ*, 122, 830

- [139] Mieske, S., Hilker, M., Infante, L., Jordan, A., 2006a, AJ, 131, 2442
- [140] Mieske, S., *et al.*, 2006b, ApJ, accepted, astro-ph/0609079
- [141] Miller, B.W., Whitmore, B.C., Schweizer, F., Fall, S.M., 1997, AJ, 14, 2381
- [142] Minniti, D., Rejkuba, M., 2002, ApJ, 575, L59
- [143] Moore, B., Diemand, J., Madau, P., Zemp, M., Stadel, J., 2006, MNRAS, 368, 563
- [144] Morgan, S., Lake, G., 1989, ApJ, 339, 171
- [145] Nelan, J.E., *et al.*, 2005, ApJ, 632, 137
- [146] Oke, J.B., *et al.*, 1995, PASP, 107, 375
- [147] Olsen, K.A.G., Miller, B.W., Suntzeff, N.B., Schommer, R.A., Bright, J., 2004, AJ, 127, 2674
- [148] Ostrov, P., Giesler, D., Forte, J.C., 1993, AJ, 105, 1762
- [149] Peng, E.W., Ford, H.C., Freeman, K.C., 2004, ApJ, 602, 705
- [150] Peng, E.W., Jordan, A., Cote, P., Blakeslee, J.P., Ferrarese, L., Mei, S., West, M.J., Merritt, D., Milosavljevic, M., Tonry, J.L., 2006, ApJ, 639, 95
- [151] Pierce, M.J., Brodie, J.P., Forbes, D.A., Beasley, M.A., Proctor, R.N., Strader, J., 2005, MNRAS, 358, 419
- [152] Pierce, M.J., *et al.*, 2006a, MNRAS, 366, 1253
- [153] Pierce, M.J., *et al.*, 2006b, MNRAS, 368, 325
- [154] Pipino, A., Matteucci, F., Chiappini, C., 2006, ApJ, 638, 739
- [155] Piotto, G., *et al.*, 2002, A&A, 391, 945
- [156] Plana, H., Boulesteix, J., 1996, A&A, 307, 391
- [157] Pritzl., B.J., Venn, K.A., Irwin, M., 2005, AJ, 130, 2140
- [158] Proctor, R.N., 2002, Ph. D. Thesis, University of Central Lancashire, UK
- [159] Proctor, R.N., Forbes, D.A., Beasley, M.A., 2004, MNRAS, 355, 1327
- [160] Proctor, R.N., Forbes, D.A., Forestell, A., Gebhardt, K., 2005, MNRAS, 362, 857
- [161] Proctor, R.N., Sansom, A.E., 2002, MNRAS, 333, 517
- [162] Prugniel, P., Simien, F., 1996, A&A, 309, 749
- [163] Puzia, T.H., Kissler-Patig, M., Goodfroom, P., 2006, ApJ, 648, 383

- [164] Puzia, T.H., Kissler-Patig, M., Thomas, D., Maraston, C., Saglia, R.P., Bender, R., Goudfrooij, P., Hempel, M., 2005, A&A, 439, 997
- [165] Puzia, T.H., Kissler-Patig, M., Thomas, D., Maraston, C., Saglia, R.P., Bender, R., Richtlet, T., Goudfrooij, P., Hempel, M., 2004, A&A, 415, 123
- [166] Puzia, T.H., Zepf, S.E., Kissler-Patig, M., Hilker, M., Minniti, D., Goudfrooij, P., 2002, A&A, 391, 453
- [167] Racine, R., 1968, PASP, 80, 326
- [168] Randall, S.W., Sarazin, C.L., Irwin, J.A., 2004, ApJ, 600, 729
- [169] Recio-Blanco, A., Aparicio, A., Piotto, G., de Angeli, F., Djorgovski, S.G., 2006, A&A, 452, 875
- [170] Renzini, A., 2006, ARA&A, 44, 141
- [171] Rhode, K.L., Zepf, S.E., 2004, AJ, 127, 302
- [172] Rhode, K.L., Zepf, S.E., Santos, M.R., 2005, ApJ, 630, L21
- [173] Rich, R.M., *et al.*, 1997, ApJ, 484, L25
- [174] Richtler, T., *et al.*, 2004, AJ, 127, 2094
- [175] Romanowsky, A.J., Douglas, N.G., Arnaboldi, M., Kuijken, K., Merrifield, M.R., Napolitano, N.R., Capaccioli, M., Freeman, K.C., 2003, Science, 301, 1696
- [176] Rose, J.A., 1984, AJ, 89, 1238
- [177] Saiz, A., Dominguez-Tenreiro, R., Serna, A., 2003, Ap&SS, 284, 411
- [178] Salaris, M., Cassisi, S., 2006, A&A, in press, astro-ph/0610252
- [179] Sanchez-Blazquez, P., Peletier, R.F., Jimenez-Vicente, J., Cardiel, N., Cenarro, A.J., Falcon-Barroso, J., Gorgas, J., Selam, S., Vazdekis, A., 2006, MNRAS, 371, 703
- [180] Sandage, A., Willey, R., 1967, ApJ, 150, 469
- [181] Scannapieco, E., Weisheit, J., Harlow, Francis., 2004, ApJ, 615, 29
- [182] Schiavon, R.P., 2006, in prep.
- [183] Schiavon, R.P., Rose, J.A., Courteau, S., MacArthur, L. 2004, ApJ, 608, L33
- [184] Schlegel, D.J., Finkbeiner, D.P., Davis, M., 1998, ApJ, 500, 525
- [185] Schweizer, F., Miller, B.W., Whitmore, B.C., Fall, S.M., 1996, AJ, 112, 1839
- [186] Schweizer, F., Seitzer, P., 1992, AJ, 104, 1039
- [187] Schweizer, F., Seitzer, P., 1998, AJ, 116, 2206

- [188] Schweizer, F., Seitzer, P., Brodie, J.P., 2004, AJ, 128, 202
- [189] Secker, J., 1992, AJ, 104, 1472
- [190] Serra, P., Trager, S.C., 2006, MNRAS accepted, astro-ph/0610343
- [191] Serven, J., Worthey, G., Briley, M.M., 2005, ApJ, 627, 754
- [192] Smith, L.J., Gallagher, J.S., 2001, MNRAS, 326, 1027
- [193] Somerville, R.S., Primack, J.R., 1999, MNRAS, 310, 1087
- [194] Spitler, L.R., Larsen, S.S., Strader, J., Brodie, J.P., Forbes, D.A., Beasley, M.A., 2006, AJ, 132, 1593
- [195] Springel, V., *et al.*, 2005, Nature, 435, 629
- [196] Strader, J., Brodie, J.P., 2004, AJ, 128, 1671
- [197] Strader, J., Brodie, J.P., Forbes, D.A., 2004a, AJ, 127, 295
- [198] Strader, J., Brodie, J.P., Forbes, D.A., 2004b, AJ, 127, 3431
- [199] Strader, J., Brodie, J.P., Schweizer, F., Larsen, S.S., Seitzer, P., 2003, AJ, 125, 626
- [200] Strader, J., Brodie, J.P., Spitler, L., Beasley, M.A., 2006, AJ, accepted, astro-ph/0508001
- [201] Terlevich, A.I., Forbes, D.A., 2002, MNRAS, 330, 547
- [202] Thomas, D., Maraston, C., Bender, R., 2003, MNRAS, 339, 897
- [203] Thomas, D., Maraston, C., Korn, A., 2004, MNRAS, 351, 19 (TMK04)
- [204] Trager, S.C., Faber, S.M., Worthey, G., Gonzarlez, J.J., 2000a, AJ, 119, 1645
- [205] Trager, S.C., Faber, S.M., Worthey, G., Gonzarlez, J.J., 2000b, AJ, 120, 165
- [206] Trager, S.C., Worthey, G., Faber, S.M., Burstein, D., Gonzalez, J.J., 1998, ApJS, 116, 1
- [207] Trippico, M.J., Bell, R.A., 1995, AJ, 110, 3035
- [208] Trippico, M.J., 1989, AJ, 97, 735
- [209] Tsujimoto, T., Shigeyama, T., 2003, ApJ, 590, 803
- [210] van den Bergh, S., 1967, AJ, 72, 70
- [211] van Dokkum, P.G., Franx, M., 1995, AJ, 110, 2027
- [212] van Dokkum, P.G., Franx, M., Fabricant, D., Illingworth, G.D., Kelson, D.D., 2000, ApJ, 541, 95

- [213] van Dokkum, P.G., Stanford, S.A., 2003, ApJ, 585, 78
- [214] Van Gorkom, J.H., Knapp, G.R., Ekers, R.D., Ekers, D.D., Laing, R.A., Polk, K.S., 1989, AJ, 97, 708
- [215] Vazdekis, A., 1999, ApJ, 513, 224
- [216] Vazdekis, A., 2006, in prep.
- [217] Vesperini, E., 2000, MNRAS, 318, 841
- [218] Vesperini, E., 2001, MNRAS, 322, 247
- [219] Vesperini, E., Zepf, S.E., 2003, ApJ, 587, L97
- [220] Vesperini, E., Zepf, S.E., Kundu, A., Ashman, K.M., 2003, ApJ, 593, 760
- [221] Wake, D.A., *et al.* , 2006, MNRAS, 372, 537
- [222] West, M.J., Cote, P., Marzke, R.O., Jordan, A., 2004, Nature, 427, 31
- [223] Whitlock, S., Forbes, D.A., Beasley, M.A., 2003, MNRAS, 345, 949
- [224] Whitmore, B.C., Schweizer, F., 1995, AJ, 109, 960
- [225] Whitmore, B.C., Schweizer, F., Kundu, A., Miller, B., 2002, AJ, 124, 147
- [226] Worthey, G., 1994, ApJS, 95, 107
- [227] Worthey, G., Ottaviani, D.L., 1997, ApJS, 111, 377
- [228] Yoon, S.-J., Yi, S.K., Lee, Y.-W., 2006, Science, 311, 1129
- [229] Zepf, S.E., Ashman, K.M. 1993, MNRAS, 264, 611
- [230] Zepf, S.E., Ashman, K.M., English, J., Freeman, K.C., Sharples, R.M., 1999, AJ, 118, 752
- [231] Zepf, S.E., Beasley, M.A., Bridges, T.J., Hanes, D.A., Sharples, R.M., Ashman, K.M., Geisler, D., 2000, AJ, 120, 2928
- [232] Zinn, R., West, M.J., 1984, ApJS, 55, 45